

AD-A084 860

NORTHROP CORP DES PLAINES IL DEFENSE SYSTEMS DIV

F/0 11/2

METAL-CERAMIC SEALS.(U)

OCT 79 Y AMER, G DOHLER

F33615-78-C-1405

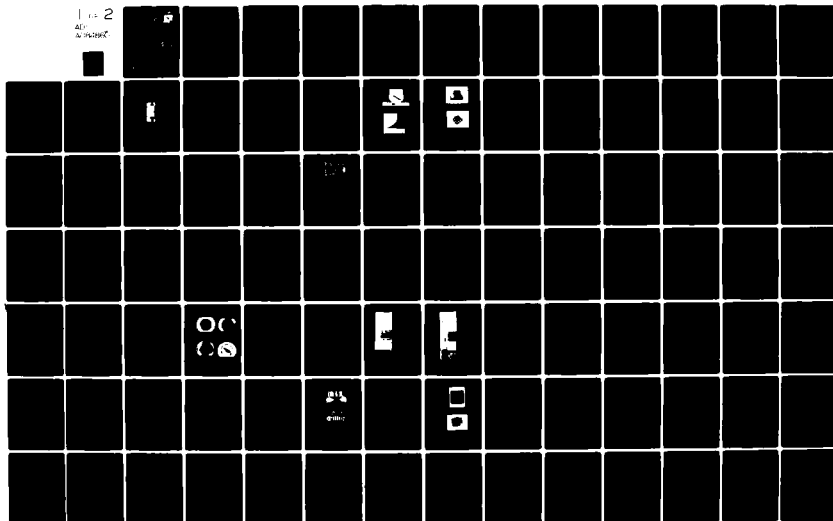
UNCLASSIFIED

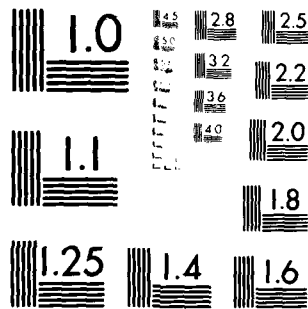
094-9169

AFAL -TR-79-1106

NL

Fig 2
ALL INFORMATION CONTAINED
HEREIN IS UNCLASSIFIED





MICROCOPY RESOLUTION TEST CHART
NATIONAL BUREAU OF STANDARDS-1963-A

AD A 084860

LEVEL

Advanced Defense Systems Division
Research Triangle Institute
Durham, NC 27709

OCTOBER 1979

Technical Report AFAL-TR-79-1106
Final Report for Period 15 Feb 78 to 15 Jun 79

DTIC
ELECTE
MAY 30 1980
S D

Approved for Public Release; Distribution Unlimited

DOC FILE COPY

AIR FORCE AVIONICS LABORATORY
AIR FORCE WRIGHT AERONAUTICAL LABORATORIES
AIR FORCE SYSTEMS COMMAND
WRIGHT-PATTERSON AIR FORCE BASE, OHIO 45433

80 5 29 009


This report contains information that is classified as "Secret" under the National Technical Information Service (NTIS) policy and is not to be released to the general public, including foreign nations.

This technical report has been reviewed and is approved for release.


DAVID H. CORNILLE, 1LT, USAF
Project Engineer
Microwave Device Group


ROBERT L. SMITH, 1LT, USAF
Microwave Device Group
Microwave Technology Branch

FOR THE COMMANDER


WILLIAM J. EDWARDS, Chief
Electronic Technology Division
Avionics Laboratory

"If your address has changed, if you wish to be removed from our mailing list, or if the addressee is no longer employed by your organization please notify AFWAL/AADM, W-PAFB, OH 45433 to help us maintain a current mailing list."

Copies of this report should not be returned unless return is required by security considerations, contractual obligations, or notice on a specific document.

REPORT DOCUMENTATION PAGE		READ INSTRUCTIONS BEFORE COMPLETING FORM	
1. REPORT NUMBER	2. GOVT ACCESSION NO.	3. RECIPIENT'S CATALOG NUMBER	
18 AFAL-TR-79-1106	AD-A084966		
4. TITLE (and Subtitle)		5. TYPE OF REPORT & PERIOD COVERED	
6 METAL-CERAMIC SEALS		Final Technical Report	
		2/15/78 to 6/15/79	
7. AUTHOR(s)		8. PERFORMING ORG. REPORT NUMBER	
10 Veldez/Amer		14 094-9169	
Gunter/Dohler		15 F33615-78-C-1405	
9. PERFORMING ORGANIZATION NAME AND ADDRESS		10. PROGRAM ELEMENT, PROJECT, TASK AREA & WORK UNIT NUMBERS	
Northrop Defense Systems Division		62204F	
Electron Tube Section		20020254	17 02
Des Plaines, Ill 60018		11. REPORT DATE	
11. CONTROLLING OFFICE NAME AND ADDRESS		October 1979	
Avionics Laboratory (AFWAL/AADM)		13. NUMBER OF PAGES	
Air Force Wright Aeronautical Laboratories		114	
AFSC, Wright Patterson AFB, OHIO 45433		15. SECURITY CLASS. (of this report)	
14. MONITORING AGENCY NAME & ADDRESS (if different from Controlling Office)		Unclassified	
12 124		15a. DECLASSIFICATION DOWNGRADING SCHEDULE	
16. DISTRIBUTION STATEMENT (of this Report)			
Approved for public release; distribution unlimited.			
17. DISTRIBUTION STATEMENT (of the abstract entered in Block 20, if different from Report)			
9 Final technical rept. 15 Feb 78-15 Jun 79			
18. SUPPLEMENTARY NOTES			
19. KEY WORDS (Continue on reverse side if necessary and identify by block number)			
RF losses		"Q" measurements	
Ceramic metallization		Liquid Brazes	
Sputtering down holes		RF windows, high power, millimeter	
Thermal Barrier		wave windows	
Reliability			
20. ABSTRACT (Continue on reverse side if necessary and identify by block number)			
This program describes the results obtained during a one year study program on high power microwave and millimeter wave windows. The objective of this program was to investigate the applicability of a new ceramic metallization process to the fabrication of waveguide windows. The new metallization process, developed recently by Northrop, consists in sputtering a Ti-Mo-Cu Layer onto the ceramic and has shown to exhibit extremely high bond strength, reliability and very low thermal barriers and rf losses when compared to the			

409984

SW

classical Mo-Mn metallization.

Three types of rf windows were fabricated, mainly for I/J band applications: circular windows, rectangular waveguide windows and coaxial windows. The advantages of the Ti-Mo-Cu metallization process as compared to the classical Mo-Mn process have been quantitatively defined, and excellent results have been obtained. The rf losses have been found to be excellent if cusil is used as brazing alloy, and extremely low thermal barriers have been measured. The use of Au/Cu brazing alloys results in higher reliability under thermal cycling conditions, but increases drastically the rf losses.

FOREWORD

This final report describes the results obtained by Northrop Corporation, Defense Systems Division, 175 West Oakton Street, Des Plaines, Illinois 60018, under contract no. F33015-78-C-1405, the Air Force Avionics Laboratory, Wright Patterson AFB, Ohio 45433. The program manager at Northrop was Dr. Gunther Dohler, the principal investigator was Yeldez Amer. The technical effort covered the period from February 1978 to June 1979. The project engineer for the Air Force was 2Lt. David Corneille. The Sputtering technique described in this program was developed by Northrop Corporation under contract no F33015-76-C-1050 from the Air Force Avionics Laboratory. This report was submitted to the Air Force Avionics Laboratory by Northrop on the 18th of May, 1979.

Accession For	
DTIC	<input checked="" type="checkbox"/>
DDC TAB	<input type="checkbox"/>
Unannounced	<input type="checkbox"/>
Justification	<input type="checkbox"/>
By _____	
Distribution _____	
Availability _____	
Dist	Accession
A	Special

TABLE OF CONTENTS

Section		Page
1.0	INTRODUCTION	1
2.0	BRAZING TECHNOLOGY	3
2.1	Compression Bonding (Flat Surface Brazing)	3
2.1.1	Bond Strength of Liquid Brazes	3
2.1.2	Reliability of Liquid Brazes	11
2.1.3	Zirconium Sputtering Substitution	13
2.1.4	Conclusion	16
2.2	Round Disc Bonding	17
2.2.1	Sputtering Into Substrate Holes	17
2.2.1.1	The Model	17
2.2.1.2	Experimental Results	21
2.2.1.3	Conclusion	25
2.2.2	Sputtering On Substrate Edges	25
2.2.3	Hermeticity of Circular Windows	29
2.2.3.1	Test Vehicles	29
2.2.3.2	OFHC Sleeves	31
2.2.3.3	Kovar Sleeves	36
2.2.3.4	Conclusion	36
2.2.4	Reliability and Tensile Strength	40
2.2.4.1	Reliability	40
2.2.4.2	Tensile Strength	40
2.2.5	Cross Sectional Analysis	49
2.2.6	Conclusion	50
2.3	Coaxial Windows	54
2.3.1	Fabrication of Coaxial Windows	54
2.3.2	Reliability and Thermal Cycle Effect on Coaxial Windows	54
2.3.3	Bond Strength Test On Coaxial Windows	60
2.3.4	Conclusion	60
2.4	Rectangular Waveguide Windows	62
2.4.1	Sputtering of Ceramics	62

TABLE OF CONTENTS (Continued)

Section		Page
3.0	HEAT TRANSFER IN ROUND WINDOWS	67
	3.1 Thermal Barrier of Liquid Brazes	67
	3.2 Thermocouple Measurements	71
	3.3 Round Discs	74
	3.3.1 Experimental Set-Up	74
	3.3.2 Diffusion Brazes	76
	3.3.3 Liquid Brazes	83
	3.4 Coaxial Samples	88
4.0	R.F. LOSSES	92
	4.1 Rectangular Waveguides	92
	4.1.1 Empty Waveguides	92
	4.1.2 The Unbrazed Window	95
	4.1.3 Brazed Windows	99
	4.1.4 Circular Windows	106
5.0	CONCLUSION AND DISCUSSION	107

LIST OF ILLUSTRATIONS

Figure		Page
1	Schematic Diagram of Pull Test Assembly for Liquid Brazing.	4
2	Liquid Brazing Fixture	5
3	Side View of Waffled Copper Rod Liquid Braze Showing Cu-Fillet	9
4	Ceramic Pull Test Samples After Pull Test Failure	10
5	Thermal Cycling Between Room Temperature and 500°C (Zr Sputtering)	15
6	Definition of Virtual Sputtering Source	18
7	Coordinate Definitions for Sputtering	19
8	Top Surface View of Aluminum Plate with Various Size Holes	22
9	Measured Copper Film Thickness vs. Depth/Diameter Ratio for 90 Minute Sputtering Time with Plate .250 Inch Thick	23
10	Amplitude $t(0) \approx t_s/2$ and Surface Film Thickness t_s a Function of Sputtering Time	24
11	Amplitude Ratio $t(0)/t_s$ versus Sputtering Time	26
12	Sputtering of Round Discs	27
13	Profile of Sputtered Layer Thickness on Sides of Round Disc	28
14	Side View of Round Window Braze Sleeve	30
15	Bond Strength Test on Round Waveguide Windows	43
16	Illustration of Round Window Sleeves After Bond Strength Test	48
17	Electron Microprobe on Sputtered Film Morphology of Sample No. 6 After 50 Thermal Cycles.	51
18	Electron Microprobe on Sputtered Film Morphology of Sample No. 19 After Brazing	52
19	Phase Diagram of Silver-Copper	53
20	Coax Pin Braze Assembly	55
21	Waveguide Window Ceramic	63
22	Sputtering of Rectangular Window Ceramics	64
23	Brazed Rectangular Windows	66
24	Thermal Barrier Measurements	68
25	Experimental Set Up for Thermal Barrier Measurements By Means Of a Thermocouple	72

LIST OF ILLUSTRATIONS (Continued)

Figure		Page
26	Thermal Barrier Measurement with a Thermocouple	73
27	Experimental Set Up for Heat Transfer Measurements through an Infrared Microscope	75
28	Calibration Curve of Temperature versus Radiance	77
29	Diffusion Brazed Al_2O_3 Disc to Cu Sleeve Mo-Mn Metallization	78
30	Diffusion Brazed Al_2O Disc to Cu Sleeve Sputtering Metallization	79
31	Sputtered Diffusion Brazed Sample #32 with Expanded Scales	80
32	Mo-Mn Metallized Diffusion Brazed Sample #35 with Expanded Scales	81
33	Linear Curve of Temperature Profile for a Mo-Mn Metallized Sample	82
34	Cross Sectional Areas at Brazed Joint of Three Different Samples Illustrating the Effect of the Presence of a Fillet	87
35	Scanning Pattern for a Coaxial Pin Assembly	91
36	Schematic of the Rectangular Waveguide Resonator	93
37	Schematic of Resonant Conditions in Waveguides With and Without Ceramic Windows	97
38	Average Measured Q as a Function of Resonant Frequency	100
39	Specific Resistivity of Au/Cu and Electrical Conductivity of Ag/Cu	101
40	Surface Resistance of Cu Plated with Mo as a Function of Coating Thickness and Frequency	105
41	Cross Sectional Area of Diffusion Brazed Sample No. 35	110
42	Relative Surface Resistivity of Copper Clad with Molybdenum	112

LIST OF TABLES

Table		Page
1	Liquid Braze Pull Tests	6
2	Pull Test Results of Diffusion Braze Samples	8
3	Summary of Thermal Cycling Tests	12
4	Zirconium Sputtering Pull Test Results	14
5	Thermal Expansion of Different Material Used for Round Window Experiments	32
6	Round Disc Seals with Copper	33
7	Round Disc Seals with Kovar	37
8	Thermal Cycling Effect On Copper Sleeves	41
9	Thermal Cycling Effect on Kovar Sleeves	42
10	Bond Strength Test On Copper Sleeves	44
11	Bond Strength Test On Kovar Sleeves	46
12	Coax Window Seals	56
13	Thermal Cycling On Coaxial Windows	58
14	Bond Strength Test On Coaxial Windows	61
15	Rectangular Waveguide Windows	65
16	Representative Values of Effective Thermal Conductivity and Calculated Thermal Resistance	70
17	Thermal Comparison Between Metallizing Schemes	85
18	Thermal Comparison Between Metallizing Schemes	86
19	Thermal Comparison Between Metallizing Schemes	89
20	Thermal Comparison Between Metallizing Schemes	90
21	Quality of Waveguide Window Seals	108
22	List of Different Elements With High Electrical Resistivity	114

SECTION 1

INTRODUCTION

High power windows for microwave devices generally rely on moly-manganese metallization to promote the required hermetic seals. This type of metal-ceramic bonding relies on a glassy phase region close to the ceramic, thus resulting in a thermal interface barrier and in rf losses due to increased resistivity and in inherent surface roughness. As a result, under high power conditions, and particularly at high frequencies, temperature differences across the bonding layer can accumulate and lead to excessive thermal gradients and stresses that precipitate failure of the vacuum joint. Furthermore, tolerances required at mm wave frequencies are difficult to achieve with such a type of thick film metallization.

This report describes the results obtained during a one year study program aimed at applying a newly developed sputtering technique to achieve highly reliable high power microwave windows with low rf losses and high thermal conductivity across the vacuum metal to ceramic seal. This sputtering metallization technique, developed previously under U.S. Air Force sponsorship* relies on a copper-copper diffusion bond between a copper substrate and a ceramic metallized by first sputtering a thin layer of titanium (200Å thick), followed by a 5000Å thick layer of molybdenum which is covered with a 10µm thick copper layer. This technique, which was successfully applied to components and subassemblies of high power microwave amplifiers such as CFA's and TWT's, results in bonding layers with high reliability, low rf losses and high thermal conductivity.

The applicability of this bonding technique to high power microwave windows is not obvious. First, the vacuum tightness of the seals was not verified and, secondly, the diffusion bond is always achieved under compression conditions.

*Contract No. F33615-76-C-1050.

It was therefore anticipated that a liquid braze would be required to warranty vacuum hermeticity and reliability. As such, the use of different liquid brazing alloys was studied together with a direct diffusion bond for coaxial windows.

Section 2 of this report describes the results obtained with regard to feasibility, vacuum tightness and reliability of the seal. Section 3 compares the thermal properties of the samples prepared as compared to classical seals using moly-manganese metallization as reference, and Section 4 discusses the rf loss of circular and rectangular windows obtained through Q measurements. Finally, Section 5 presents a summary of the results and discusses possible future investigations.

SECTION 2

BRAZING TECHNOLOGY

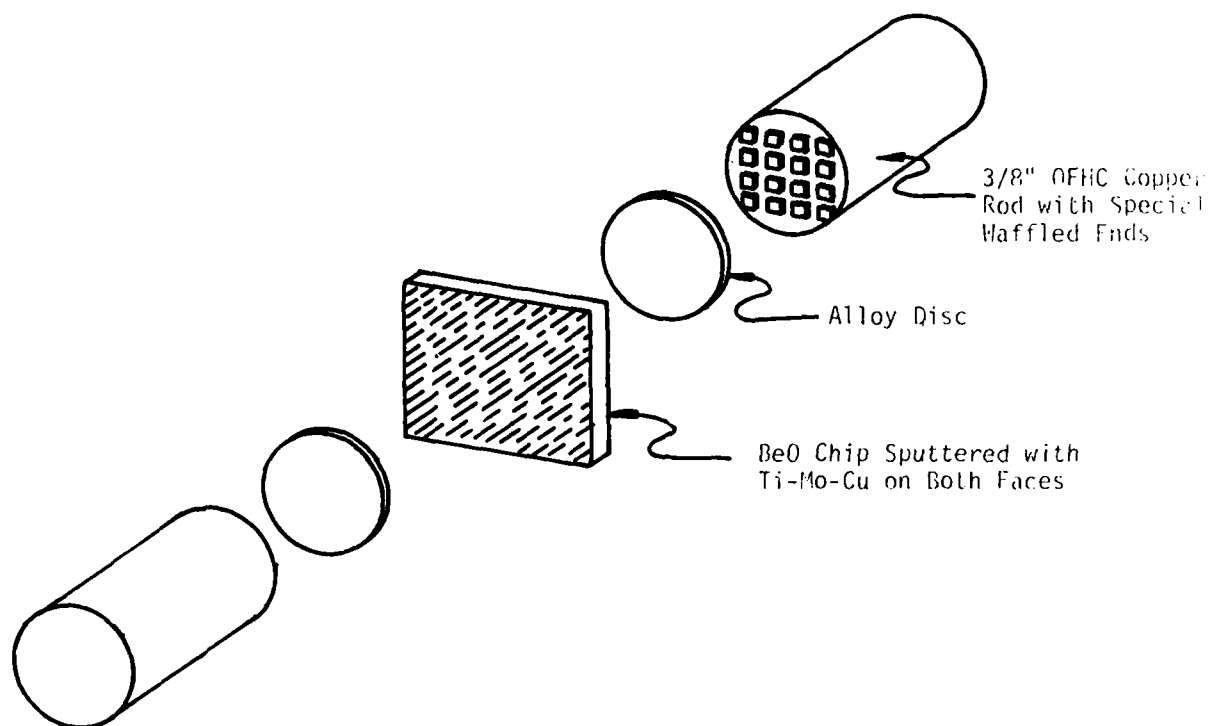
The study program was initiated by directly comparing the bond strength of liquid braze samples to diffusion braze samples on flat BeO substrates metallized in conformance with processes defined previously*. The fabrication of coax windows (as well as rectangular windows) require the determination of a sputtering technique into small holes (coax-center pins) and along the side of samples. Furthermore, once windows have been brazed, the hermeticity as well as their bond strength and reliability must be defined. As such, the following tasks have been undertaken.

2.1 Compression Bonding

2.1.1 Bond Strength of Liquid Brazes (Compression Bonding)

2" x 2" flat beryllia substrates were metallized on both sides with the optimized Ti-Mo-Cu layers as defined previously and as used in current production IBCFA and TWT subassemblies. After sputtering, these coupons were cut into .5" square pieces which were positioned between two waffled rods, as shown in Figure 1. For liquid braze samples, a 3/8" diameter, .001" thick alloy disc was placed between the substrate and the rods. Fixturing, as shown in Figure 2, was used to accommodate the space available in the furnace. Brazing was accomplished in wet hydrogen, leaving the sample approximately for 1 minute at the melting temperature of the corresponding alloy. Bond strength was obtained by measuring the pulling force required on the rods for fracture of the bond to occur, and converting the measured value to bond strength by dividing the measured force by the effective area of the waffles (see Figure 1). Table 1 shows the results obtained with different alloys.

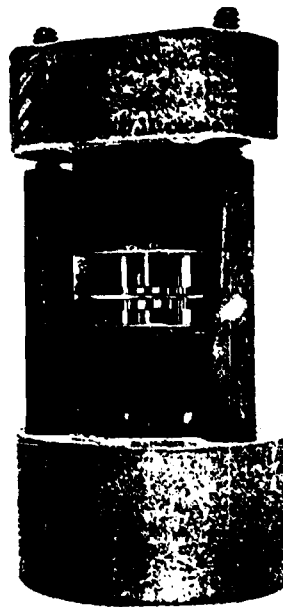
*Contract No. F33615-76-C-1050.



158-020418-001

Schematic Diagram of Pull Test Assembly for Liquid Brazing

Figure 1. Schematic Diagram of Pull Test Assembly for Liquid Brazing



156-026418-002

Figure 2. Liquid Brazing Fixture

TABLE 1. LIQUID BRAZE PULL TESTS (BeO)

ALLOY	MELTING POINT (°C)	FRACTURE STRESS (lb _f /in ²)	AVERAGE FOR GROUP (lb _f /in ²)
35 Au/65 Cu	1020	9,410	10,145
"	1020	9,725	
"	1020		
35 Au/65 Cu + Ni	1020	18,430	18,040
"	1020	17,650	
50 Au/50 Cu	975	8,630	9,675
"	975	9,800	
"	975	10,590	
28 Cu/72 Ag	780	20,570	20,325
"	780	20,790	
"	780	19,610	
3 Ni/15 Cu/83 Au	910	14,510	16,210
"	910	18,040	
"	910	16,080	
Au	1063	4,315	5,698
		4,820	
		7,960	
Ag	960	1,765	2,117
		2,275	
		2,310	

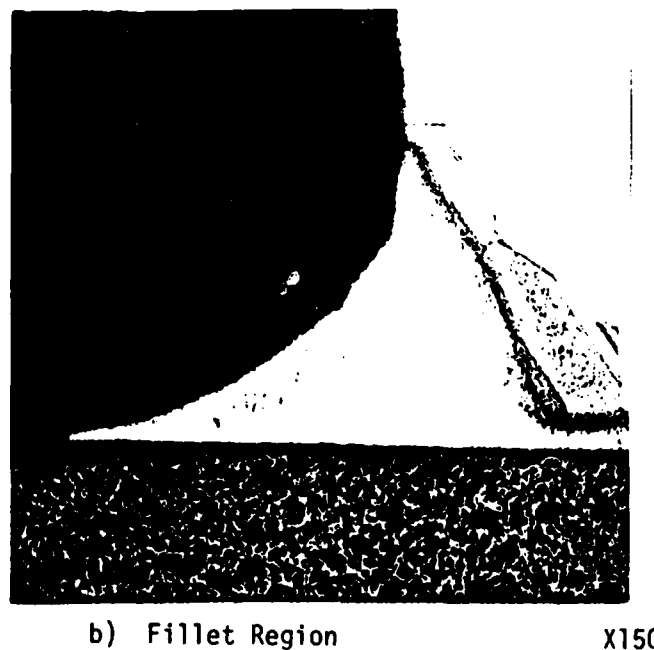
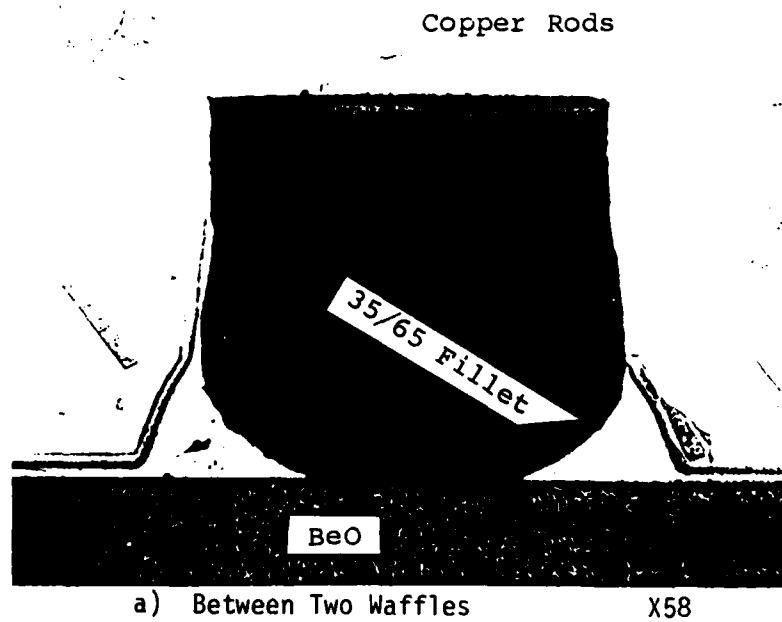
To compare the values obtained, reference was made to a diffusion braze reference group, where 3 samples of 3 different coupons were tested, see Table 2. (Note that these results correspond to those obtained previously, indicating proper metallization process for all samples).

The observed fracture stress for liquid brazed samples seems to be greater than the strength of diffusion brazed samples, with a few exceptions. Figure 3 shows a cross section of a 35/65 Au/Cu liquid braze waffle. Clearly seen on the left side is a fillet of alloy which effectively increases the contact area. Figure 4 also shows the influence of the fillet. The top picture shows the diffusion brazed ceramic after pull test failure: the waffles of the copper rod are clearly visible. The lower picture shows the liquid braze ceramic after pull test failure: here, the effective area of the waffles increased the contact area. Furthermore, these pictures clearly show that fracture of the ceramic occurs in the case of the diffusion bond, while the failure of the liquid alloy braze occurs at the metallized layer and/or the fillet (the ceramic is not clearly visible), indicating erosion of the metallized layer.

The erosion of the sputtered film prompted the plating of the sputtered samples with a nickel layer. With nickel plating, the erosion was still observed, although at a lesser degree, and the bond strength was enhanced by a factor of 2. Additional evidence of reduced bond strength due to erosion (or dissolution) of the films by gold was found when a 35/65 gold/copper liquid braze was held for four minutes at the melting temperature of the alloy (instead of 1 minute). The failure occurred then at only 4310 psi.

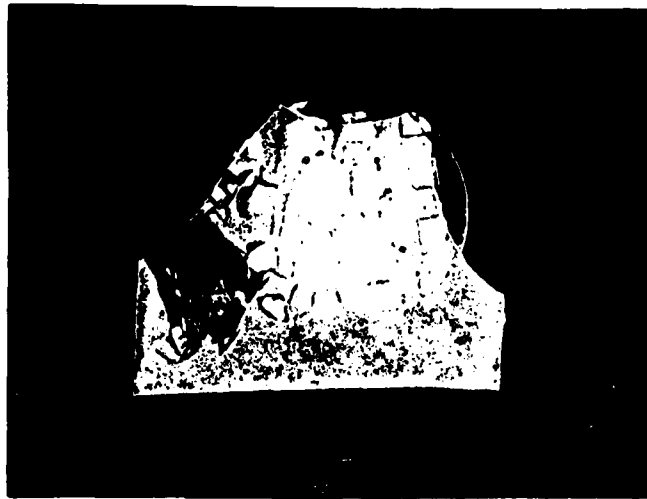
TABLE 2. PULL TEST RESULTS OF REFERENCE DIFFUSION BRAZE SAMPLES

COUPON	PULL TEST STRESS (lb _f /in ²)	AVERAGE (lb _f /in ²)
871	8,840	9,900
871	12,630	
871	8,235	9,900
872	10,900	
872	7,255	
872	8,765	8,980
873	8,900	
873	10,900	
873	7,685	9,160
Overall Average		9,347

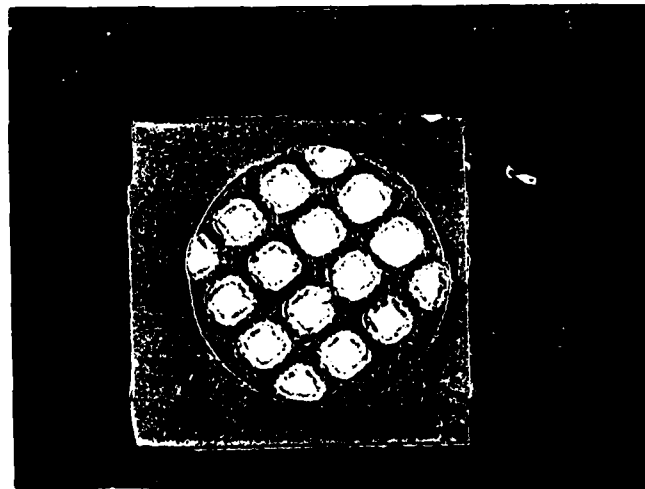


158-026418-003

Figure 3. Side View of Waffled Copper Rod Liquid Braze Showing Cu-Fillet



Diffusion Brazed Pull Test Sample
After Testing. (Q782, 8785 psi)



35Au/65Cu Liquid Alloy Brazed Pull
Test After Testing (Q873, 9410 psi)

158-028418-004

Figure 4. Ceramic Pull Test Samples after Pull Test Failure

Increasing the gold content in the braze alloy to 50% (50/50 Cu-Au) did not alter the bond strength (see Table 1). This can be attributed to the slower melting temperature of this alloy. Increasing the gold content even further and adding Nickel (3 Ni/15 Cu/82 Au) produced greater bonding fracture stress attributed also to the lower melting temperature of this alloy. Thus, the use of gold alters the metallized film, and increased gold content, which reduces the brazing temperature, does not influence significantly the erosion. Pure gold, however, reduces the bond stress to about 4300 psi.

The use of silver/copper alloys reduces the brazing temperature further. Greatest strength values were observed with Cusil (28 Cu/72 Ag), see Table 1, attributed mainly to the fillet. Pure silver, however, also dissolves the metallized layer, and results in low bond strength.

In conclusion, therefore, both 35/65 and 50/50 Au/Cu alloy can be used (with and without Ni), but Cusil produces stronger bonds.

2.1.2 Reliability of Liquid Brazes

Information on reliability was obtained by thermal cycling the test samples between room temperature and 500°C, with 10 minutes at each extreme temperature. The test sample is inserted into a wet hydrogen furnace at 500°C for 10 minutes, then removed into a cold zone for 10 minutes to complete 1 thermal cycle. Table 3 shows the average failure stress of liquid braze samples as a function of number of thermal cycles.

The alloys containing gold have failure stress comparable to the diffusion braze, and degrade as a function of number of thermal cycles. Cusil liquid brazing samples do not show degradation. It is thus concluded that Cusil, 35 Au/65 Cu and 50/50 Au/Cu can be used as brazing alloy, with preference given to Cusil because of its resistance to degradation during thermal cycling.

TABLE 3. SUMMARY OF THERMAL CYCLING TESTS

BRAZE TYPE	MELTING TEMPERATURE (°C)	AVERAGE FAILURE STRESS (lb _f /in ²)		
		No Cycles	25 Cycles	50 Cycles
DIFFUSION	1050	9,345	9,865	7,585
35 Au/65 Cu	1020	10,145	10,680	8,280
50 Au/50 Cu	975	9,675	6,300	6,575
28 Cu/72 Ag	780	21,025	25,560	22,365

2.1.3 Zirconium Sputtering Substitution

The aim of this experiment was to evaluate the relative merits of a compositional change on the bonding. The compositional change is by substituting titanium by zirconium in the Ti-Mo-Cu sputtering process.

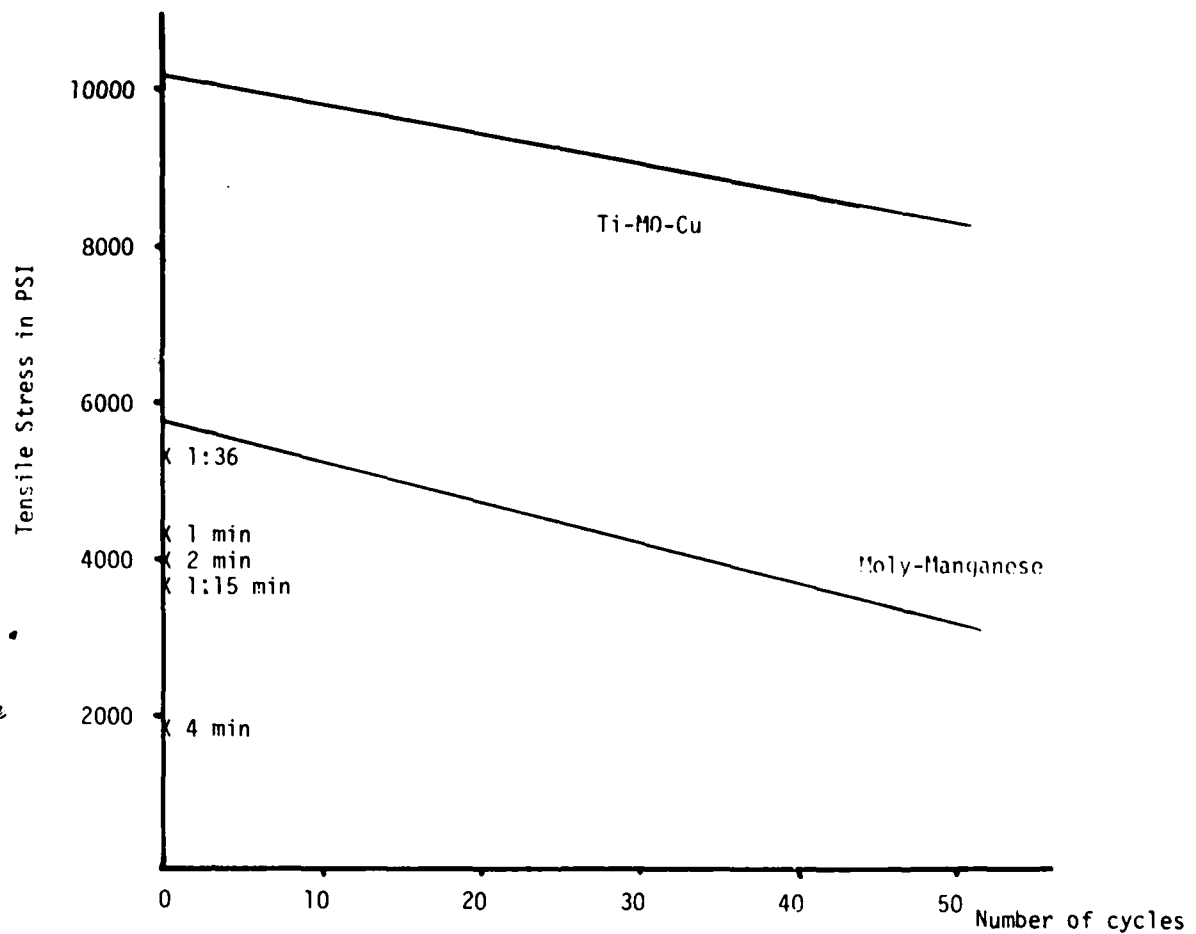
Standard diffusion brazing pull tests were performed on 2" x 2" beryllia coupons. Sputtering time for zirconium was varied; 2, 4, 1:36, 1:15, and 1 minute. The results obtained are shown in Table 4 and in Figure 5

The tensile strength results obtained indicate that the bond strength is weaker when Zr instead of titanium is used. Therefore, no liquid braze tests with Zr were attempted.

Table 4. Zirconium Sputtering Pull Test Results

Coupon No.	Zirconium Sputtering Time	Brazing Process	Average Tensile Strength
Q 899	2	Diffusion	3398 lb_f/in^2
Q 900	2	Diffusion	4313 lb_f/in^2
Q 901	4	Diffusion	1804 lb_f/in^2
Q 902	4	Diffusion	2038 lb_f/in^2
Q 903	1:36	Diffusion	4849 lb_f/in^2
Q 904	1:36	Diffusion	6574 lb_f/in^2
Q 905	1	Diffusion	3960 lb_f/in^2
Q 906	1	Diffusion	4195 lb_f/in^2
Q 958	1:15	Diffusion	3567 lb_f/in^2
Q 959	1:15	Diffusion	3580 lb_f/in^2

ZIRCONIUM SPUTTERING RESULTS



(X Data related to zirconium: time of sputtering as parameter)

Figure 5. Thermal Cycles Between Room Temperature and 500°C

2.1.4 Conclusion

The preliminary tests made on flat surface under compression bonding conditions clearly indicate that:

- a) pure noble metals such as Au and Ag should not be used as brazing alloy because of erosion of the metallized layer and poor adhesion occurring at brazing temperature.
- b) copper/gold alloys exhibit bond strength and reliability similar to diffusion brazes.
- c) cusil alloy exhibits the highest tensile stress (probably due to fillets) and the least degradation during thermal cycling.
- d) the use of Nickel in conjunction with copper/gold alloys enhances the tensile strength.

2.2 Round Disc Bonding

The fabrication of coaxial windows requires (1) a sputtering technique to metallize the side of ceramic discs (also applicable to rectangular windows), (2) a sputtering technique to metallize through the center hole for insertion of the center conductor, and (3) a sleeve and a center pin (test vehicle) of compatible material to assure good and reliable hermetic seals. As such, the following tasks have been accomplished.

2.2.1 Sputtering into Substrate Holes

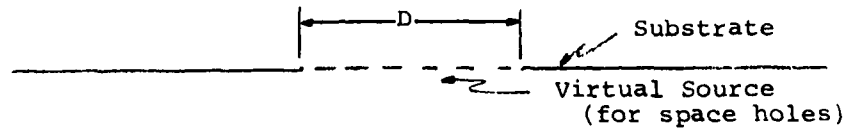
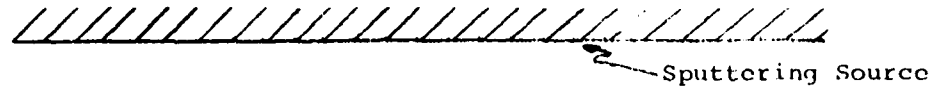
2.2.1.1 The Model

If one considers a sputtering source and a receiving substrate containing a hole, each of infinite extent and parallel to each other, then the material deposited onto the substrate is uniform and the deposited layer thickness is equal to the layer thickness lost by the source, see Figure 6. Assuming then that the particles arriving onto the substrate have the same velocity distribution as those leaving the source, the opening of the substrate hole plays the role of a virtual sputtering source for the space below the hole opening, see Figure 6. It is therefore possible to assume that the number of particles (and their velocity distribution) which pass through the hole opening of diameter D (virtual source) per second is equal to the number of particles per second leaving the real source of the same dimension D .

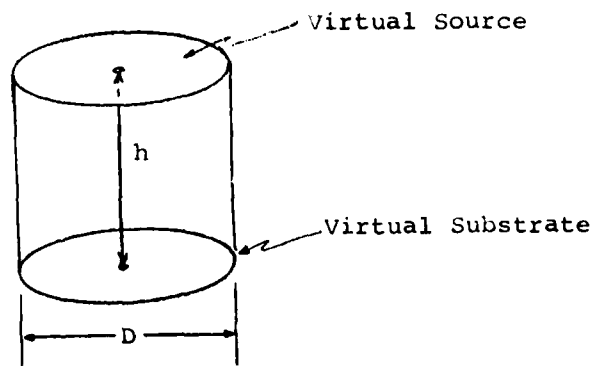
The thickness d_0 of material deposited onto a small surface dA_r of a plane substrate located a distance h away from a circular disc source of radius $D/2 = s$ (see Figure 4) is a function of the distance x between the surface element dA_r and the axis of symmetry of the system, and is given by*:

$$d_0 = \frac{M_e}{2\pi\rho s^2} \left[1 - \frac{1 + x'^2 - s'^2}{[(1 - x'^2 + s'^2)^2 + 4x'^2]^{\frac{1}{2}}} \right] \quad (1)$$

*L.I. Marssel, R. Glang, Handbook of Thin Film Technology, McGraw Hill, pp. 1-59, 1970.

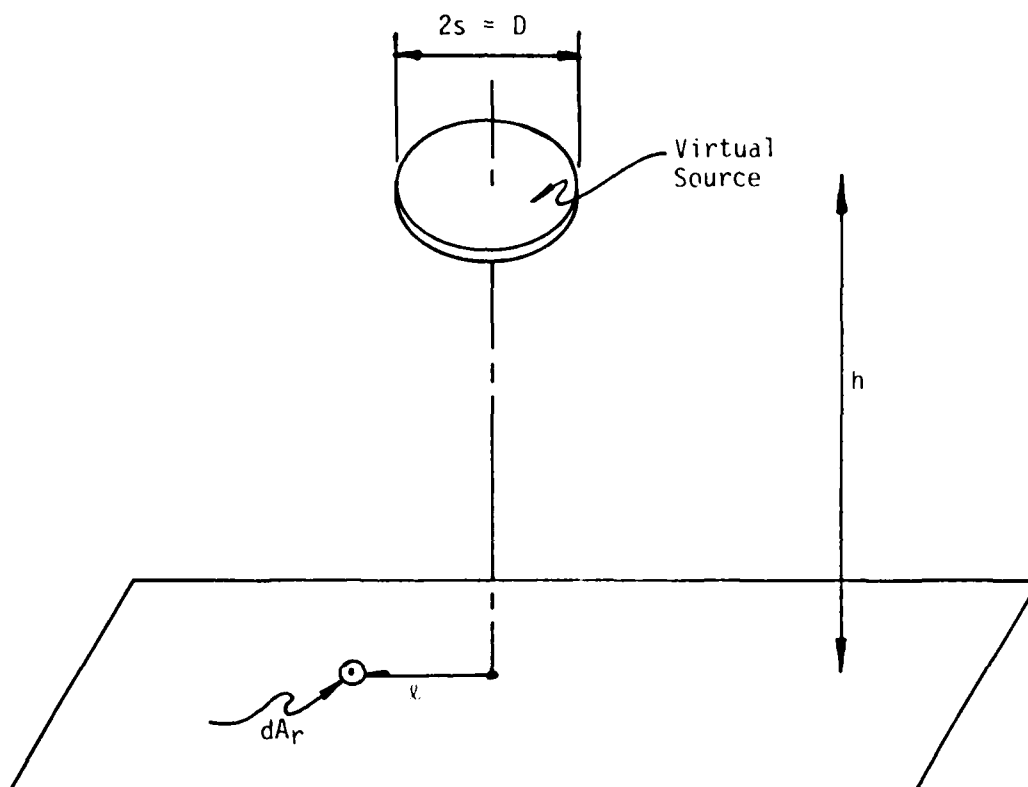


Substrate Definition



188-628418-008

Figure 6. Definition of Virtual Sputtering Source



156-026418-008

Figure 7. Coordinate Definitions for Sputtering

where ℓ and S have been normalized with respect to h ($\ell' = \ell/h$, $s' = s/h$). Here, the total evaporated mass, M_e , from the virtual source is proportional to the sputtering time t and proportional to its surface area πs^2 .

The thickness d is defined as being the ratio (dM_r/dA_r) of the mass dM_r received by the surface element dA_r divided by the density ρ of the deposit. Thus, the total mass received by the virtual substrate of diameter $D = 2s$ located at a distance h away from the virtual source is obtained by simple integration:

$$M_r = \int_0^{2\pi} \int_0^S d_0 \rho(\ell d\rho)$$

Once this integral has been calculated, the thickness t of the deposit on the wall as a function of h is given by:

$$t(h) = - \frac{1}{\pi \rho D} \frac{\partial M_r}{\partial h} \quad (2)$$

which can be calculated to give:

$$t(h) = \frac{t_s}{2} \frac{[\sqrt{1+x^2} - x]^2}{\sqrt{1+x^2}} ; \quad x = h/D \quad (3)$$

where t_s is the thickness which could have been deposited onto the actual substrate if no hole was present.

For small values of x ($h \ll D$), it follows that:

$$t(0) \approx \frac{t_s}{2} \left(1 - \frac{2h}{D}\right)$$

showing that the maximum thickness is equal to $t_s/2$. For large values of x ($h \gg D$) one obtains:

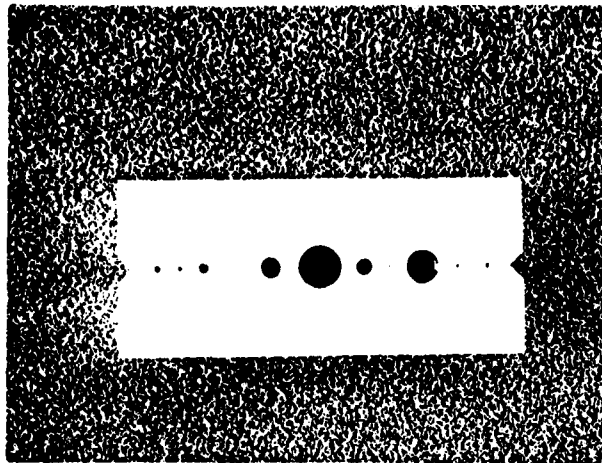
$$t(h) \approx \frac{t_s}{8} \left(\frac{D}{h}\right)^3$$

2.2.1.2 Experimental Results

Aluminum plates with a series of holes of different diameters were constructed, as shown for one example in Figure 8. The plates have a width of 1" and a length of 2.5", and have V-slots on both sides to mark the center line of the holes. After sputtering copper onto these plates, each block was sectioned down the center line, and the film thickness measured with a microscope as a function of hole depth. Simultaneously, the film thickness deposited onto the flat surface of the plate was also measured, thus determining t_s .

Figure 9 shows a typical result obtained for a sputtering time of 90 minutes, the aluminum plate thickness being .250" and the hole diameter D being the parameter. The same figure also shows the curve determined by best fitting a function (3), minimizing the square of the deviations. It is seen that the curve fits rather well at values $H/D \leq 1$, but that deviations occur at larger values of H/D . Also, the film thickness for zero depth ($H = 0$) is found by extrapolation to be 4×10^{-4} inches. From relation (3) it follows that the surface coverage should be twice this value, i.e., 8×10^{-4} inches. The measured average surface film thickness was measured to be 6.6×10^{-4} inches, which is not far from the theoretical value.

Similar results were obtained by varying the aluminum plate thickness and the sputtering time. As expected, the influence of the plate thickness was negligible, and the film thickness was proportional to the sputtering time, at least in first approximation. Figure 10 shows the amplitude $t(0) = t_s/2$ (see relation 3) as obtained from best curve fitting methods, as a function of sputtering time. The same figure also shows the thickness of the surface film as



Hole Diameters for Test Plate

<u>Hole Number</u>	<u>Hole Diameter</u>	<u>Min. Depth of Hole</u>
1	.0468	.075"
2	.0313	.050"
3	.0625	.100"
4	.0156	.025"
5	.125	.200"
6	.250	THRU
7	.0995	.160"
8	.0200	.030"
9	.1990	THRU
10	.0250	.040"
11	.0400	.065"

158-020418-007

Figure 8. Top Surface View of Aluminum Plate with Various Size Holes

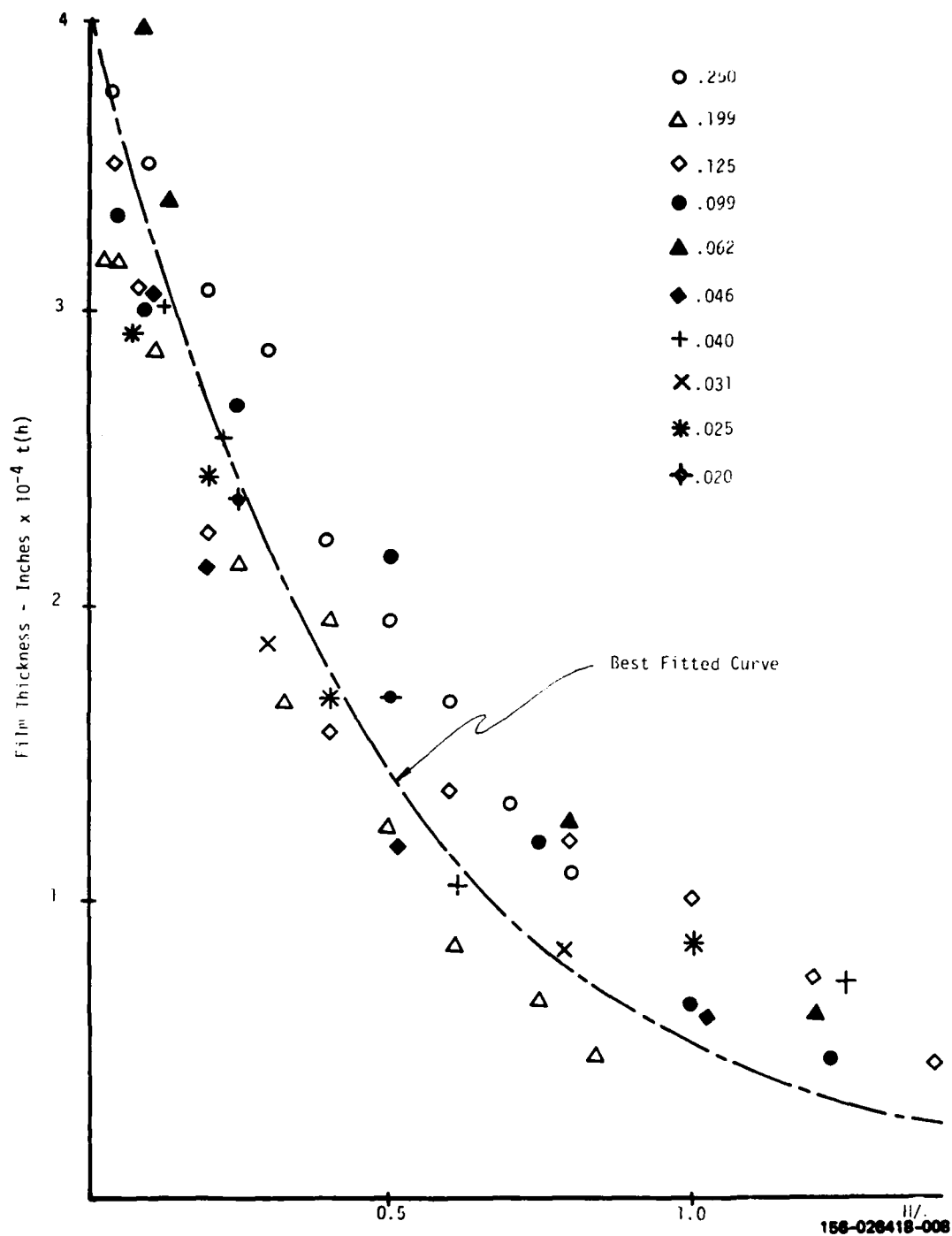


Figure 9. Measured Copper Film Thickness vs. Depth/Diameter Ratio for 90 Minute Sputtering Time with Plate .250 in thick

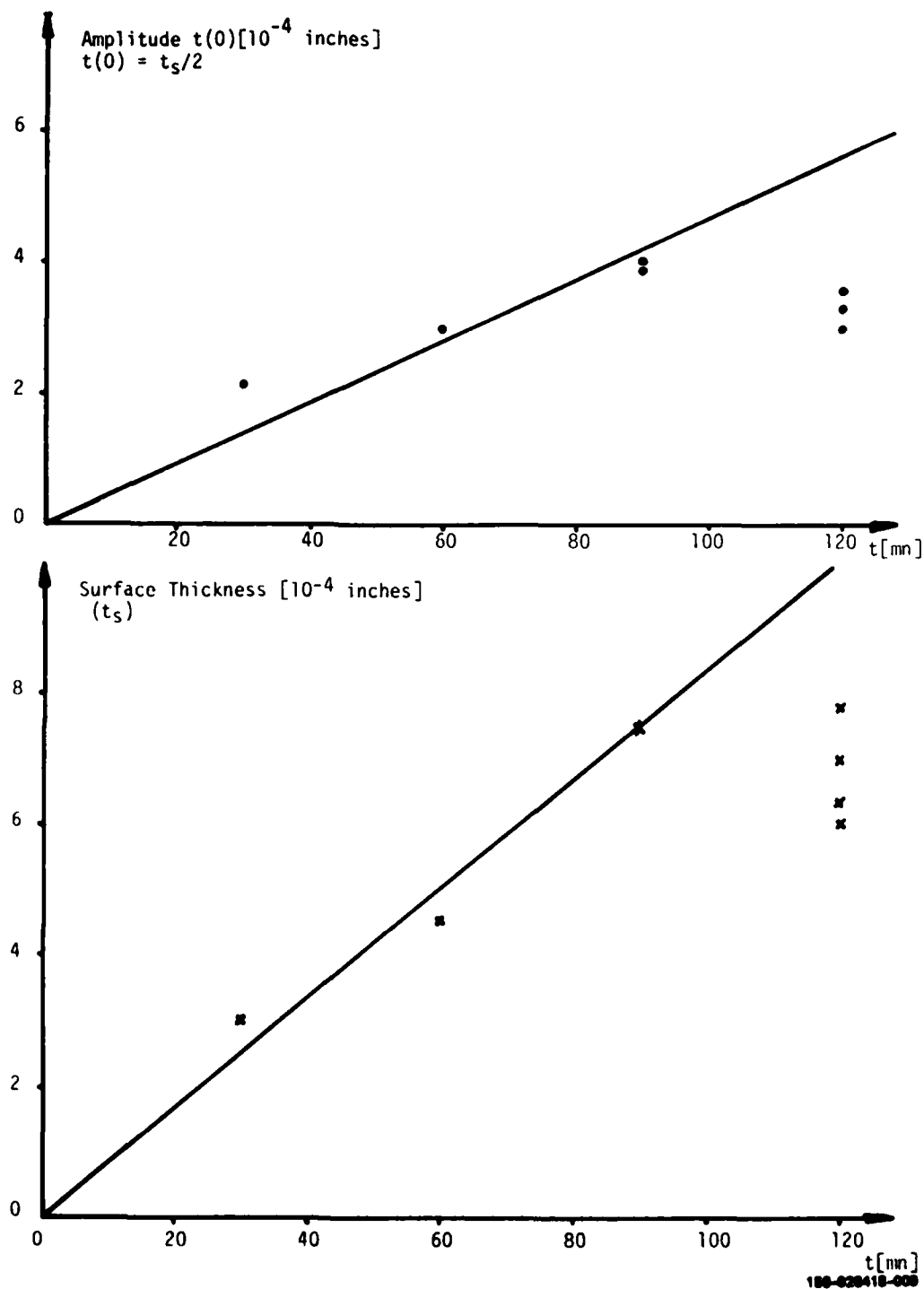


Figure 10. Amplitude $t(0) \approx t_s/2$ and Surface Film Thickness (t_s) as a Function of Sputtering Time

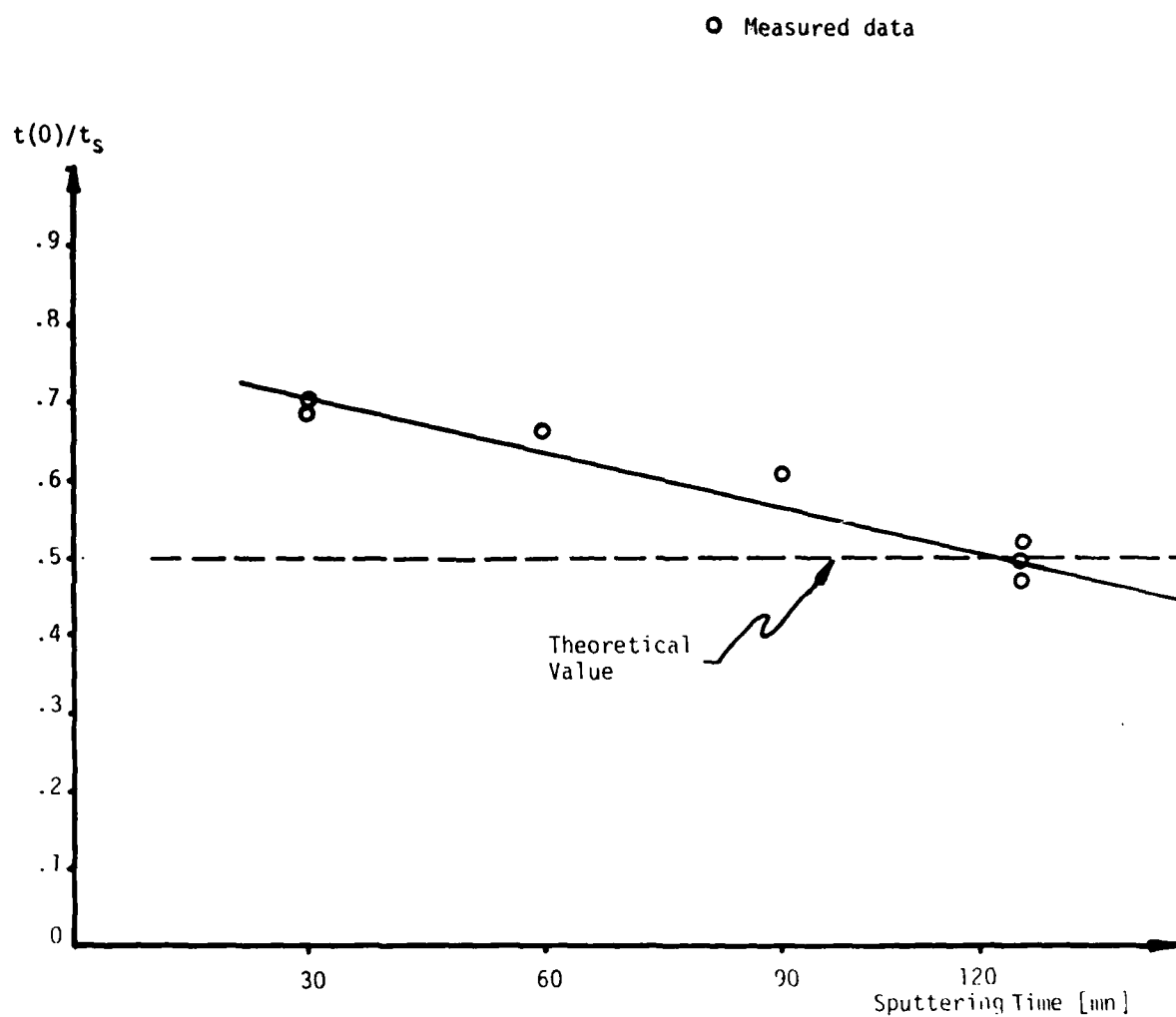
a function of sputtering time. It is not understood at this point why the data for $t = 120\text{mn}$ fall so far from the expected curve. However, within the experimental error, it is found that the sputtering rate of Cu onto the flat surface is approximately $2000\text{\AA}/\text{mn}$, while the amplitude $t(0)$, is given by the sputtering rate of $1120\text{\AA}/\text{mn}$ (about one half of the sputtering rate onto the surface). Figure 11 shows in detail the dependence $t(0)/t_s$ as a function of sputtering time.

2.2.1.3 Conclusion

A relationship giving the sputtered surface coverage on the walls of holes perpendicular to flat surfaces has been obtained theoretically and verified experimentally. Some slight discrepancies between theory and experiments at large distances from the surface are attributed to shocks between the sputtered molecules, to a variable "sticking" coefficient and to diffusion. For all practical purposes, however, relation (3) is well verified and can be used as design guideline.

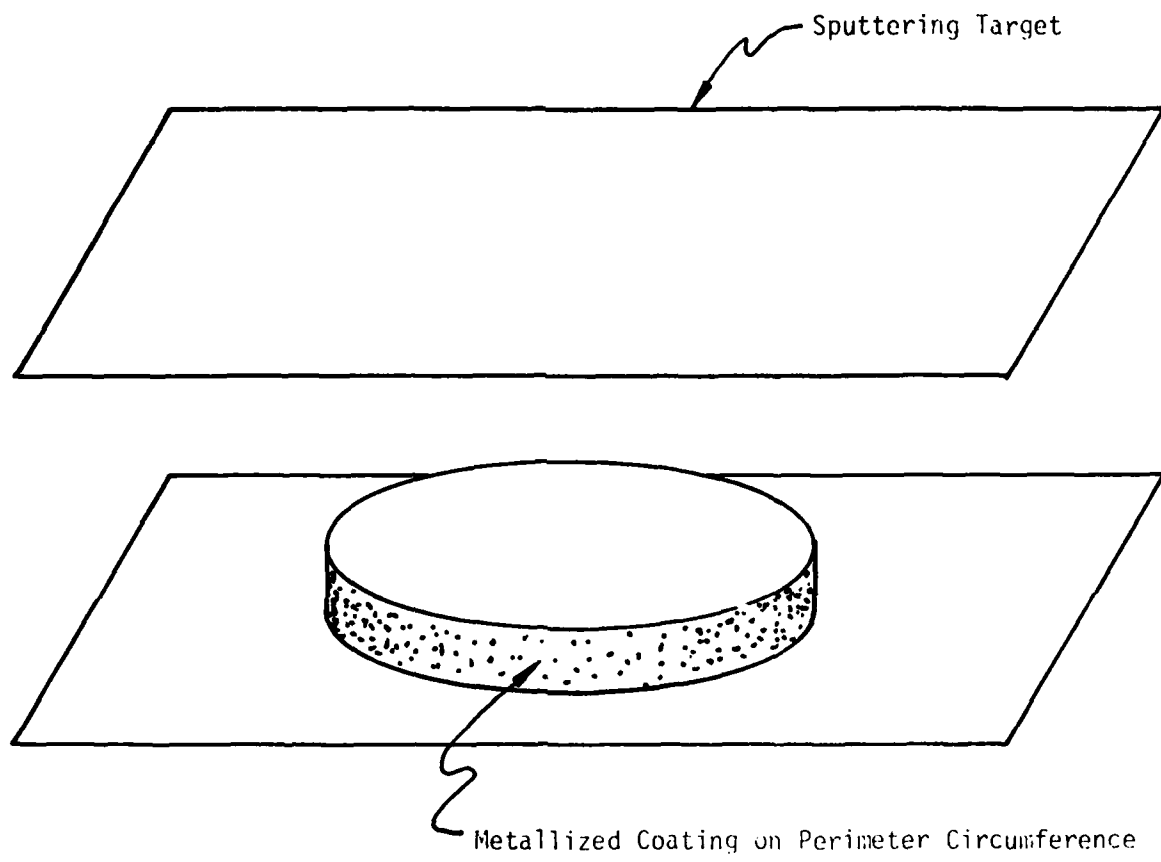
2.2.2 Sputtering on Substrate Edges

A certain number of experiments were carried out to determine the surface coverage on the sides of a flat substrate lying parallel to the target during sputtering (see Figure 12). A typical result is shown in Figure 13. where the film thickness on the edge at a certain distance from the top is plotted as a function of h . It is seen that the film thickness is approximately 40% of the surface thickness just beneath the surface ($h = 0$), and decreases to about 20% at a distance of $.060''$.



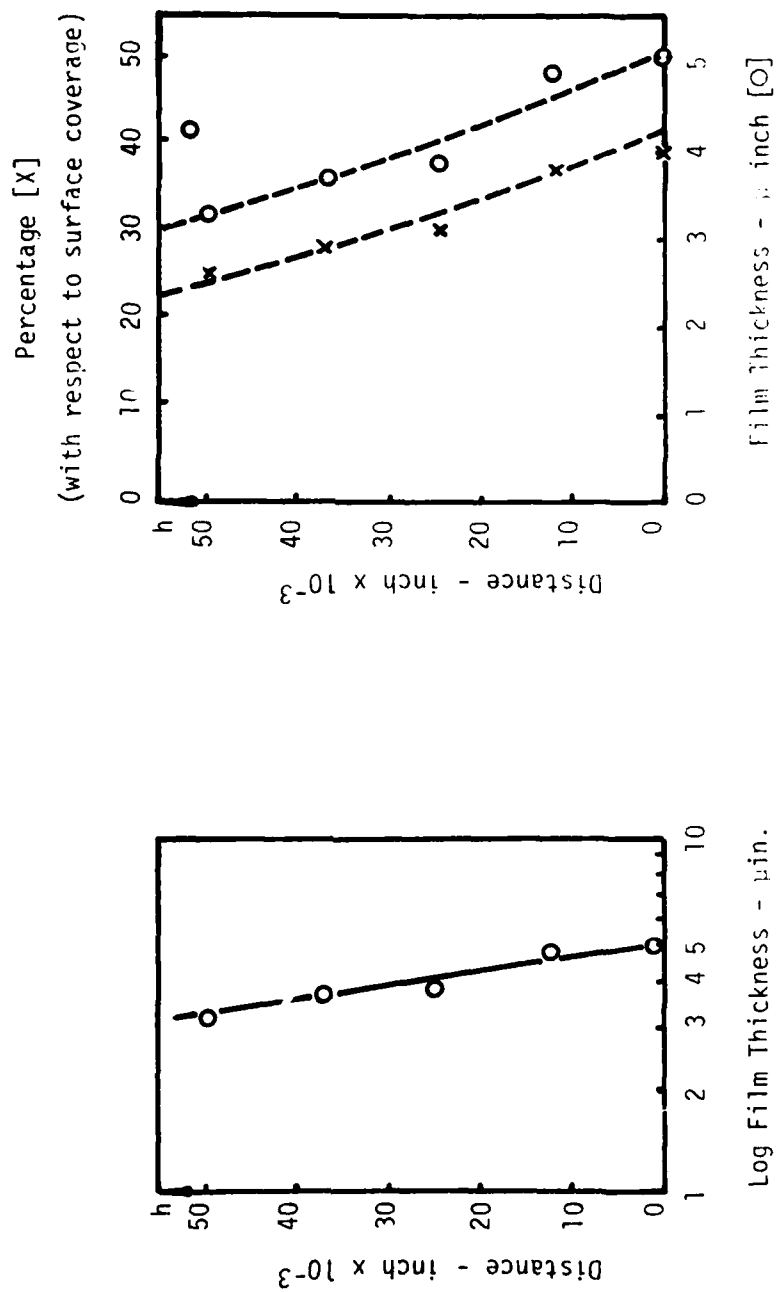
156-029418-010

Figure 11. Amplitude Ratio $t(0)/t_s$ versus Sputtering Time



158-028418-011

Figure 12. Sputtering of Round Discs



158-026418-012

Figure 13. Profile of Sputtered Layer Thickness on Sides of Round Disc.

2.2.3 Hermeticity of Circular Windows

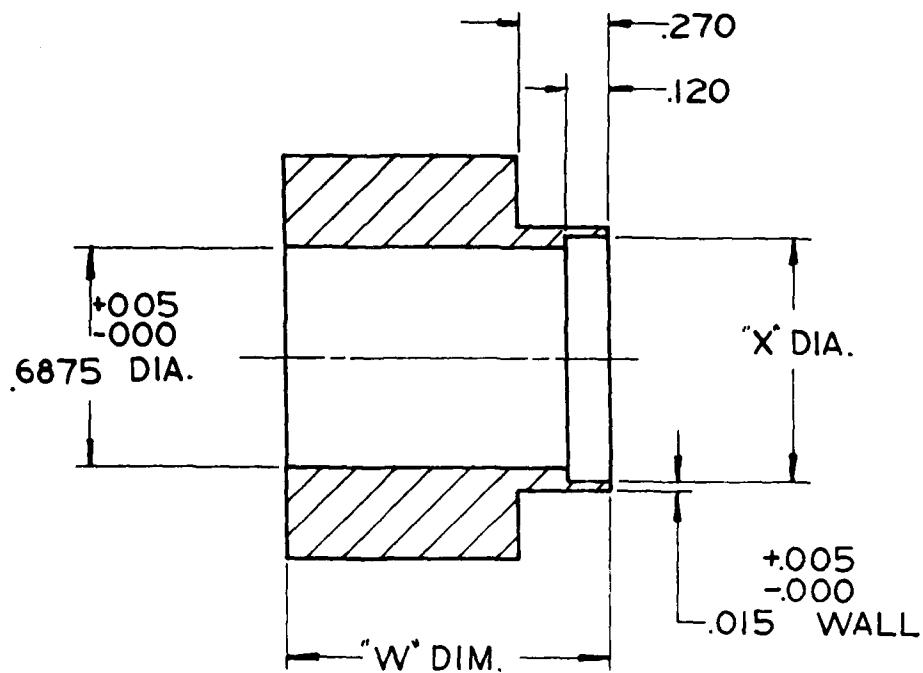
Diffusion brazes are presently used in production of high power microwave tubes. In this case, the brazing layer is under constant compression during the entire brazing cycle, thus leading to an intimate contact between ceramic and metal surface areas to be joined. These brazes have been well characterized with respect to bond strength, reliability, thermal conductivity and rf losses. However, the vacuum hermeticity of these bonds have never been checked.

The fabrication of microwave windows does not necessarily rely on brazing cycles during which the brazing layer is under constant compression, and the resulting seal must be hermetic to maintain the vacuum in the tube. It was therefore of primary importance to study the hermeticity of rf window seals by using windows of relatively large dimensions, where the thermal expansion between the components is more critical.

2.2.3.1 Test Vehicles

Figure 14 shows a cross section of the circular metal sleeve used as test vehicle to determine hermeticity, bond strength and reliability of rf window seals. The sleeve material used was mainly OFHC and Kovar, and the diameter "X" was adjusted corresponding to the O.D. of the ceramic window (and its thermal expansion) to be used. Under certain conditions, the inner surface of the sleeves were coated with nickel or copper.

Both 96% and 99% Al_2O_3 as well as BeO were used as ceramic material. The ceramic discs were metallized by either the classical moly-manganese process or by the optimized Ti-Mo-Cu sputtering technique developed previously at Northrop, adjusted for edge coating by increasing the sputtering time by roughly a factor of 3 (see Section 2.2.2). In the latter case, the flat surface of the ceramic



DASH NO	MATERIAL	"W" DIM.	"X" DIM.
- 001	OFHC COPPER	1.00 $\begin{smallmatrix} +.01 \\ -.05 \end{smallmatrix}$.752 $\begin{smallmatrix} +.001 \\ -.000 \end{smallmatrix}$
- 002	OFHC COPPER	1.25 $\begin{smallmatrix} +.01 \\ -.05 \end{smallmatrix}$.752 $\begin{smallmatrix} +.001 \\ -.000 \end{smallmatrix}$
- 003	MOLYBDENUM	1.25 $\begin{smallmatrix} +.01 \\ -.05 \end{smallmatrix}$.754 $\begin{smallmatrix} +.001 \\ -.000 \end{smallmatrix}$
- 004	KOVAR	1.25 $\begin{smallmatrix} +.01 \\ -.05 \end{smallmatrix}$.752 $\begin{smallmatrix} +.001 \\ -.000 \end{smallmatrix}$

156-026-18-013

Figure 14. Side View of Round Window Braze Sleeve

disc was lapped to remove the sputtered layer. Certain tests were conducted by slightly chamfering one edge of the ceramic side.

The samples were set vertically into the furnace, and, when liquid braze was performed, braze alloy wire ring corresponding to the ID of the sleeve was located on top of the ceramic disc.

Table 5 shows the inner diameter of the sleeves and the outer diameter of the ceramic discs used, both at room and alloy melting temperature.

2.2.3.2 OFHC Sleeves

Since the thermal expansion coefficient of copper is larger than the thermal coefficient of expansion for ceramics, a molybdenum "keeper" ring was slid onto the outer diameter of the copper sleeve, the brazing layer will be under continuous compression during the entire cooling cycle of the brazing cycle.

Table 6 shows a list of some of the results obtained, indicating the materials and brazing temperatures used in each case. In the first experiment (No. 1) no Moly "keeper" was used, allowing the copper sleeve to expand freely during the brazing cycle. Note that Sample 32 relied on a diffusion bond, indicating that the compression was not strong enough to assure hermeticity of the seal. Hermeticity was checked by using a typical helium leak detector. Note also that Sample No. 17 was brazed in a vacuum furnace and not in wet hydrogen. This procedure was recommended by Battelle*. The sample was thermal cycled 50 times and was checked to be leak tight. Undergoing a bond strength test, the ceramic cracked at 512.5 lbs with a failure stress of about 4346 lbf/in^2 . This result is significantly lower than the results obtained when samples were brazed in wet hydrogen. The high number of samples (more than 60 were prepared) was required to allow bond strength and thermal cycling testing of the seals.

*Battelle

	OD 96% Al ₂ O ₃ (inches)	OD 99.5% Al ₂ O ₃ (inches)	OD BeO (inches)	ID Cu Sleeve (inches)	ID Kovar Sleeve (inches)
T ₀	.751	.751	.751	.752	.752
T ₅₀₀	.752	.752	.7525	.754	.7535
T _{CuSi1}	.754	.755	.7541	.758	.7558
T _{35/65}	.7557	.756	.756	.760	.757
T ₀	.750	.750	.750	.753	.753
T ₅₀₀	.751	.751	.7515	.755	.7545
T _{CuSi1}	.753	.7536	.7537	.7589	.756
T _{35/65}	.7547	.755	.755	.761	.758
T ₀	.749	.749	.749	.754	.754
T ₅₀₀	.750	.750	.7505	.756	.755
T _{CuSi1}	.752	.7526	.7527	.7599	.757
T _{35/65}	.7537	.754	.754	.762	.759

Table 5. Thermal expansion of different material used for round window experiments.

Table 6. Round Disc Seals with Copper

NO.	SLEEVE MATERIAL	DISC MATERIAL	EDGE COATING	BRAZE ALLOY	WIRE DIA (.N)	BRAZE TEMP(°C)	MOLY KEEPER	VACUUM TIGHT JOINT
1	Cu	96% Al ₂ O ₃	Sputtered Ti-Mo-Cu	35-65 Au Cu	.025	1050	NO	NO
2	Cu	96% Al ₂ O ₃	Sputtered Ti-Mo-Cu	35-65 Au Cu	.025	1050	YES	Leak tight
3	Cu	99% Al ₂ O ₃	Sputtered Ti-Mo-Cu	35-65 Au Cu	.020	1050	YES	Leak tight
4	Cu	99% Al ₂ O ₃	Moly-Mang	35-65 Au Cu	.020	1050	YES	Leak tight
5	Cu	96% Al ₂ O ₃	Moly-Mang	35-65 Au Cu	.020	1050	YES	Leak tight
6	Cu	96% Al ₂ O ₃	Sputtered Ti-Mo-Cu	28-72 Cu Ag	.020	830	YES	Leak tight
7	Cu	99% Al ₂ O ₃	Sputtered Ti-MO-Cu	28-72 Cu Ag	.020	830	YES	Leak tight
8	Cu	96% Al ₂ O ₃	Moly-Mang	28-72 Cu Ag	.020	830	YES	Leak tight
9	Cu	99% Al ₂ O ₃	Moly-Mang	28-72 Cu Ag	.020	830	YES	Leak tight
10(dupl. of No.2)	Cu	96% Al ₂ O ₃	Sputtered Ti-Mo-Cu	35-65 Au Cu	.025	1050	YES	Leak tight

Table 6. Round Disc Seals with Copper (con't)

NO.	SLEEVE	DISC	SPUTTER DATE	ALLOY	SIZE OF DISC SIZE OF WIRE	TEMP.	TIME	MOLY RETAINER	REMARKS
12	Cu	Al ₂ O ₃ 96%	9/1/78	Cusil	.750 .020	830	1 min	YES	Leak tight
13	Cu	Al ₂ O ₃ 99%	9/1/78	35/65 Ni-flashed	.750 .020	1050	1 min	YES	Leak tight
14	Cu	Al ₂ O ₃ 96%	Moly Mang.	Cusil	.750 .020	830	1 min	YES	Leak tight
15	Cu	Al ₂ O ₃ 96%	9/1/78	Cusil	.749 .020	830	1 min	YES	Leak tight
16	Cu	Al ₂ O ₃ 96%	9/1/78	35/65 Ni-flashed	.750 .020	1050	1 min	YES	Leak tight
*17	Cu	Al ₂ O ₃ 96%	10/2/78	35/65 Ni-flashed	.751 .020	1050	1 min	YES	Leak tight Assembly was brazed in vacuum furnace
18	Cu	Al ₂ O ₃ 96%	Moly Mang.	Cusil	.751 .020	830	1 min	Yes	Leak tight
19	Cu	BeO 99.5%	10/2/78	Cusil	.751 .020	830	1 min	Yes	Leak tight
20	Cu	BeO 99.5%	10/2/78	35/65	.750 .020	1050	1 min	Yes	Leak tight
21	Cu	BeO 99.5%	Moly Mang.	Cusil	.750 .020	830	1 min	Yes	Leak tight

Table 6. Round Disc Seals with Copper

NO.	SLEEVE MATL	DISC	SPUTTER DATE	ALLOY	SIZE OF DISC SIZE OF WIRE	TEMP.	TIME	MOLY RETAINER	REMARKS
22	Cu	BeO	10/25/78	35/65	.750 .020	1050	1 min	YES	Leak tight
23	Cu	BeO	10/25/78	Cusi1	.750 .020	830	1 min	YES	Leak tight
27	Cu	BeO	Moly Mang	35/65	.750 .020	1050	1 min	YES	Leak tight
26	Cu	BeO	11/22/78	Cusi1	.750 .020	830	1 min	YES	Leak tight
28	Cu	BeO	Moly Mang	Cusi1	.750 .020	830	1 min	YES	Leak tight
29	Cu	BeO	Moly Mang	Cusi1	.750 .020	830	1 min	YES	Leak tight
32	Cu	Al ₂ O ₃ 99	10/2/78	Diffusion		1015	12 min	YES	Leaks
33	Cu	BeO	Moly Mang	Cusi1	.750 .020	830	1 min	YES	Leak tight
34	Cu	BeO	Moly Mang	35/65	.750 .020	1050	1 min	YES	Leak tight
35	Cu	Al ₂ O ₃ 99	Moly Mang	Diffusion	.750	1015	12 min	YES	Leaks

2.2.3.3 Kovar Sleeves

The coefficient of thermal expansion of Kovar is smaller than the thermal expansion coefficient of copper, but slightly larger than the thermal expansion coefficient of ceramics. Therefore, during the cooling process, the braze layer will be in compression.

Table 7 shows some of the results obtained with Kovar sleeves. Note that No. 17 to No. 20 were not plated and when checked for hermeticity, 2 pin hole leaks were detected. Brazing in dry hydrogen was suggested with silver-bearing filler metals, because Kovar is subject to stress corrosion and to cracking due to intergranular penetration of silver.*

2.2.3.4 Conclusion

The hermeticity of round window seals is assured if Kovar or Copper are used as outer sleeves and if proper precautions are taken related to the matching of thermal coefficients of expansion. Diffusion braze with Cu sleeves did not result in leak tight seals, at least with the diameter of ceramics used during these experiments. It is believed that diffusion bonding becomes possible at smaller window dimensions, particularly windows for mm wave application.

* Rosebury, Fred, "Handbook of Electron Tube and Vacuum Techniques", edited by Addison Wesley Publishing Company, Inc., p.334.

Table 7. Round Disc Seals with Kovar

NO.	SLEEVE	DISC	SPUTTER DATE	ALLOY	SIZE OF DISC SIZE OF WIRE	TEMP.	TIME	REMARKS
1	Kovar	99% Al ₂ O ₃	9/1/78	Cu511	.749 .020	830	1 min	Leak tight Sleeve was Ni-plated
2	Kovar	99% Al ₂ O ₃	10/2/78	35/65	.750 .020	1050	1 min	Leak tight Sleeve was Ni-plated
3	Kovar	96% Al ₂ O ₃	10/2/78	35/65	.750 .020	1050	1 min	Leaked-rebrazed and still leaked. Sleeve was Cu-plated
4	Kovar	96% Al ₂ O ₃	10/2/78	Cu511	.750 .020	830	1 min	Leak tight Sleeve was Cu-plated
5	Kovar	96% Al ₂ O ₃	10/2/78	35/65	.750 .020	1050	1 min	Leak tight Sleeve was Cu-plated
6	Kovar	96% Al ₂ O ₃	Moly Mang.	Cu511	.750 .020	830	1 min	Leak tight Sleeve was Cu-plated
7	Kovar	96% Al ₂ O ₃	Moly Mang.	35/65	.020	1050	1 min	Leak tight Sleeve was Ni-plated
8	Kovar	99% BeO	Sputtered Ti-Mo-Cu	Cu511	(.750) .020	830	1 min	Leak tight Sleeve was Ni-plated
9	Kovar	99% BeO	Sputtered Ti-Mo-Cu	35/65	(.750) .020	1050	1 min	Leak tight Sleeve was Ni-plated

Table 7. Round Disc Seals with Kovar (con't)

NO.	SLEEVE	DISC	SPUTTER DATE	ALLOY	SIZE OF DISC SIZE OF WIRE	TEMP.	TIME	REMARKS
10	Kovar	99% BeO	Sputtered Ti-Mo-Cu	CuSi1	.750 .020	830	1 min	Leak tight Sleeve was Cu-plated
11	Kovar	99% BeO	Sputtered Ti-Mo-Cu	35/65	.750 .020	1050	1 min	Leak tight Sleeve was Cu-plated
12	Kovar	99% Al ₂ O ₃	Sputtered Ti-Mo-Cu	CuSi1	.750 .020	830	1 min	Leak tight Sleeve was Cu-plated
13	Kovar	99% Al ₂ O ₃	Moly Mang.	CuSi1	.750 .020	830	1 min	Leak tight Sleeve was Cu-plated
14	Kovar	99% BeO	Moly Mang.	CuSi1	.750 .020	830	1 min	Leak tight Sleeve was Cu-plated
15	Kovar	99% BeO	Moly Mang.	35/65	.750 .020	1050	1 min	Leak tight Sleeve was Cu-plated
16	Kovar	99% BeO	Moly Mang.	CuSi1	.750 .020	830	1 min	Leak tight Sleeve was Ni-plated
17	Kovar	99% BeO	Sputtered Ti-Mo-Cu	Copper	.750 .020	1150	1 min	Leaks Sleeve was not plated
18	Kovar	99% BeO	Sputtered Ti-Mo-Cu	CuSi1	.750 .020	830	1 min	Leaks No plating
19	Kovar	99% BeO	Moly Mang.	CuSi1	.750 .020	830	1 min	Leaks No plating
20	Kovar	99% BeO	Moly Mang.	CuSi1	.750 .020	830	1 min	2 pin hole leaks No plating

Table 7. Round Disc Seals with Kovar (con't)

NO.	SLEEVE	DISC	SPUTTER DATE	ALLOY	SIZE OF DISC SIZE OF WIRE	TEMP.	TIME	REMARKS
21	Kovar	94% Al ₂ O ₃	Sputtered	Copper	.751 .020	1150	1 min	2 pin hole leaks No plating
22	Kovar	94% Al ₂ O ₃	Sputtered	Copper	.751 .020	1150	1 min	Leak tight No plating Braze in dry H ₂
23	Kovar	99% BeO	Moly Mang.	CuSi1	.750 .020	830	1 min	Leak tight Braze in dry H ₂
24	Kovar	99% BeO	Moly Mang.	CuSi1	.750 .020	530	1 min	Leak tight Braze in dry H ₂

2.2.4 Reliability and Tensile Strength

2.2.4.1 Reliability

To measure the reliability of round disc seals, samples were thermal cycled between room temperature and 500°C in wet hydrogen, leaving the samples ten minutes at each extreme temperature.

a) Cu-Sleeves

Results obtained with copper sleeves are shown in Table 8. The samples metallized by sputtering a Ti-Mo-Cu composite layer and brazed with Cusil exhibited leaks after 10 thermal cycles. All other samples were leak tight after 10 and 25 thermal cycles.

Those samples prepared by sputtering the Ti-Mo-Cu composite layer and brazed with 35Au/65Cu also exhibited leaks after 50 thermal cycles. All other samples were still leak tight, especially those prepared with the classical Moly manganese metallization process.

b) Kovar Sleeves

The results obtained with Kovar sleeves are shown in Table 9. All samples tested up to 50 thermal cycles remained leak tight, with either alumina or BeO as ceramic disc material.

2.2.4.2 Tensile Strength

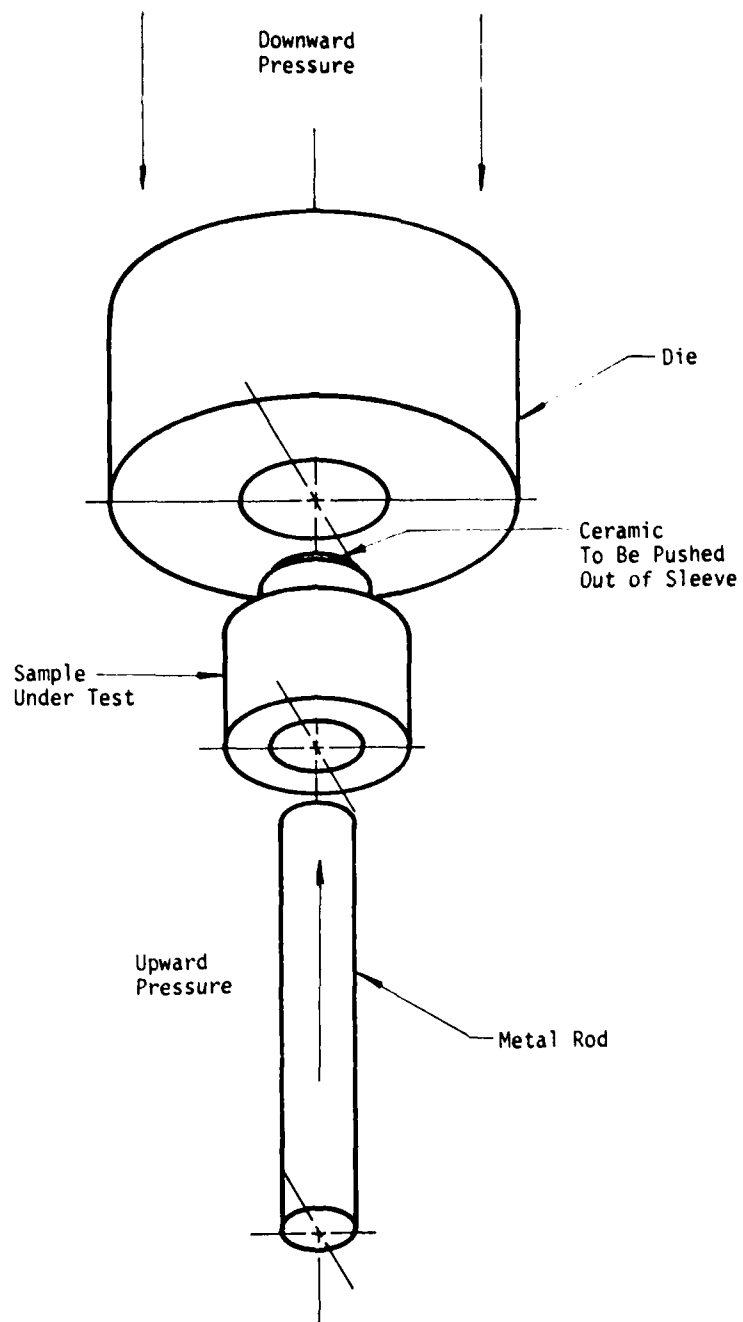
Brazed assemblies were mechanically tested after 50 thermal cyclings to examine the bond strength of the braze joint. Each assembly was placed in a die, then a ground rod was inserted inside the braze assembly (see Figure 15) and the load required to cause failure was recorded. Results obtained with the copper sleeves are shown in Table 10. Results obtained with the Kovar sleeves are given in Table 11. In all the assemblies examined the fracture location occurred in the ceramic disc and not at the brazed joint as shown typically in Figure 16.

Table 8. Thermal Cycling Effect On Copper Sleeves

NO.	SLEEVE MATERIAL	DIS MATERIAL	EDGE COATING	BRAZE ALLOY	VACUUM TIGHT JOINT	AFTER 10 CYCLES	AFTER 25 CYCLES	AFTER 50 CYCLES
1	Cu	96% Al ₂ O ₃	SPUTTERED Ti-Mo-Cu	35-65	NO			
2	Cu	96% Al ₂ O ₃	SPUTTERED Ti-Mo-Cu	35-65	YES			
3	Cu	99% Al ₂ O ₃	SPUTTERED Ti-Mo-Cu	35-65	YES	YES	YES	YES
4	Cu	99% Al ₂ O ₃	Moly-Mang	35-65	YES	YES	YES	YES
5	Cu	96% Al ₂ O ₃	Moly-Mang	35-65	YES	YES	YES	YES
6	Cu	96% Al ₂ O ₃	SPUTTERED Ti-Mo-Cu	CuSi1	YES	NO	NO	NO
7	Cu	99% Al ₂ O ₃	SPUTTERED Ti-Mo-Cu	CuSi1	YES	NO	NO	NO
8	Cu	96% Al ₂ O ₃	Moly-Mang	CuSi1	YES	YES	YES	YES
9	Cu	99% Al ₂ O ₃	Moly-Mang	CuSi1	YES	YES	YES	YES
10	Cu	96% Al ₂ O ₃	SPUTTERED Ti-Mo-Cu	35-65	YES	YES	YES	NO
19	Cu	BeO	SPUTTERED	CuSi1	YES	NO	NO	NO
20	Cu	BeO	SPUTTERED	35/65	YES	YES	YES	NO
21	Cu	BeO	Mo-Mn	CuSi1	YES	YES	YES	YES

Table 9. Thermal Cycling Effect on Kovar Sleeves

NO.	SLEEVE MATERIAL	DISC MATERIAL	EDGE COATING	BRAZE ALLOY	VACUUM TIGHT JOINT	AFTER 10 CYCLES	AFTER 26 CYCLES	AFTER 50 CYCLES
1	Kovar	99% Al ₂ O ₃	Sputtering	Cusil	YES	YES	YES	YES
2	Kovar	99% Al ₂ O ₃	Sputtering	35/65	YES	YES	YES	YES
4	Kovar	96% Al ₂ O ₃	Sputtering	Cusil	YES	YES	YES	YES
5	Kovar	96% Al ₂ O ₃	Sputtering	35/65	YES	YES	YES	NO
6	Kovar	96% Al ₂ O ₃	Moly-Mang.	Cusil	YES	YES	YES	YES
7	Kovar	96% Al ₂ O ₃	Moly-Mang.	35/65	YES	YES	YES	YES
	Cu	96% Al ₂ O ₃	Sputtering	35/65	YES	YES	YES	YES
8	Kovar	BeO	Sputtered Ti-Mo-Cu	Cusil	YES	YES	YES	YES
9	Kovar	BeO	Sputtered Ti-Mo-Cu	35/65	YES	YES	YES	YES
15	Kovar	BeO	Moly-Mang.	35/65	YES	YES	YES	YES
16	Kovar	BeO	Moly-Mang.	Cusil	YES	YES	YES	YES



155-020418-014

Figure 15. Bond Strength Test on Round Waveguide Windows

Table 10. Bond Strength Test on Copper Sleeves

NO.	SLEEVE MATERIAL	DISC MATERIAL & EDGE COATING	BRAZE ALLOY	MOLY KEEPER	THERMAL CYCLING	MAXIMUM LOAD (lbf/in ²)	FAILURE MODE & LOCATION
1	Cu	Al ₂ O ₃ Sputtered Ti-Mo-Cu	35/65	NO	50 cycles	1207.6 1500	Ceramic disc fracture at first load & bond failed at second
2	Cu	Al ₂ O ₃ Sputtered Ti-Mo-Cu	35/65	YES	No cycling	5084	Fractured ceramic disc
3	Cu	Al ₂ O ₃ Sputtered Ti-Mo-Cu	35/65	YES	50 cycles	2593	Fractured ceramic disc
5	Cu	Al ₂ O ₃ Moly-Mang.	35/65	YES	50 cycles	5094	Fractured ceramic disc
8	Cu	Al ₂ O ₃ Moly-Mang.	Cusil	YES	50 cycles	6779.6	Fractured ceramic disc
9	Cu	Al ₂ O ₃ Moly-Mang.	Cusil	YES	50 cycles	4220	Fractured ceramic disc
22	Cu	BeO Sputtered Ti-Mo-Cu	35/65	YES	No cycling	5084	Fractured ceramic disc
29	Cu	BeO Sputtered Ti-Mo-Cu	Cusil	YES	No cycling	3389	Fractured ceramic disc
33	Cu	BeO Sputtered Ti-Mo-Cu	Cusil	YES	No cycling	3215	Fractured ceramic disc

Table 10. Bond Strength Test on Copper Sleeves (continued)

NO.	SLEEVE MATERIAL	DISC MATERIAL & EDGE COATING	BRAZE ALLOY	MOLY KEEPER	THERMAL CYCLING	MAXIMUM LOAD (lbf/in ²)	FAILURE MODE & LOCATION
34	Cu	BeO Moly-Mang.	35/65	YES	No cycling	4237.	Fractured ceramic disc
36	Cu	BeO Sputtered Ti-Mo-Cu	Cu511	YES	No cycling	4237.	Fractured ceramic disc
37	Cu	BeO Sputtered Ti-Mo-Cu	35/65	YES	No cycling	3815	Fractured ceramic disc

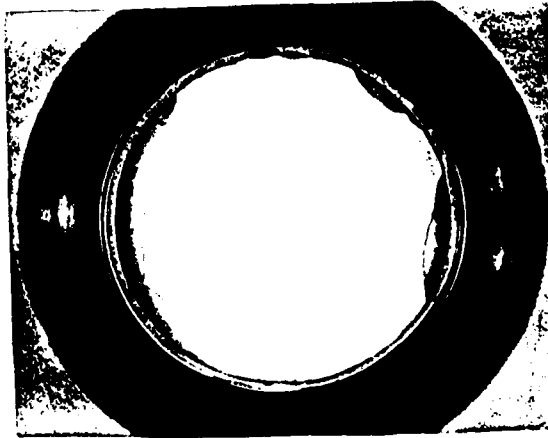
Table 11. Bond Strength Test on Kovar Sleeves

NO.	SLEEVE MATERIAL	DISC MATERIAL & EDGE COATING	BRAZE ALLOY	THERMAL CYCLING	MAXIMUM LOAD (lb _f /in ²)	FAILURE MODE/ LOCATION
1	Kovar	Al ₂ O ₃ Sputtered Ti-Mo-Cu	Cu51	50 cycles	6631	Fractured ceramic disc
2	Kovar	Al ₂ O ₃ Sputtered Ti-Mo-Cu	35/65	50 cycles	8114	Fracture in ceramic and bond
4	Kovar	Al ₂ O ₃ Sputtered Ti-Mo-Cu	Cu51	50 cycles	9195	Fracture in ceramic and bond
5	Kovar	Al ₂ O ₃ Sputtered Ti-Mo-Cu	35/65	50 cycles	9691	Fracture in ceramic and bond
6	Kovar	Al ₂ O ₃ Moly-Mang.	Cu51	50 cycles	7669	Fracture in ceramic and bond
7	Kovar	Al ₂ O ₃ Moly-Mang.	35/65	50 cycles	4873 5403	Fracture cracked at first load & bond failed at second
8	Kovar	BeO Sputtered Ti-Mo-Cu	Cu51	50 cycles	8474	Fractured ceramic
9	Kovar	BeO Sputtered Ti-Mo-Cu	35/65	50 cycles	9322	Fractured ceramic

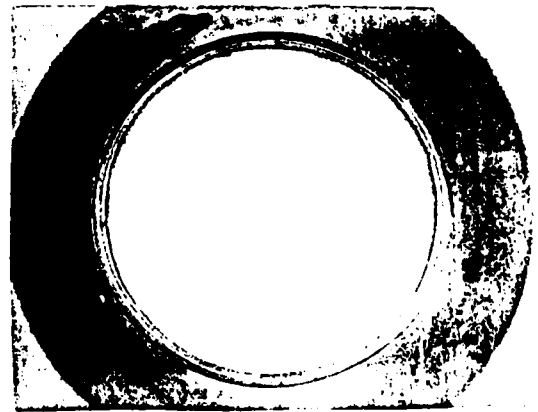
Table 11. Bond Strength Test on Kovar Sleeves (continued)

NO.	SLEEVE MATERIAL	DISC MATERIAL & EDGE COATING	EPAZE ALLOY	THERMAL CYCLING	MAXIMUM LOAD (lbf/in ²)	FAILURE MODE/ LOCATION
15	Kovar	BeO Moly-Mang.	35/65	50 cycles	11,864	Fractured ceramic
16	Kovar	BeO Moly-Mang.	Cusil	50 cycles	8,051	Fractured ceramic
17	Kovar	Al ₂ O ₃ Sputtered Ti-Mo-Cu	Copper	No cycling	8,474	Fractured ceramic
22	Kovar	Al ₂ O ₃ Sputtered Ti-Mo-Cu	Copper	No cycling	9,322	Fractured ceramic
23	Kovar	BeO Moly-Mang.	Cusil	No cycling	8,474	Fractured ceramic
24	Kovar	BeO Sputtered Ti-Mo-Cu	Cusil	No cycling	5,034	Fractured ceramic

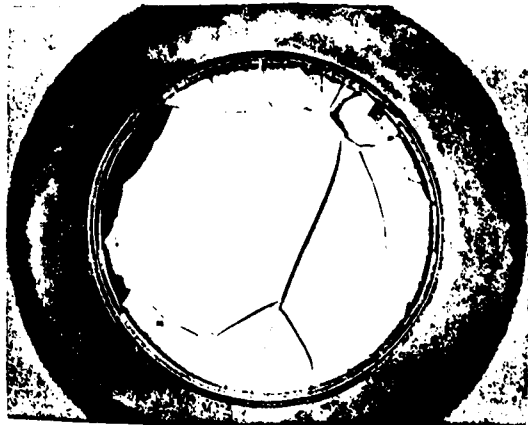
Sample No. 1



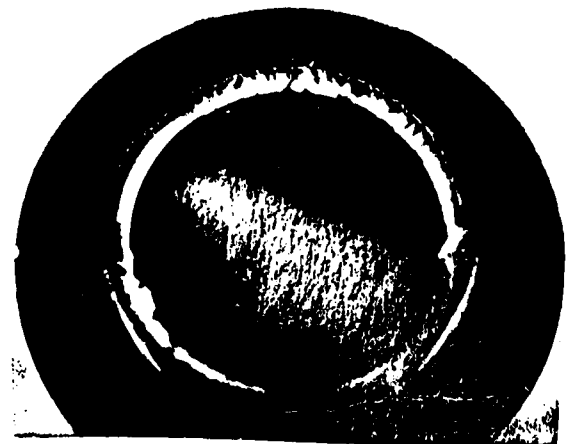
Sample No. 4



Sample No. 6



Sample No. 7



156-020418-015

Figure 16. Illustration of Round Window Sleeves After Bond Strength Test.

As reference, Tables 10 and 11 show the maximum strength observed on samples which were not subjected to thermal cycling. (It is seen that no difference between the results obtained before and after thermal cycling exists, strongly indicating that failure occurs in the ceramic and not at the braze joint).

2.2.5 Cross Sectional Analysis

In an attempt to determine the cause of failure of round disc windows, particularly those fabricated with Cusil, microprobe analysis of cross sectional areas were made, before and after thermal cycling. No direct correlation between failure mode and microprobe analysis could be found. In certain cases, failure could be attributed to a non-homogeneous coverage of the ceramic, as shown for example, in Figure 17, for sample #6. Clearly seen in the pictures are the interruptions in the coatings (this sample failed after 10 temperature cycles, and the micrographs were taken after 50 cycles). As reference, Figure 18, shows the micrograph of sample 19 after brazing. Here also, the interruption in the coverage is detectable. It was therefore concluded that the failure of cusil brazed windows with copper sleeves is only due to the mechanical problems associated with the thermal expansion coefficients of the materials. This is substantiated by the observation that cusil brazed windows with Kovar sleeves are much more reliable. However, the problem of non-uniform coverage remains to be solved, and may remain a problem for reproducible sputtering of coupons in production.

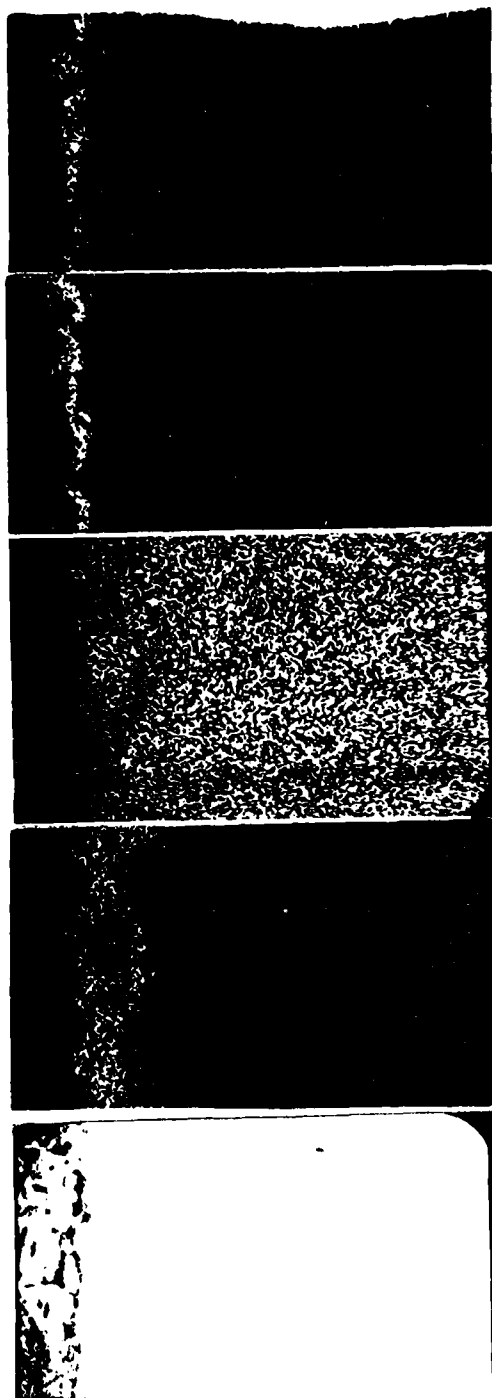
It is interesting to note that cusil brazes exhibit islands of copper in the bonding layer, see Figures 17 and 18. This can be explained by considering the phase diagram shown in Figure 19. During the brazing cycle,

the temperature is raised above the melting point of the copper silver alloy (about 30-50°C). At the brazing temperature, copper from the walls or from the ceramic metallizing is dissolved into the liquid, and the concentration of Cu increases in the melt, as indicated by the arrow in Figure 19. During the cooling cycle, therefore, a range of temperatures exist in which Cu will precipitate from the liquid phase and form the observed islands.

2.2.6 Conclusion

From the data obtained while testing round disc windows of .750" diameter, the following conclusions were drawn:

- 1) Both Cu and Kovar sleeves can be used for brazing windows with either the sputtering or moly-manganese metallization technique. Preference, however, should be given to Kovar, since slightly higher tensile strength was obtained with Kovar, although fracture always occurred in the ceramic.
- 2) Kovar sleeves are more reliable than copper sleeves, which failed after maximally 25 thermal cycles.
- 3) Moly-manganese and composite layer sputtering are equivalent in bond strength and reliability when Kovar sleeves are used. Ni and Cu plating of the Kovar sleeves improves metal wetting and reliability.
- 4) diffusion braze leads to leaky seals when Cu-sleeves are used.



Sample No. 6

Distribution of Ti layer

X1200

Distribution of Mo layer

X1200

Distribution of Cu layer

X1200

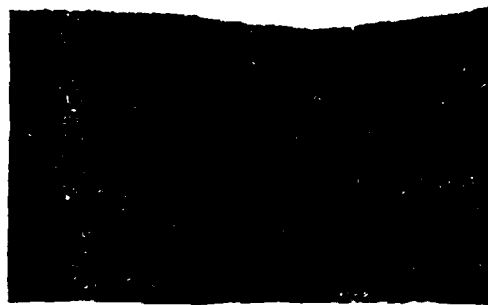
Distribution of Ag layer

X1200

SEM

166-028418-018

Figure 17. Electron Microprobe on Sputtered Film Morphology of Sample No. 6 After 50 Thermal Cycles.

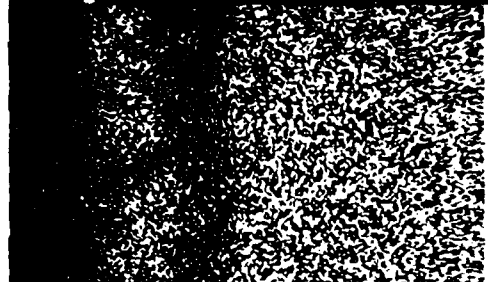


Sample No. 19

Distribution of titanium layer X1200



Distribution of Moly layer X1200



Distribution of Cu layer X1200



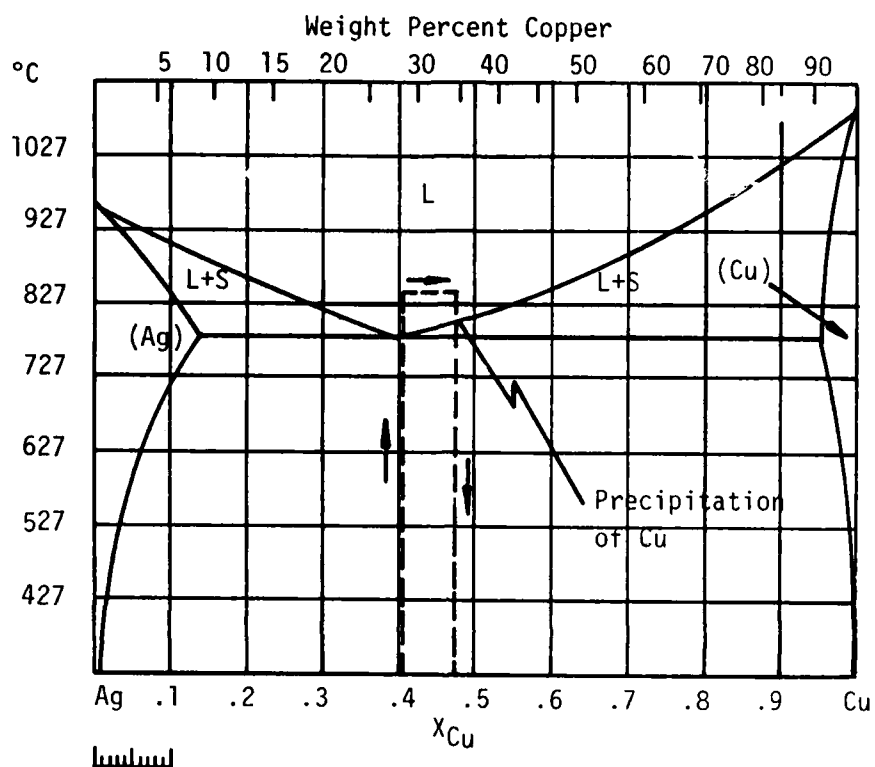
Distribution of Ag layer X1200



SEM

155-026418-017

Figure 18. Electron Microprobe on Sputtered Film Morphology of Sample No. 19, After Brazing.



158-028418-018

Figure 19. Phase Diagram of Silver-Copper (after Heltgren, Desai, Hawkins, Gleiser, Kelly, "Selected Values of the Thermodynamic Properties of Binary Alloys", American Society for Metals, pg. 46)

2.3 Coaxial Windows

2.3.1 Fabrication of Coaxial Windows

A test vehicle as shown in Figure 20 was used for assembling and brazing coaxial windows. The ceramic material used was alumina and the ID and the OD of the ceramic were .052" and .327" respectively. The ID/OD ratio was chosen so that approximately 50 ohm coax transmission impedance is obtained, and corresponds to dimensions actually used in the development of the traveling wave tubes at Northrop Electron Tubes. Some ceramics were chamfered before metallization.

The materials used for the center pin were molybdenum and copper. The materials used for the sleeves were copper, cupro-nickel and Kovar. Sixteen samples were brazed with cusil alloy and 50Au/50Cu. Table 12 shows the results obtained. The first four samples in the table were sputtered and Ni flashed. As shown in Table 12 leak tight joints were obtained in all samples, except No.6 which leaked possibly due to contamination.

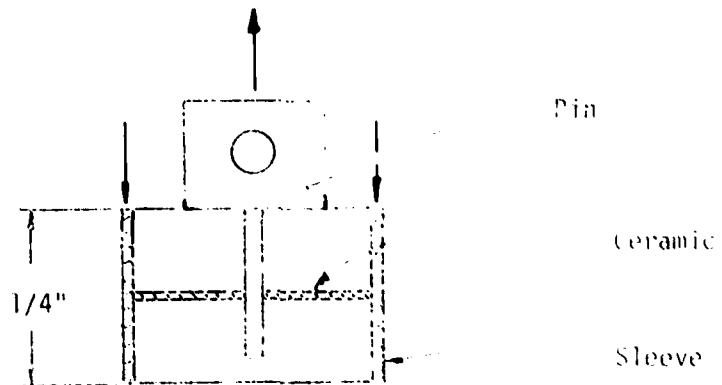
2.3.2 Reliability and Thermal Cycle Effect on Coaxial Windows

Brazed coaxial windows were thermal cycled between room temperature and 500°C for 10 minutes at each extreme to check for the reliability of the brazed joint after heat treatment.

After 10 thermal cycles, braze assemblies No. 1, 3, 6 and 8 were checked and found to be leaking, while the rest of the samples were leak tight. (See Table 13) The explanation here is that Samples No.1, 3 and 8 were brazed with a copper center pin. According to the Handbook of Thin Film Technology*, feedthroughs of the type where a metal rod is used at the center is only possible if the thickness or diameter of the metal rod does not exceed .040". The thermal expansion of the ceramic should be greater than that of the metal used at the center,

* Maissel & Glaug, Thin Film Technology, McGraw-Hill, 1970, p.2-76.

Pin Pulled Out



	OD	ID	Thickness
Ceramic:	.327"	.052"	.040"
Pin:	Mo: .051" Dia		
	Cu: .050" Dia		
Sleeve:	Cu: ID: .330"	OD: .360"	
	Copper Nickel ID: .330"	OD: .360"	
	Kovar ID: .330"	OD: .360"	

158-026418-019

Figure 20. Coax Pin Braze Assembly

Table 12. Coaxial Window Seals

NO.	SLEEVE	PIN	CERAMIC	ALLOY	SIZE OF WIRE	TEMP	TIME	REMARKS
1	Cu	Cu	Al ₂ O ₃ Sputtered	CuSi1	.020	830	1 min	Leak tight
2	Cu	Mo	Al ₂ O ₃ Sputtered	CuSi1	.015	830	1 min	Leak tight
3	Cu+Ni	Cu	Al ₂ O ₃ Sputtered	CuSi1	.015	830	1 min	Leak tight
4	Cu+Ni	Mo	Al ₂ O ₃ Sputtered	CuSi1	.015	830	1 min	Leak tight
5	Cu+Ni	Mo	Al ₂ O ₃ Moly-Mang	CuSi1	.015	330	1 min	Leak tight
6	Cu	Mo	Al ₂ O ₃ Moly-Mang.	CuSi1	.015	830	1 min	Leaks
7	Kovar	Moly	Al ₂ O ₃ Moly-Mang	50/50	.015	1000	1 min	Leak tight

Table 12. Coaxial Window Seals (continued)

NO.	SLEEVE	PIN	CERAMIC	ALLOY	SIZE OF WIRE	TEMP	TIME	REMARKS
8	Cu+Ni	Cu	Al ₂ O ₃ Mo17-Mang.	Cusil	.015"	830	1 min	Leak tight
9	Kovar	Mo	Al ₂ O ₃ Sputtered	Cusil	.015"	830	1 min	Leak tight
10	Cu+Ni	Mo	Al ₂ O ₃ Sputtered	Cusil	.015"	830	1 min	Leak tight
11	Cu	Mo	Al ₂ O ₃ Sputtered	Cusil	.015"	830	1 min	Leak tight
12	Kovar	Mo	Al ₂ O ₃ Sputtered	50/50	.015"	1000	1 min	Leak tight
13	Cu	Cu	Al ₂ O ₃ Sputtered	Cusil	.015"	830	1 min	Leak tight
14	Cu	Cu	Al ₂ O ₃ Sputtered	Cusil	.015"	830	1 min	Leak tight
15	Cu	Cu	Al ₂ O ₃ Mo17-Mang.	Cusil	.015"	830	1 min	Leak tight
16	Cu	Cu	Al ₂ O ₃ Sputtered	Cusil	.015"	830	1 min	Leak tight

Table 13. Thermal Cycling of Coaxial Windows

NO.	SLEEVE MAT'L	CENTER PIN MAT'L	CERAMIC MAT'L & EDGE COATING	ALLOY & SIZE OF WIRE	TIME & TEMP. FURNACE	Vacuum Tight Joint		
						No.	10	25
						Cy	Cy	Cy
1	Cu	Cu	Al ₂ O ₃ Sputtered Ni-plated	Cusil .015"	1 min 830°C	Leak tight	No	No
2	Cu	Mo	Al ₂ O ₃ Sputtered Ni-plated	Cusil .015"	1 min 83 °C	Leak tight	Yes	Yes
3	Cu	Cu	Al ₂ O ₃ Sputtered Ni-plated	Cusil .015"	1 min 830°C	Leak tight	No	No
4	Cu+Ni	Mo	Al ₂ O ₃ Sputtered Ni-plated	Cusil .015"	1 min 830°C	Leak tight	Yes	Yes
5	Cu+Ni	Mo	Al ₂ O ₃ Moly-Mang.	Cusil .015"	1 min 830°C	Leak tight	Yes	Yes
6	Cu	Mo	Al ₂ O ₃ Moly-Mang.	Cusil .015"	1 min 830°C	Leak tight	No	No
7	Kovar	Mo	Al ₂ O ₃ Moly-Mang.	50/50 .015"	1 min 1000°C	Leak tight	Yes	Yes
8	Cu+Ni	Cu	Al ₂ O ₃ Moly-Mang.	Cusil .015"	1 min 830°C	Leak tight	No	No
9	Kovar	Mo	Al ₂ O ₃ Sputtered	Cusil .015"	1 min 830°C	Leak tight	Yes	Yes

Table 13. Thermal Cycling of Coaxial Windows (con't)

NO.	SLEEVE MAT'L	CENTER PIN MAT'L	CERAMIC MAT'L & EDGE COATING	ALLOY & SIZE OF WIRE	TIME & TEMP. IN FURNACE	Vacuum Tight Joint				
						No	10	25	50	Cy.
10	Cu+Ni	Mo	Al ₂ O ₃ Sputtered	CuSi1 .015"	1 min 830°C	Leak tight	Yes	Yes	No	50 Cy.
11	Cu	Mo	Al ₂ O ₃ Sputtered	CuSi1 .015"	1 min 830°C	Leak tight	Yes	Yes	No	
12	Kovar	Mo	Al ₂ O ₃ Sputtered	50/50 .015"	1 min 1000°C	Leak tight	Yes	Yes	No	

which is not the case. Brazed assemblies with Molybdenum center pins were further thermal cycled. After 25 and 50 cycles, they were all leak tight.

2.3.3 Bond Strength Test on Coaxial Windows

After thermal cycling, a pull test as shown in Figure 20 was performed on coaxial windows to examine the tensile strength. From the results obtained, Table 14 clearly shows that moly center pins should be used with both the moly-manganese and the sputtering metallization.

Kovar and cupronickel sleeves can be used. Tensile strengths obtained are higher. Higher tensile strength is obtained when the ceramic is not chamfered before metalization and not Ni-plated after metallization.

2.3.4 Conclusion

Reliable and vacuum tight coaxial windows can be obtained if moly is used as a center pin and Cupronickel or Kovar used as outside sleeves. The thermal expansion coefficients are matched when using the above mentioned metals when 94% alumina ceramics are used, but special attention should be given to dimensions. Both the sputtering and the moly-manganese metallization produce comparable tensile strengths.

Table 14. Bond Strength Test on Coaxial Windows

NO.	SLEEVE MATERIAL	CENTER PIN MATERIAL	ALLOY	TIME & TEMP. IN FURNACE	MAXIMUM LOAD AT CENTER PIN (lb_f/in^2)
1	Cu	Cu	CuSi1	1 min/830°C	7,692
2	Cu	Mo	CuSi1	1 min/830°C	8,615
3	Cupro-Nickel	Cu	CuSi1	1 min/830°C	9,538
4	Cupro-Nickel	Mo	CuSi1	1 min/830°C	10,600
5	Cupro-Nickel	Mo	CuSi1	1 min/830°C	12,615
6	Cu	Mo	CuSi1	1 min/830°C	8,462
7	Yovar	Mo	50Au/50Cu	1 min/1000°C	13,846
8	Cupro-Nickel	Cu	CuSi1	1 min/830°C	8,462
9	Yovar	Mo	CuSi1	1 min/830°C	13,538
10	Cupro-Nickel	Mo	CuSi1	1 min/830°C	15,246
11	Cu	Mo	CuSi1	1 min/830°C	6,154
12	Yovar	Mo	50Au/50Cu	1 min/1000°C	10,246

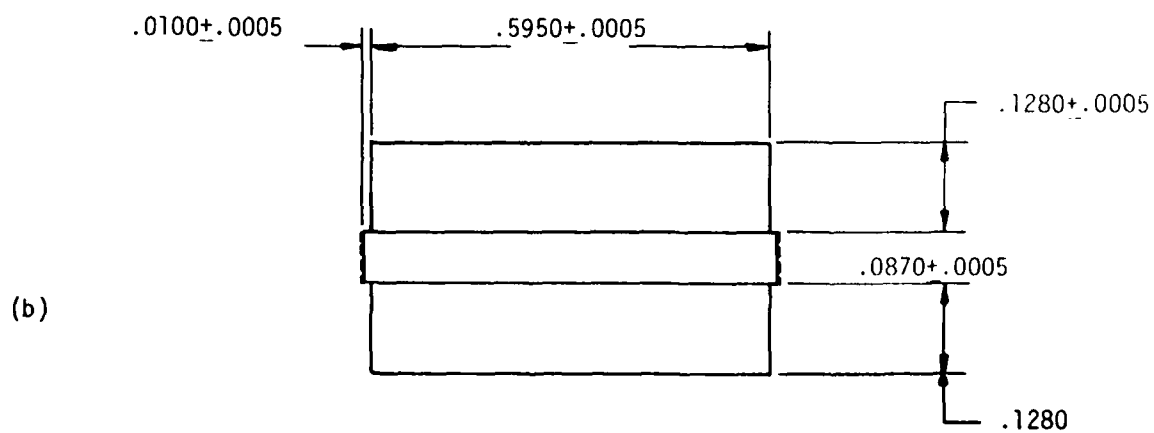
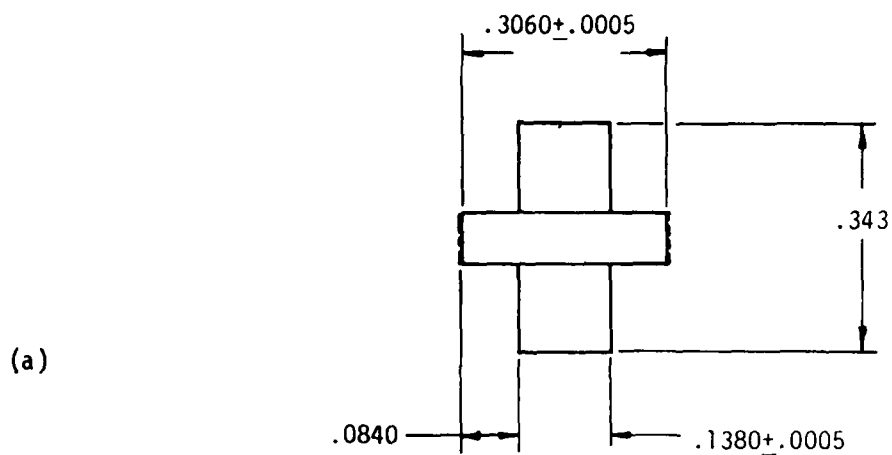
2.4 Rectangular Waveguide Windows

Fabrication of rectangular waveguide windows was accomplished using an existing window design developed by Northrop during a previous contract for a KU band CFA (12-18GHz). Material used for the ceramic was BeO of the given design and dimensions (Figure 21). Material used for the waveguide window was OFHC-copper.

2.4.1 Sputtering of Ceramics

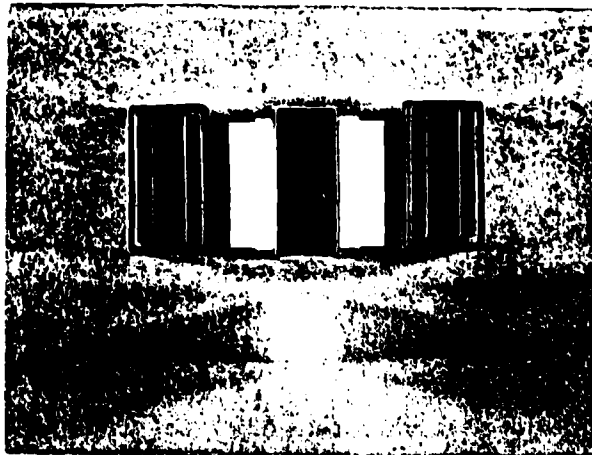
In order to sputter the four sides of the rectangular ceramic, a fixture shown schematically in Figure 22 was made to mask off the sides that needed no metallization. By sputtering from the top onto the 2 long sides of the rectangle, the two shorter sides were sputtered, similar to the process of sputtering the sides of the round discs, as discussed in Section 2.

Sputtered and moly-manganese metallized ceramics were brazed to waveguides (Figure 23) using gold-copper and silver-copper alloys. Table 15 shows the results obtained. Numbers 6 and 8 were diffusion brazed for comparison.

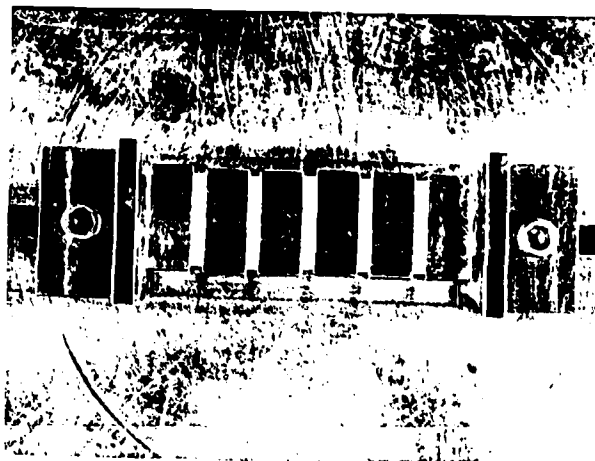


155-026418-020

Figure 21. Waveguide Window Ceramic



Masking ceramics with Cu-pieces



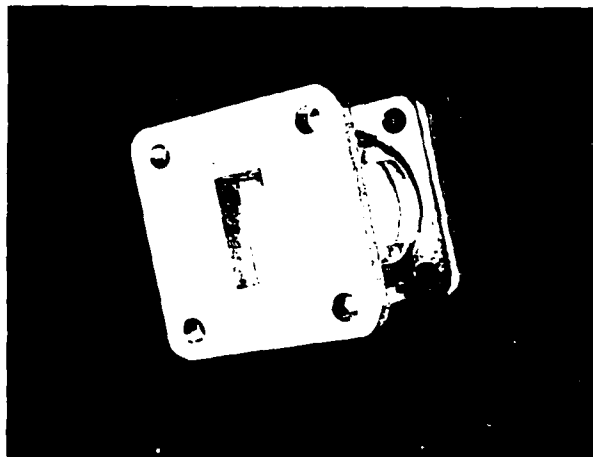
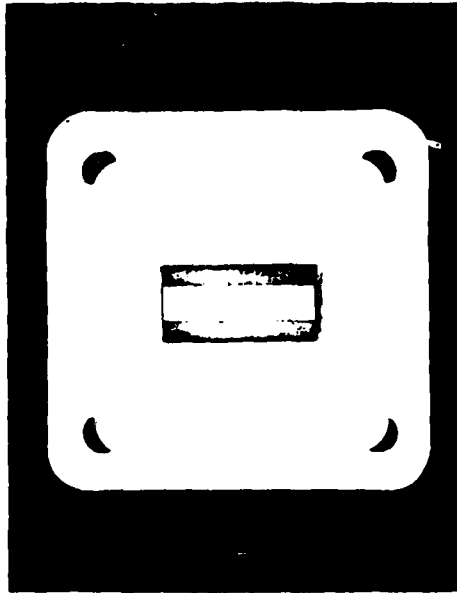
Clamping 5 ceramics together ready for sputtering

156-028418-021

Figure 22. Sputtering of Rectangular Window Ceramics

Table 15. RECTANGULAR WAVEGUIDE WINDOWS

<u>No.</u>	<u>Sleeve</u>	<u>Ceramic</u>	<u>Metallization</u>	<u>Alloy</u>	<u>Time</u>	<u>Temp</u>	<u>Remarks</u>
1	Cu	BeO	Mo-Mn	CuSi1	2 min	830	Leak tight
2	Cu	BeO	Mo-Mn	CuSi1	2 min	830	1 pin hole leak in 9th scale
3	Cu	BeO	Sputtered Ti-Mo-Cu	CuSi1	2 min	830	1 pin hole leak in 8th scale
4	Cu	BeO	Sputtered Ti-Mo-Cu	CuSi1	2 min	830	Leak tight
5	Cu	BeO	Sputtered Ti-Mo-Cu	35/65	2 min	1050	Leak tight
6	Cu	BeO	Mo-Mn	Diffusion	12 min	1015	leaks
7	Cu	BeO	Mo-Mn	CuSi1	2 min	830	1 pin hole leak on one side
8	Cu	BeO	Sputtered Ti-Mo-Cu	Diffusion	12 min	1015	Leaks



156-028418-022

Figure 23. Brazed Rectangular Window

3.0 HEAT TRANSFER IN ROUND WINDOWS

3.1 Thermal Barrier of Liquid Brazes

The application of the diffusion bonding process developed by Northrop resulted in enhanced heat transfer through the brazing layer. It was therefore believed that the use of the sputtering technique together with a liquid braze would also lead to enhanced thermal transport through the brazing layer. Considerable amount of effort has been spent to demonstrate enhanced thermal conductivity of the liquid-sputtered brazing layer when compared to the classical moly-manganese liquid braze.

To discuss the measurement techniques employed, it is useful to summarize the results obtained from the diffusion bonding process as applied to the CFA meander line.

Figure 24(a) shows schematically the cross section of a finger of the meander line. Assuming a stationary heat flow Q from the meander line to the cooling block, the temperature distribution as shown in Figure 24(a) is obtained with:

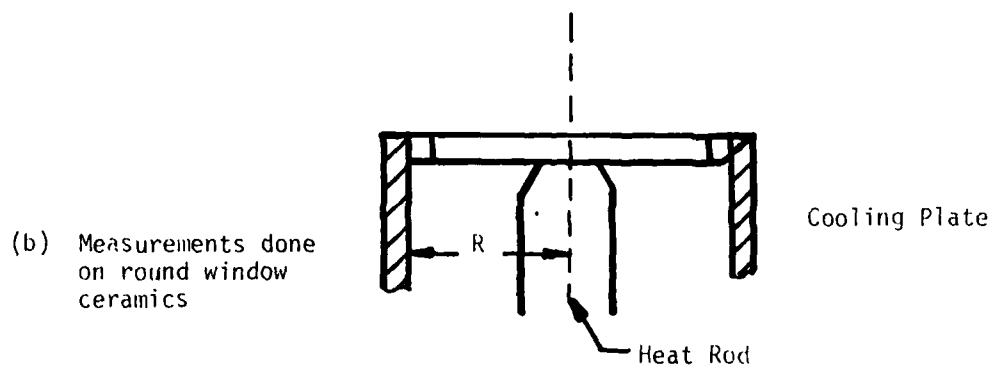
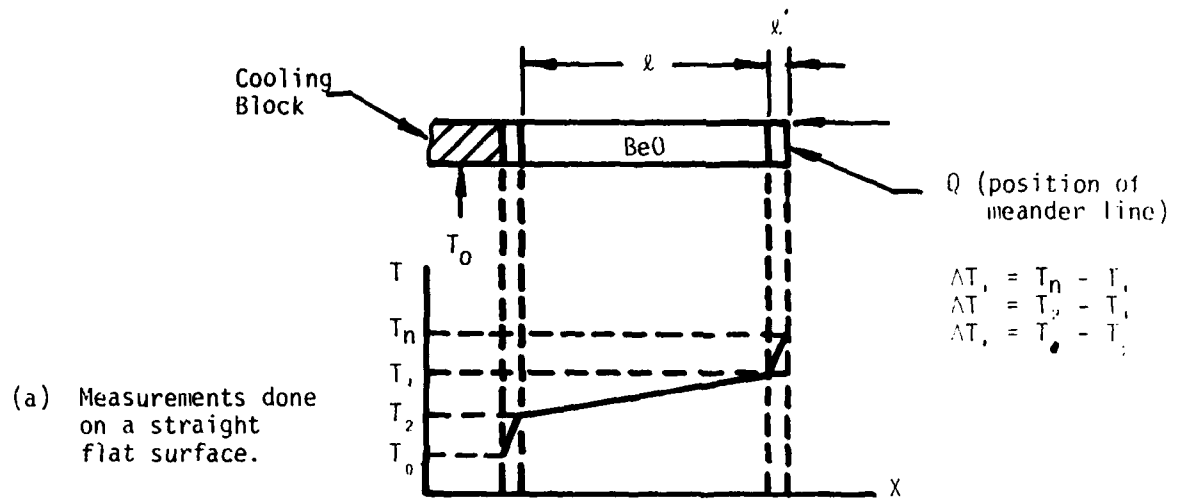
$$Q = s'k' \Delta T_s / \ell' = sk \Delta T / \ell$$
$$s = \text{cross section}$$

where we assumed the two brazing layers to be identical with a heat conductivity k' and length ℓ' . It is then possible to define an effective thermal conductivity k_{eff} and a thermal barrier R_t by assuming $\ell' \ll \ell$.

$$T_h - T_o = \Delta T_s + \Delta T + \Delta T_c = (Q\ell/s)(1/k_{\text{eff}})$$

$$\frac{1}{k_{\text{eff}}} = \left[2 \frac{\ell'}{\ell} \frac{s}{s'} \frac{1}{k'} \right] + \frac{1}{k} = \frac{2R_t}{\ell} + \frac{1}{k}$$

$$R_t = \frac{\ell's}{k's'} = \ell \left[\frac{1}{k_{\text{eff}}} - \frac{1}{k} \right]$$



158-028418-023

Figure 24. Thermal Barrier Measurements

Figure 24(b) shows the schematic of the set up for measuring the heat transfer through the round discs. A heat rod in intimate contact with the center area of the ceramic disc is heated sufficiently so that adequate heat flow through the ceramic disc to the sleeve occurs. If a point P_0 is located at a distance r_0 from center larger than the radius of the heating rod, then the stationary thermal distribution in the ceramic is given by:

$$T(r) = T(r_0) - \frac{Q}{2\pi tk} \ln r/r_0 \quad (5)$$

where Q is the total heat flow, t the thickness of the ceramic disc and k its heat conductivity.

Similarly, the temperature drop ΔT_b across the brazed layer of inner radius R and outer radius $R + \Delta R$ is given by:

$$\Delta T_b = \frac{Q}{2\pi k' t'} \ln \left(1 + \frac{\Delta R}{R}\right) \approx \frac{Q}{2\pi k' t'} \frac{\Delta R}{R}$$

Typical values for Q were 50-100W, with $R = .94\text{cm}$ and $t = .13\text{cm}$. Using these values with $t' = t$, together with the thermal resistance R_t as discussed above, it follows:

$$\Delta T_b \sim 68 \times R_t$$

As a result, the values ΔT_b as shown in Table 16 were expected, ranging from less than 1°C to about 10°C . These values were believed to be large enough to be detectable by simple thermocouple temperature measurements.

Table 16*

Representative Values of Effective Thermal Conductivity
(W/cm °C) and Calculated Thermal Resistance** (cm² °C/W)

Metallization	Braze	k _{eff}	R _t = average (s=s')	ΔT _b (°C)
Mo-Mn	Au-Cu-Alloy	.42-.25	.09-.16	6-11
Mo-Mn	Au-Cu-Diffusion	.51	.07	4.8
Mo-Mn	Au-Cu-Diffusion (high compression)	.65-.95	.05-.03	3.4-2
Mo-Cu (sputtered)	Cu-Cu-Diffusion (high compression)	1.8-2.5	.003-0	.2-0

* Cooke, M., Moats, R., IEEE Conference Record of 1973 on Electron Device Techniques, p.76.

**Note: the barrier resistance calculated assumes only 1 barrier, the second barrier being assumed negligible since the ceramics bars are buried into the base block. As such, R_t must be multiplied by a factor between 1 and 1/2.

3.2 Thermocouple Measurements

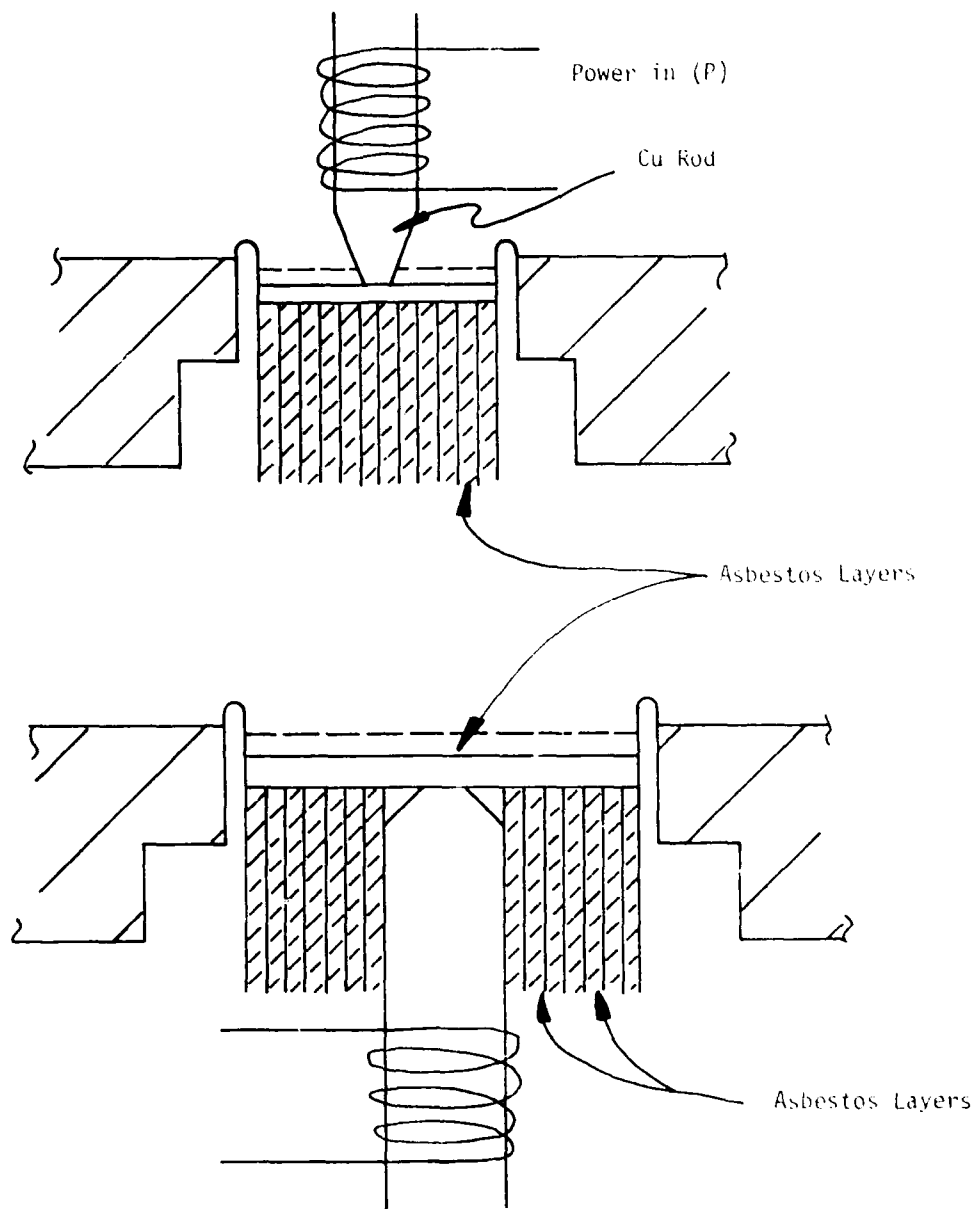
First measurements were performed by probing the surface temperature of the ceramic with a small thermocouple probe. Heat input to the ceramic disc was achieved by pressing a copper rod onto the center of the ceramic disc, as shown in Figure 25. Cooling was achieved by inserting the sleeve into a water cooled copper plate. Care was taken to avoid convective thermal cooling or convective thermal conduction by using asbestos isolation, as shown in Figure 25a.

Figure 26 shows a typical result. Here the measured temperature on the surface of the ceramic is plotted as a function of $D = 2r$, where r is the radial distance from the ceramic center. The value of T measured at $D = 1.782$ corresponds to the sleeve temperature. The temperature drop ΔT across the brazing layer can be obtained by extrapolating the curve $T(r)$ of the ceramic surface temperature to the sleeve position. For a heater input power of 80W, 1°C temperature difference is obtained by this method.

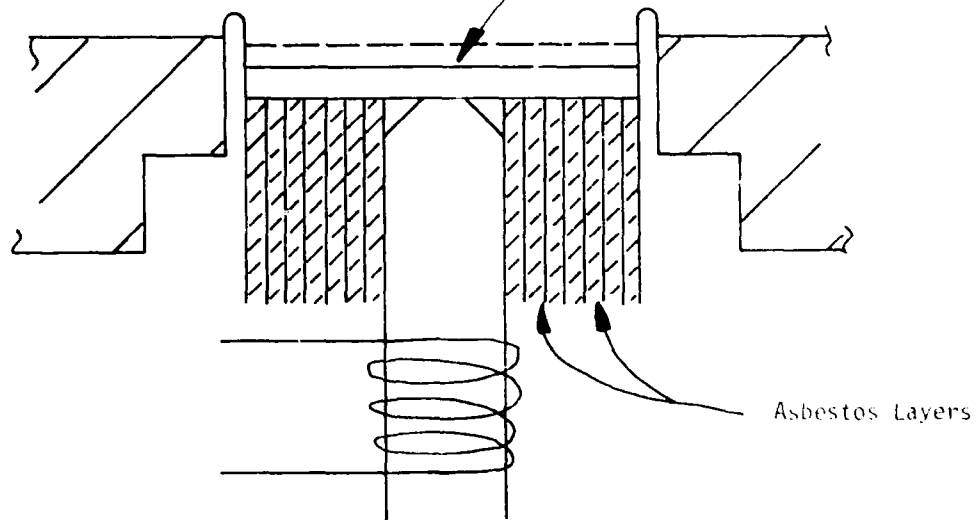
For higher input powers, this temperature drop seems to disappear, indicating that the method is not accurate enough to predict the exact value of the temperature drop. Other data have shown that even at low heater power ($P < 80\text{W}$), the measurement technique is not repeatable enough to obtain accurate conclusions. Placing the rod as shown in Figure 25b did not improve the accuracy of the method. However, the following conclusions could be made.

- 1) when detectable, the temperature drop across the barrier depends strongly on the position along the ceramic ID.
- 2) when detectable, the temperature drop across the barrier varies from sample to sample.

(a) Heating Rod Pressed Onto the Center of the Ceramic



(b) Heating Rod Inserted Inside Sleeve



156-026418-024

Figure 25. Experimental Setup for Thermal Barrier Measurements by Means of a Thermocouple.

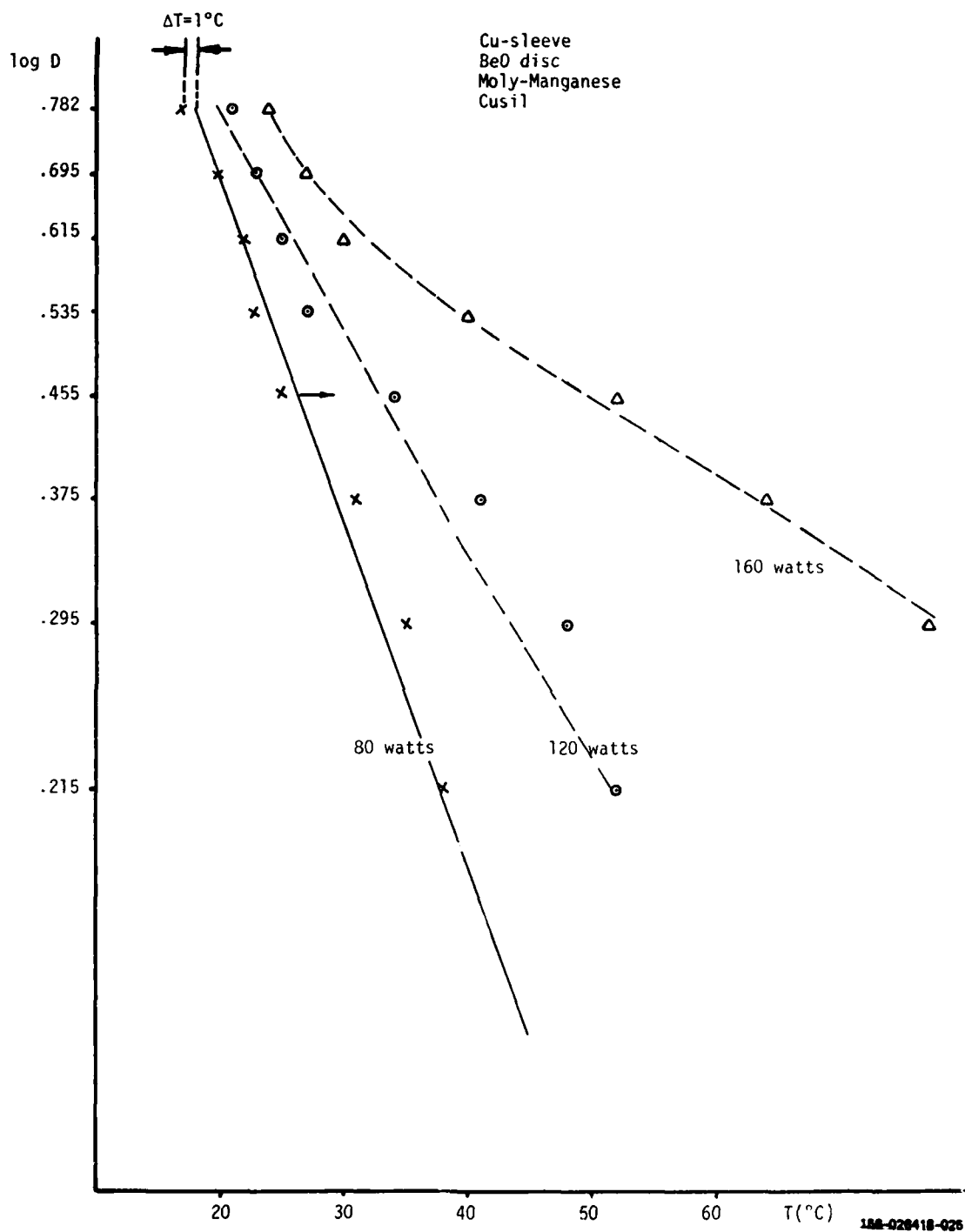


Figure 26. Thermal Barrier Measurement with a Thermocouple

- 3) the power flow Q through the ceramic as determined from Figure 26 and equation (4), i.e.,

$$Q(80W) \sim 34 W$$

$$Q(120W) \sim 52 W$$

$$Q(160W) \sim 61 W$$

is approximately proportional to the heating power.

- 4) Convection heating of the thermocouple probe could be detected.

To obtain more accurate data, an infrared microscope* was used to scan the interface layer.

3.3 Round Discs

3.3.1 Experimental Set-up

Figure 27 shows the automated experimental set-up: a carrier supporting the sample under test is moved in two directions, A and B, and passed under the microscope. Once proper alignment in radial direction is obtained (A direction), the "temperature" distribution in B direction is automatically obtained and recorded.

The spot size of the microscope was set to the manufacturer's recommended operating conditions, and was estimated to be 0.0014" in diameter. The read-out of the microscope is essentially proportional to the power radiated from the device at the spot position, in a certain frequency band, and converted to a black body temperature. As such, the indicated temperature (or radiance) are strongly dependent on the emissivity of the sample under test, and calibration of the test set up must be performed. However, since comparative

* Infrared Radiometric Microscope, Model RM-2A Barnes Engineering Company.

values between Mo-Mn metallized and sputtered samples were first desired, the first tests were conducted without proper calibration. The testing techniques were improved step by step:

1) the variation of sample distance to microscope was found to be a source of errors, due to the depth of focusing of the microscope. The shoulder of the sleeve above the ceramic was mechanically removed, and care was taken to adjust horizontal movement of the carrier under the microscope.

2) the burrs left by the machining operation were found to be sources of errors. Thus, the samples, after machining, were diamond polished to warranty burr free sleeves in the ceramic plane.

3) even on a comparative evaluation, the variation of emissivity was too large from sample to sample for proper evaluation. The samples and the cold plate were then covered with a thin layer of an aquadag for more homogeneous and repeatable sample emission of radiation.

4) calibration was obtained by measuring the true temperature (thermocouple) of a sample prepared with aquadag to be .95. Figure 28 shows the calibration curve obtained, where "0" radiance is referenced to ambient temperature.

3.3.2 Diffusion Brazes

For reference, the first samples tested were diffusion brazed samples with Mo-Mn metallization and with sputtering metallization. Figures 29 and 30 show the results obtained, where the radiance as a function of radial position is plotted (Cu sleeves, Al_2O_3 ceramic discs). The three curves represent on each figure three runs at the same position.

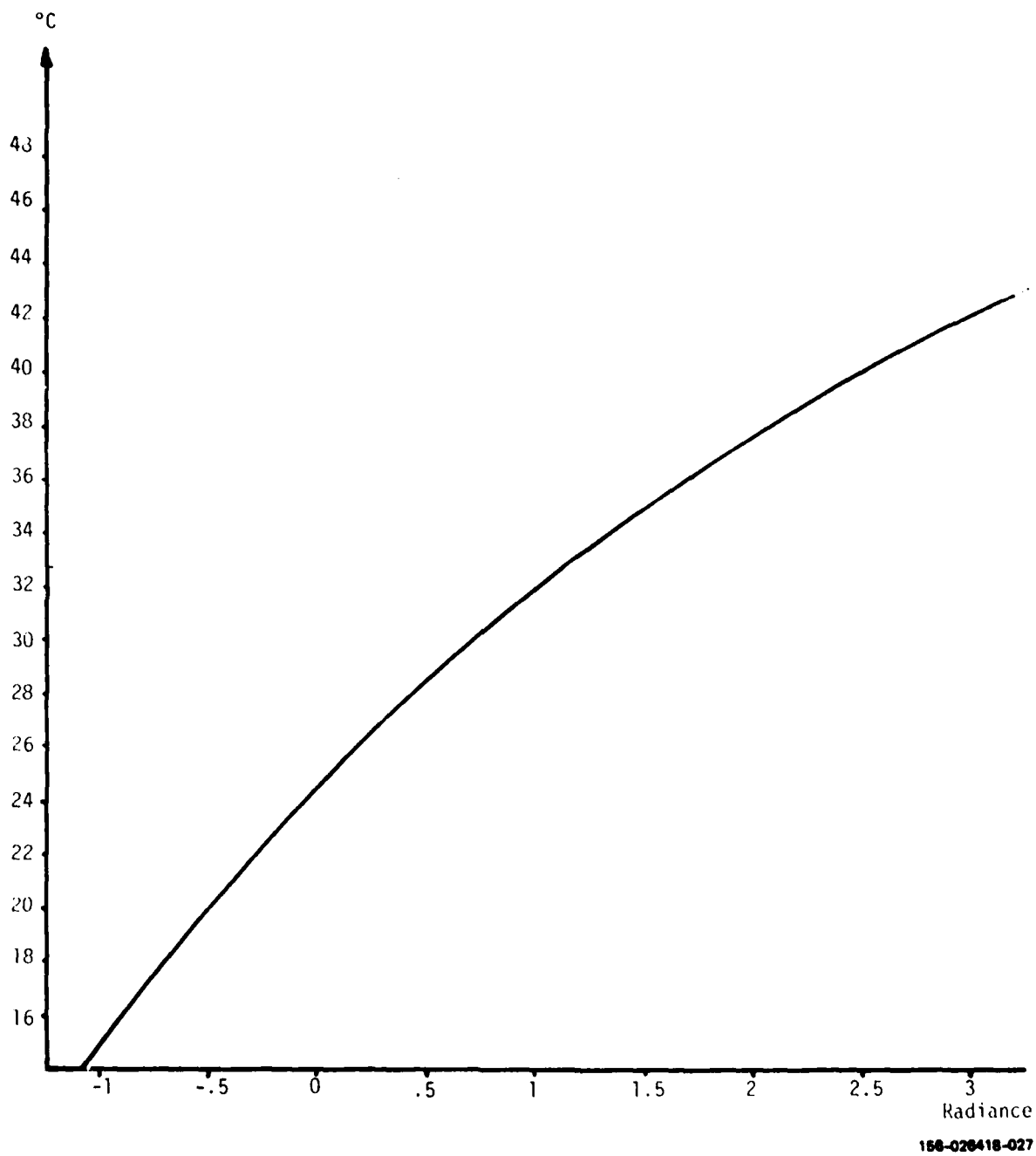


Figure 28. Calibration Curve of Temperature Versus Radiance

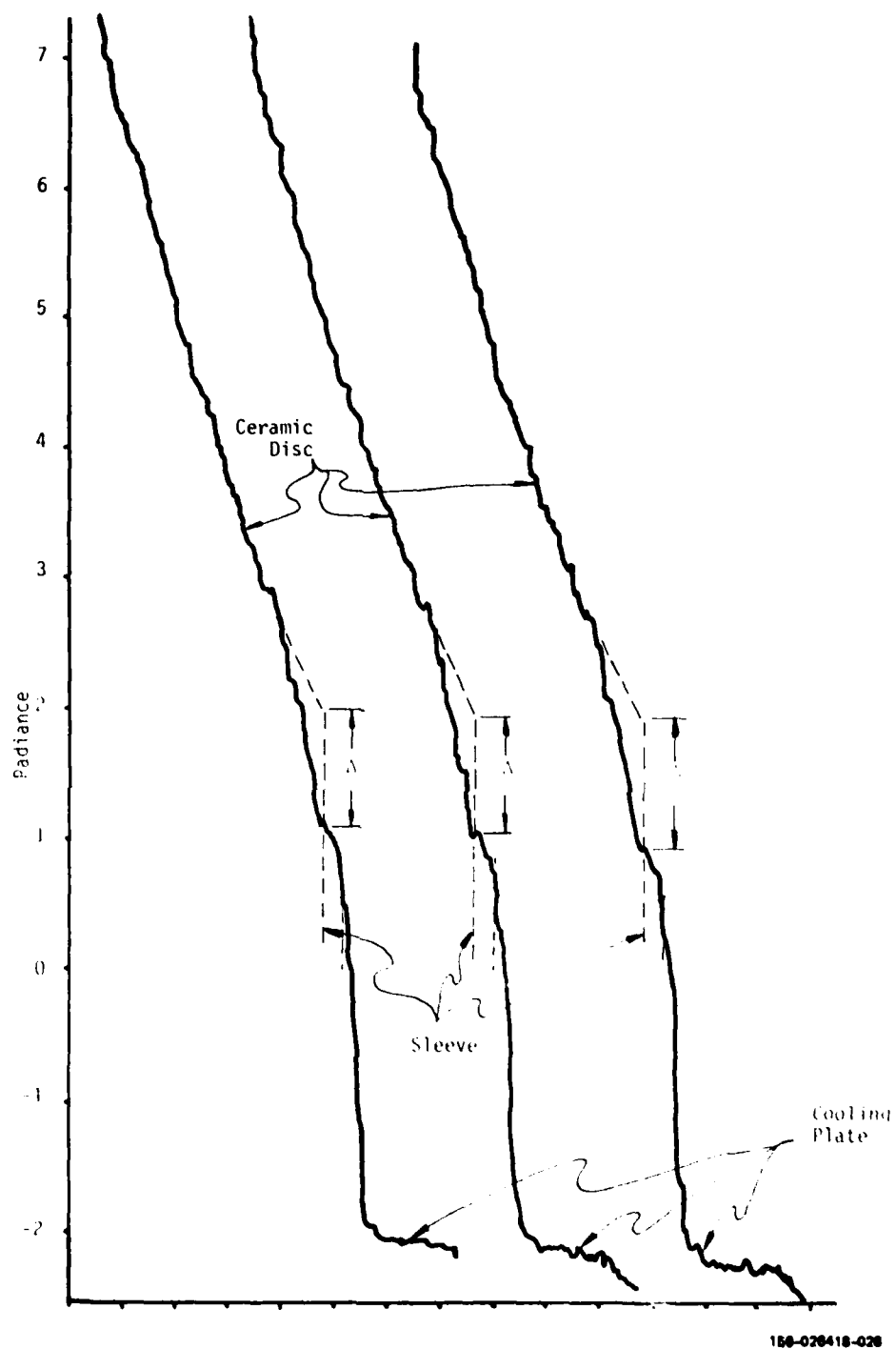


Figure 29. Sample #35 - Diffusion brazed Al_2O_3 Disc to Cu sleeve
Mo-Mn metallization

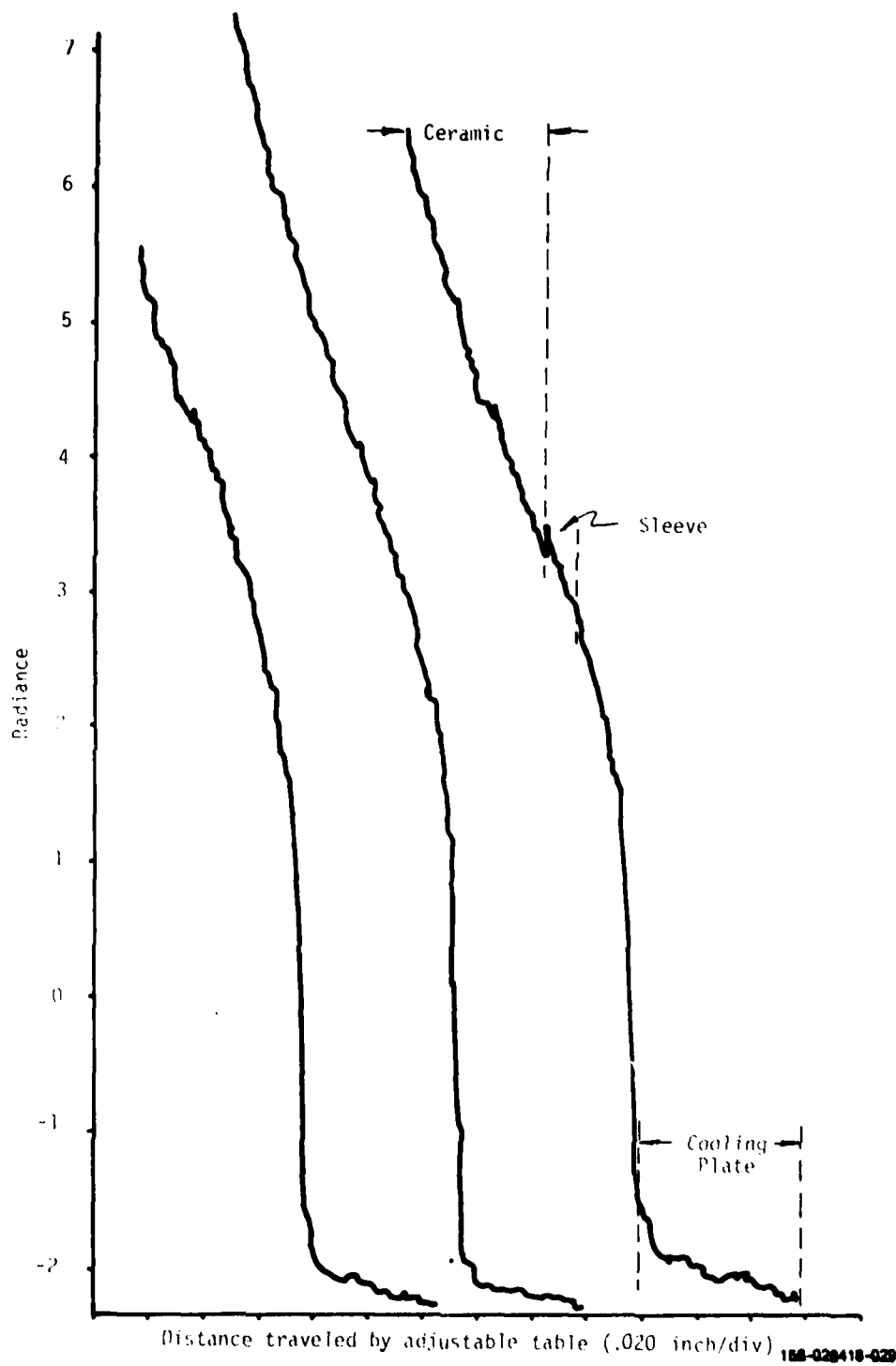


Figure 30. Sample #32 - Diffusion brazed Al_2O_3 disc to Cu sleeve
Sputtering metallization

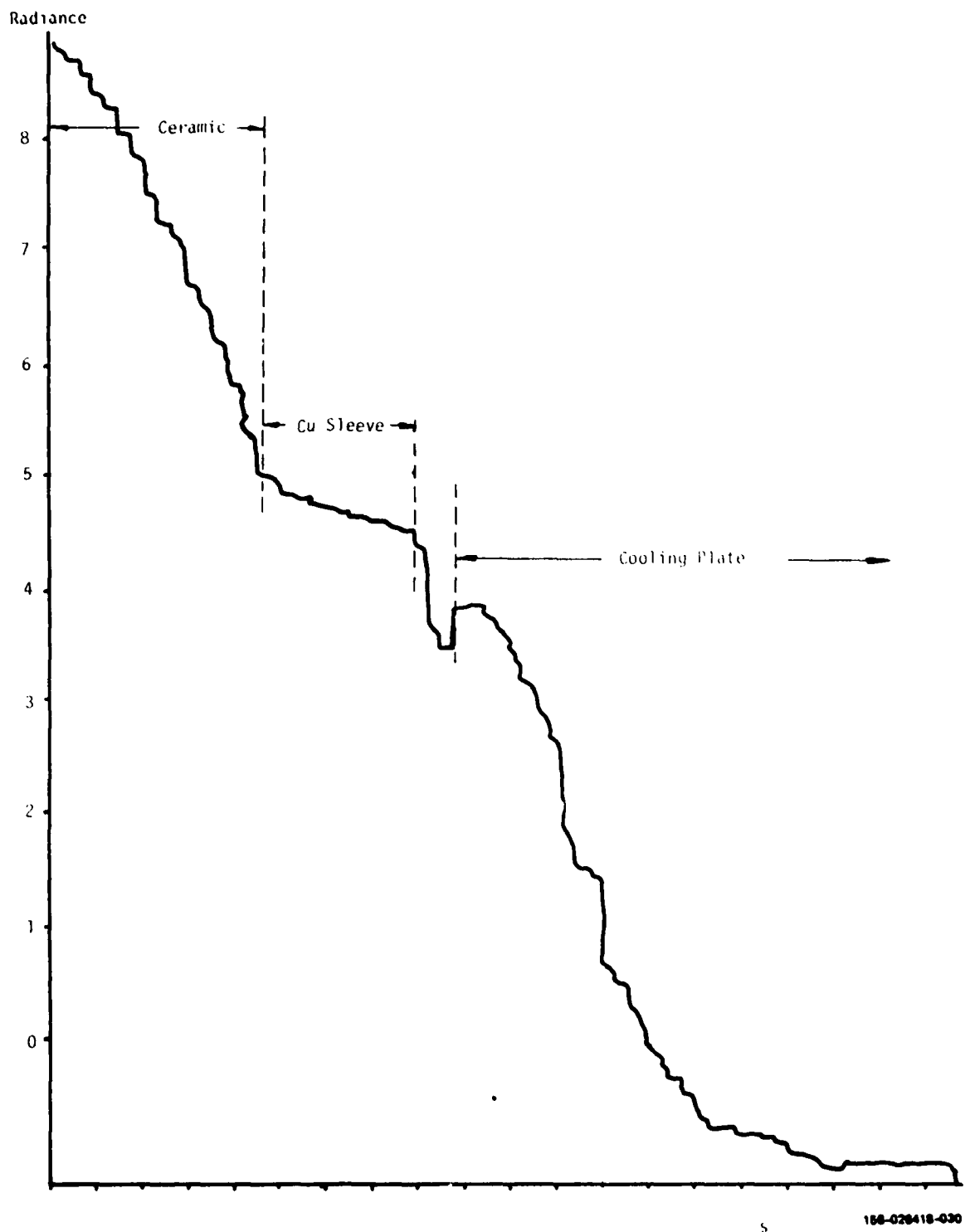


Figure 31. Sputtered Diffusion Brazed Sample #32 with Expanded Scales

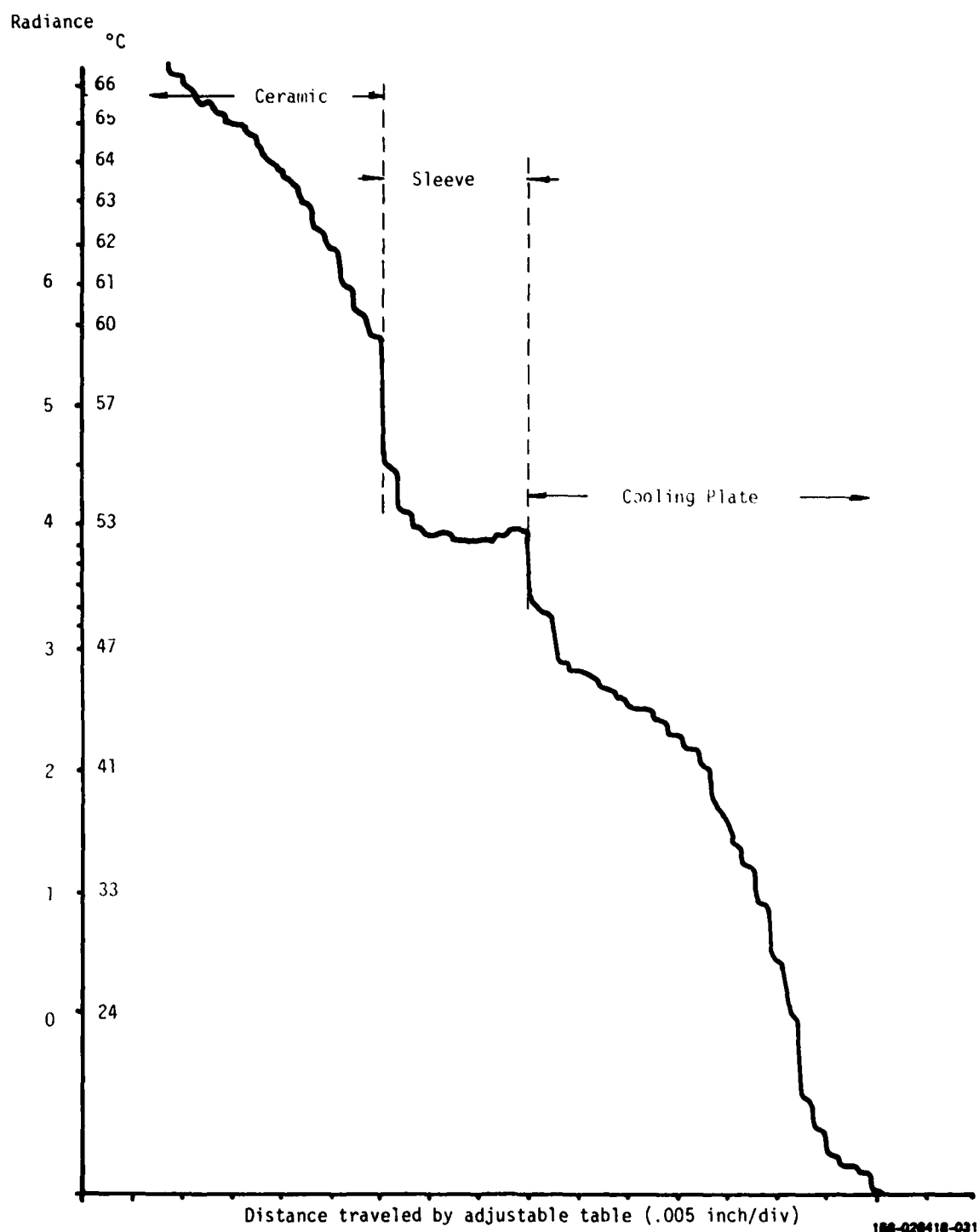
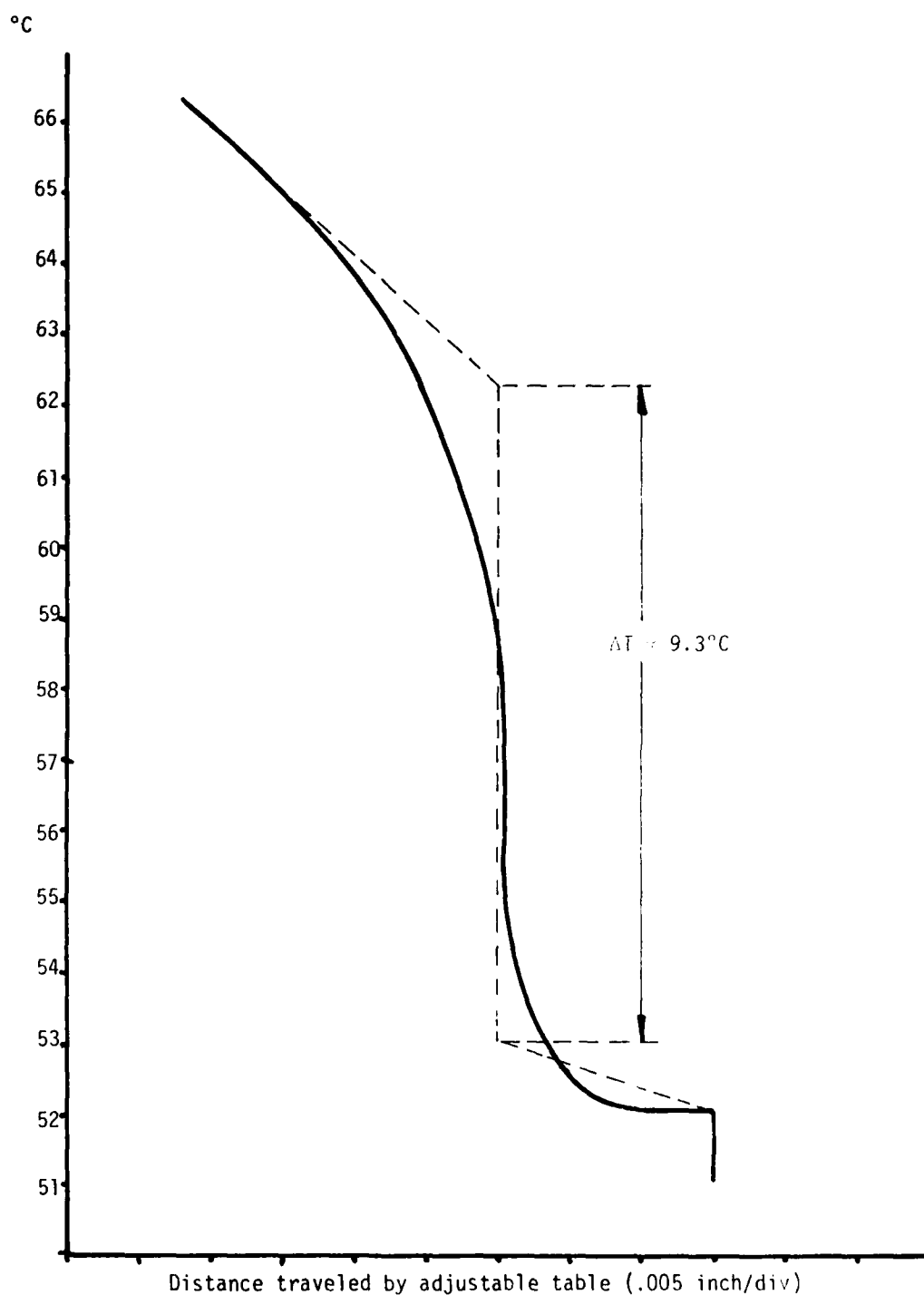


Figure 32. Mo-Mn Metallized, Diffusion Brazed Sample #35 with Expanded Scales



158-028418-032

Figure 33. Linear Curve of Temperature Profile for Mo-Mn Metallized Sample #35

The MoMn sample (Figure 29) clearly shows a drop in radiance at the interface between the alumina and the copper sleeve. In first approximation, a drop Δ of about 1 radiance at 1 radiance above room temperature is observed, corresponding roughly to 9°C. The curves for the sputtered metallized sample (Figure 30) do not show such a distinctive drop: even the sleeve position in the plot is not clearly discernible.

In order to evaluate these data further, the curves obtained were measured once again by expanding the scales in both variables (distance and radiance) Figures 31 and 32 show the curves obtained. Clearly visible is the temperature drop across the interface layer of the MoMn sample, while nearly no drop is visible across the sputtered layer sample. Figure 33 shows a linear plot of the temperature profile for the case of the Mo-Mn sample. The same figure shows the idealized dashed curve one would expect. From this expected curve, one can calculate $Q=21W$ and obtain the barrier resistance. Note, however, that such a barrier is not always observed as the measurement location around the ID of the ceramic is varied. In fact, positions have been found on the diffusion bonded Mo-Mu samples where no temperature barrier was observable. Furthermore, some positions around the ID of the ceramic of the sputtered diffusion brazed sample showed a small thermal barrier.

These measurements demonstrate that the interface layer is very inhomogeneous with respect to thermal transport properties. Correlation of high thermal barrier with pin leaks could not be made.

3.3.3 Liquid Brazes

A certain number of measurements on different samples have been made using the infrared microscope. Tables 17 through 20 show some typical results

obtained by comparing the thermal properties of the metallizing schemes, all other fabrication materials and processes being identical.

The total power (first column) is obtained by determining $\Delta T/\Delta R$ from the graphs at the edge of the ceramic. A value $\epsilon = 1$ was assumed to convert "radiance" scale to true temperature (room temperature assumed = 25°C).

$$P = 2\pi k t R \Delta T/\Delta R$$

t = thickness of sample

k = thermal conductivity (= 2.5 W/°C cm for BeO)
(= .36 W/°C cm for Al₂O₃)

The thermal barrier R is obtained through the relation:

$$R = \Delta T/(2\pi R t Q)$$

Table 17 compares the two metallizing schemes when BeO is used with a Cusil liquid braze and a copper sleeve. Comments should be made.

- the power P exceeds 200 watts in certain cases, while the input power was maximally 260 watts. Such high values may be due to a slight eccentricity of the heating rod with respect to the ceramic center.
- the barrier resistance varies from .037°C/W cm² to 0, depending on the position around the circumference of the disc. The barrier resistance is low as compared to the diffusion bonding result, strongly indicating that the fillet formed by the liquid braze alloy play a major role, and as such are responsible for the spread measured in the barrier resistance. Figure 34 shows, for example, two cross sections through the brazed joint.
- it is indicative that the barrier resistance for the sputtered samples is about 3 times smaller, although an average value of the barrier resistance is not a representative measurement.

Table 17

THERMAL COMPARISON BETWEEN METALLIZING SCHEMES

- Copper Sleeve, BeO-ceramic, Cusil liquid braze

Mn-Mo Metallizing (Sample No. 28)

Power Through Ceramic (W)	ΔT (°C)	R (°/Wcm ²)	Position
144	.7	.006	1
186	1.0	.007	2
186	1.5	.012	2
200	1.5	.010	2
188	0	0	3
200	0	0	3
168	0	0	3
156	3.0	.025	4
160	3.5	.029	4
180	4.0	.029	4
165	.8	.006	5
184	1.0	.007	5
200	1.5	.010	5
200	1.5	.010	5
190	0	0	6
160	4.0	.033	7
170	4.0	.037	7
		$\overline{R} = .013$	

Sputtering (Sample No. 26)

180	1.0	.007	1
176	.7	.005	1
165	1.0	.008	1
168	0	0	2
210	0	0	2
187	1.0	.007	2
199	0	0	3
210	0	0	3
180	1.0	.007	3
210	0	0	4
210	.8	.005	4
211	1.4	.009	4

Sputtering (Sample No. 29)

190	0	0	1
130	0	0	1
165	0	0	2
		$\overline{R} = .004$	

Table 18
THERMAL COMPARISON BETWEEN METALLIZING SCHEMES
- Cu-Sleeve, BeO discs, 35/65 Braiding alloy

MoMn (Sample No. 27)

Power Through Ceramic (W)	ΔT (°C)	R (°C/Wcm ²)	Position
126	.3	.003	1
115	.3	.003	1
130	.5	.005	1
100	0	0	2
112	0	0	3
		$\overline{R} = .002$	

Sputtering (Sample No. 37)

127	0	0	1
123	0	0	1
138	.3	.003	2
145	.5	.005	2
128	0	0	3
127	.5	.005	3
		$\overline{R} = .002$	

AD-A084 860

NORTHROP CORP DES PLAINES IL DEFENSE SYSTEMS DIV

F/G 11/2

METAL-CERAMIC SEALS.(U)

OCT 79 Y AMER, G DOHLER

F33615-78-C-1405

UNCLASSIFIED

094-9169

AFAL -TR-79-1106

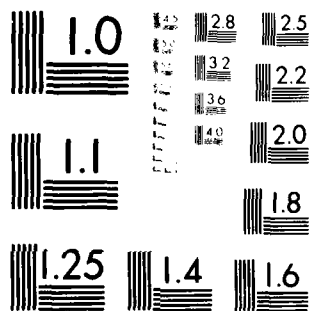
NL

2 2

AL
2-9-80/7



END
DATE
FILMED
7 80
DTIC



MICROCOPY RESOLUTION TEST CHART
NATIONAL BUREAU OF STANDARDS-1963-A



No Fillet
No Champfer
(both sides)



Fillet
Champfered



Fillet
No Champfer

158-028418-033

Figure 34. Cross sectional areas at brazed joint of three different samples illustrating the effect of the presence of a fillet.

- no barrier resistance was measured with the Al_2O_3 sputtered metallizing process, see Table 19. The power through the samples is smaller since the thermal conductivity of alumina is about 8 times smaller than the thermal conductivity of BeO : the heat losses from the rod are thus larger, since the ceramic is hotter.
- Table 20 shows a typical example obtained with Kovar sleeves. Here, a drop $\Delta T \approx 15\text{-}25^\circ\text{C}$ was found between the Kovar sleeve and the cooling plate, thus reducing P further.

3.4 Coaxial Samples

With the diameter of the ceramic disc being .83 cm, the measurements were more critical with respect to alignment errors. The center pins were contacted to the heating rod, and a typical scanning pattern is shown in Figure 35 for an Al_2O_3 ceramic disc metallized with the MoMn process (Cu-sleeve). The power through the ceramic can be estimated to be roughly 20 watts. No barrier at the interface can be detected, even if the scale is increased by a factor of 10. More than 3 samples were tested, and the temperature drop across the brazing layer, was less than the resolution of the experimental set-up (less than $.1^\circ\text{C}$), independent on Mo-Mn or sputtering metallization. The following sample types were measured:

<u>No.</u>	<u>Sleeve</u>	<u>Ceramic</u>	<u>Braze Alloy</u>	<u>Metallization</u>	<u>Center Pin</u>
13	Cu	Al_2O_3	CuSi1	Sputtered Ti-Mo-Cu	Cu
15	Cu	Al_2O_3	CuSi1	Mo-Mn	Cu
16	Cu	Al_2O_3	CuSi1	Sputtered Ti-Mo-Cu	Cu

Table 19

THERMAL COMPARISON BETWEEN METALLIZING SCHEMES

- Copper Sleeve, Al₂O₃ ceramic, CusilMoMn (Sample 24)

Power Through Ceramic (W)	ΔT (°C)	R (°C/Wcm ²)	Position
25	.7	.037	1
35	1.2	.045	1
32	1.0	.041	1
20	.5	.033	2
18	.3	.022	2
25	1.1	.057	2
30	1.0	.044	2
25	0	0	3
23	2.0	.114	3
45	1.8	.052	4
45	.8	.023	4
		$\overline{R} = .042$	

Sputtering (Sample 25)

30	0	0	1
32	0	0	1
48	0	0	2
54	0	0	2
39	0	0	3
45	0	0	4
		$\overline{R} = 0.0$	

Table 20
THERMAL COMPARISON BETWEEN METALLIZING SCHEMES
- Kovar sleeve, Al₂O₃ ceramic, Cusil Liquid Braze

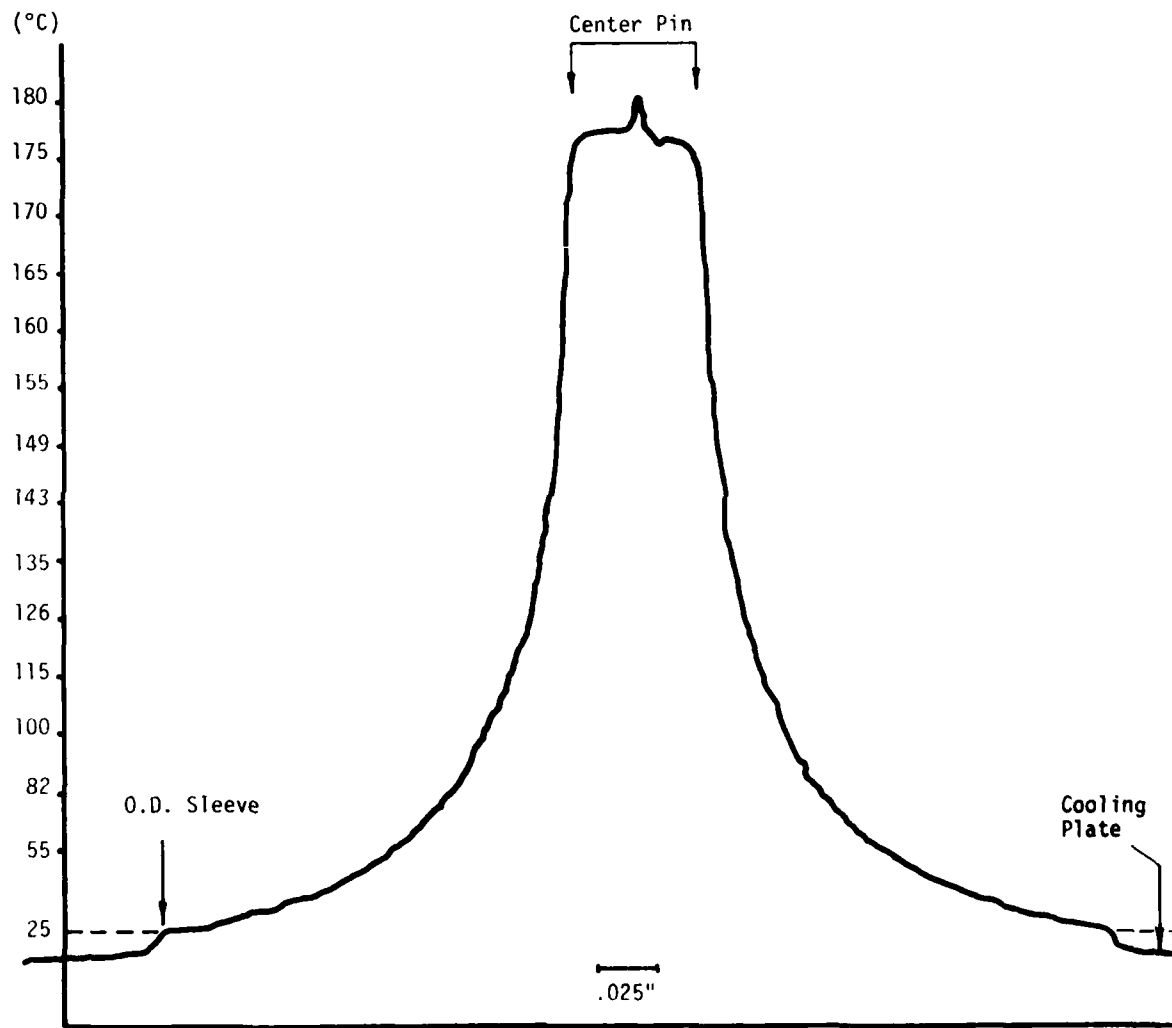
Mo-Mn Metallizing (Sample No. 19)

<u>Power Through Ceramic (W)</u>	<u>ΔT (°C)</u>	<u>R (°C/Wcm²)</u>	<u>Position</u>
25	0	0	1
30	0	0	1
30	0	0	1
35	0	0	2
35	0	0	2
30	0	0	2
25	0	0	2
24	0	0	3
32	0	0	3
31	0	0	3

Sputtering [Large T-drop,sleeve to Cooling Plate](Sample No. 18)

14	0	0	1
10	0	0	1
12	0	0	1
10	0	0	2
11	0	0	2
15	0	0	3
14	0	0	3
12	0	0	3

Pheater = 180 watts ($c = .9$)



168-028418-034

Figure 35. Scanning pattern for a coaxial pin assembly

4.0 RF LOSSES

The additional rf losses of metallized layers in brazed windows can be measured either by direct insertion loss measurements or by Q measurements of properly designed cavities. The first method is more direct, but sensitive measurements are difficult to achieve. The second method is generally more sensitive to small variations in rf losses, but the interpretation of the results is more difficult. On a comparative basis, Q measurements are more easily made. As such, this technique has been applied to both the circular and rectangular windows. In sequence, the Q's were measured in each case on empty waveguide sections, waveguide sections containing unmetallized ceramic windows at the proper location, and waveguide sections containing brazed windows. The results were then compared and preliminary analysis made.

4.1 Rectangular Waveguides

4.1.1 Empty Waveguide

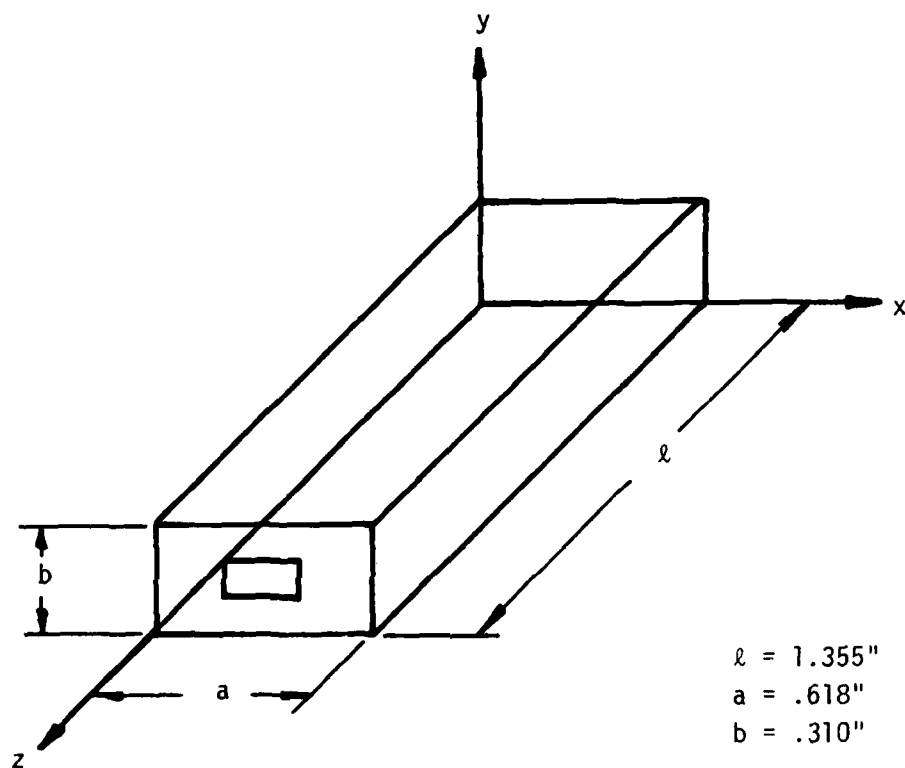
Rectangular waveguide sections of length $\ell = 1.355"$ were closed on both ends, a rectangular iris having been placed in the center portion of one of the smallest cross sections, see Figure 36. The resonance frequencies of these empty waveguide sections were measured in the range from 12 to 18GHz, and were found to be $12.875 \pm .005$ and $16.079 \pm .004$ GHz for a single cavity. Using the relation for resonant frequencies $f_{m,n,v}$ for rectangular waveguide sections of dimensions a, b and ℓ :

$$f_{m,n,v} = \frac{c}{2} \left[\left(\frac{m}{a} \right)^2 + \left(\frac{n}{b} \right)^2 + \left(\frac{v}{\ell} \right)^2 \right]^{1/2} \quad (5)$$

where c is the light velocity and m, n, v integers, one finds *

$$f_{1,0,2} = 12.93 \text{ GHz}; \quad f_{1,0,3} = 16.19 \text{ GHz}; \quad f_{1,0,4} = 19.88 \text{ GHz}$$

* The (2,0,1) and (0,1,1) modes do resonate respectively at 19.58 and 19.52GHz.



156-028418-036

Figure 36. Schematic of the rectangular waveguide resonator

if the values a , b and l as given in Figure 36 are used. Thus, it is concluded that the TE modes (1,0,2) and (1,0,3) are the resonant modes detected in the empty waveguide sections:

$$E_x = E_z = H_y = 0 \quad (6)$$

$$H_x = -v \frac{a}{l} \sin \frac{\pi x}{a} \cos \frac{v \pi z}{l}$$

$$H_z = \cos \frac{\pi x}{a} \sin v \pi z / l$$

$$E_y = -j \frac{\omega \mu}{c} \frac{a}{\pi} \sin \frac{\pi x}{a} \sin \frac{v \pi z}{l}$$

The Q of the cavities at these resonance frequencies can be calculated: *

$$Q = \frac{2}{\delta} \frac{\int_V H^2 dv}{\int_S H^2 ds}$$

where δ is the skin depth of the wall material at the resonant frequency, the volume integral extending over the total volume $V = abl$ of the resonator, and s being the total wall surface:

$$Q_{1,0,v} = \frac{1}{\delta} \frac{(1/a)^2 + (v^2/l^2)}{(1/a^2)(2/a + 1/b) + (v^2/l^2)(2/l + 1/b)} \quad (7)$$

resulting in the following values if the walls are assumed to be pure copper:

$$\begin{aligned} Q_{1,0,2} &= 7732 \\ Q_{1,0,3} &= 9226 \\ Q_{1,0,4} &= 10,635 \end{aligned} \quad (8)$$

* J.C. Slater, Microwave Electronics, D. Van Nostrand Co., New York (1950), p. 70.

The average Q measured on unplated copper cavities were found way below these values, namely 5400 and 5900 for the two detected modes respectively. Copper plating the walls did not improve these values drastically, so that silver plating of the walls became necessary. The average Q's measured were as follows:

$$\bar{Q}_{1,0,2} = 7382 \quad (9)$$

$$\bar{Q}_{1,0,3} = 8930$$

Compared to the theoretical value determined in (8), the skin depth δ_p of the plating is determined as a function of the copper skin depth δ_{cu} :

$$\delta_p = 1.047 \delta_{cu} (1,0,2) \quad (10)$$

$$\delta_p = 1.033 \delta_{cu} (1,0,3)$$

The Q was remeasured for the lower frequency mode just after recleaning the surfaces. With Q = 7500 another value for δ_p was obtained:

$$\delta_p = 1.031 \delta_{cu}$$

Thus within the model presented, one can assume that the conductivity of the walls is within 3% of the conductivity of pure copper.

4.1.2 The Unbrazed Window

The insertion of an unbrazed window into the empty waveguide disturbs the field pattern within the resonant cavity. With the window unbrazed and unmetallized at the design position in the center of the resonator, the resonant frequencies detected were as follows:

$$f_1 = 13.699 \text{ GHz}$$

$$f_2 = 16.370 \text{ GHz}$$

Since these frequencies are higher than the resonant frequencies observed earlier with the empty waveguide, one must assume that the 16.44 GHz frequency must be correlated to the (1,0,4) mode, while the frequency of 13.75 GHz must be correlated to the (1,0,3) mode. Furthermore, the resonant frequency of 12.9 GHz of the (1,0,2) mode is shifted below the 12 GHz equipment limitation. Thus, the $f_{1,0,4}$ frequency is shifted down from 19.88 GHz to 16.5 GHz, the $f_{1,0,3}$ resonant frequency being shifted to 13.75 GHz, while the $f_{1,0,2} \approx 12.9$ GHz frequency is shifted below 12 GHz. This is schematically shown in Figure 37. Here, the window, which is of complex geometry (see Figure 21), has been simulated by a dielectric slab inserted into the center of the cavity. Both sketches (a) and (b) of Figure 37 represent schematically the resonance conditions for the empty waveguide and for the waveguide containing the simulated window, for both the (1,0,3) and (1,0,4) mode respectively.

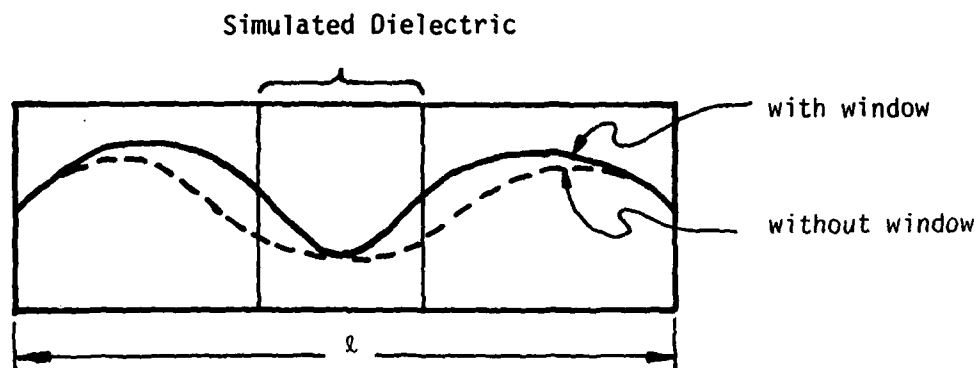
If one assumes, in first approximation, that the insertion of the unbrazed window into the cavity can be simulated by the filling of the entire resonator with a dielectric of effective dielectric constant $\bar{\epsilon}$, then the resonant frequency shifts observed must determine the value of $\bar{\epsilon}$. For a given mode (1,0,n), the ratio $f_{1,0,n}$ of the empty waveguide to the $f_{1,0,n}$ of the waveguide with the window is equal to the square root of the effective dielectric constant. Considering the values obtained previously, one obtains the value $\bar{\epsilon} = 1.37$ [(1,0,3) mode shift] and $\bar{\epsilon} = 1.42$ [(1,0,4) mode shift]. Furthermore, the effective dielectric constant $\bar{\epsilon}$ defined by the expression:

$$\bar{\epsilon} \approx \frac{V - \Delta V + \epsilon \Delta V}{V} \approx 1.61$$

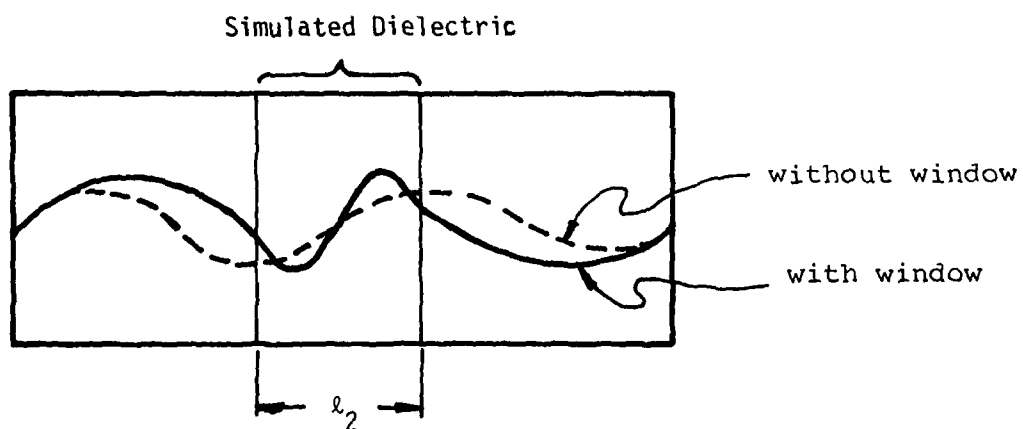
V: total volume of the cavity

ΔV : total volume occupied by the dielectric

ϵ : dielectric constant of BeO = 6.7



(a) (1,0,3) mode



(b) (1,0,4) mode

156-028418-036

Figure 37. Schematic of resonant conditions in waveguides with and without ceramic windows

is close enough to these two values to demonstrate the validity of the simplified model. Note also that the resonant frequency $f_{1,0,2}$ shifts in this model to a value of 10.9GHz, well below the 12-18 GHz test range.

The respective average Q's measured at those two frequencies after insertion of the unmetallized windows were:

$$\bar{Q}_{1,0,3} = 8160 \quad (11)$$

$$\bar{Q}_{1,0,4} = 9580$$

These values have to be compared to the theoretical values determined in relation (8). Assuming that the actual skin depth is about 3% larger than the skin depth for copper, the modified expected values of Q are:

$$Q_{1,0,3} = 8950$$

$$Q_{1,0,4} = 10,320$$

The reduction of the Q' from these values to the values shown in Equation 11 can be attributed to:

- change of the electromagnetic field profile due to the insertion of the unmetallized windows. A careful analysis by computer code shows, for example, that the magnitude of the magnetic field in the center of the waveguide (transversal component) is 2.38 times larger than the amplitude at the cavity ends.

- losses due to the loss tangent of the window material (and possible surface contamination).

The values of Q in relation to Equation 11 will be used as reference for the data obtained with brazed windows.

4.1.3 Brazed Windows

A large number of rectangular waveguide window sections were fabricated and tested. The results obtained were not always reliable or reproducible. As such, only some of the most pertinent data will be presented in the following.

Figure 38 shows a summary of the results obtained. The average Q measured for a given sample is plotted as a function of resonant frequency (no continuous dependence of Q versus resonant frequency is inferred). The two Q values measured as reference in cavities containing unmetallized windows are also plotted. The resonance observed at around 18.7GHz has not been clearly identified, and is believed to be due to a mode closely related to the window geometry. The resonance observed at 19.3GHz is believed to be of the TE-type, either the (1,0,5) or the (2,0,3) mode. Furthermore, the resonance observed at around 11.8GHz is just at the lower limit of the resolution of the equipment used, and was not always observed.

The Q ' related to sputter metallization and cusil braze are consistently higher than those measured with windows prepared with Mo-Mn. Furthermore, clearly seen are the low Q 's obtained when gold/copper alloys are used. This becomes understandable when the electrical resistivity of copper-gold alloys is considered (see Figure 39a): at a 50/50 mixture, a resistivity 7 times higher than the resistivity of pure copper is obtained. The lower part of the same figure, 39b, shows that Cu-Ag alloy only exhibit a maximum increase in resistivity of approximately 20% when compared to copper.

Analytical evaluation can be made as follows. From the Q definition given in Section 4.1.1, it follows that if Q_0 is the Q of the cavity containing an

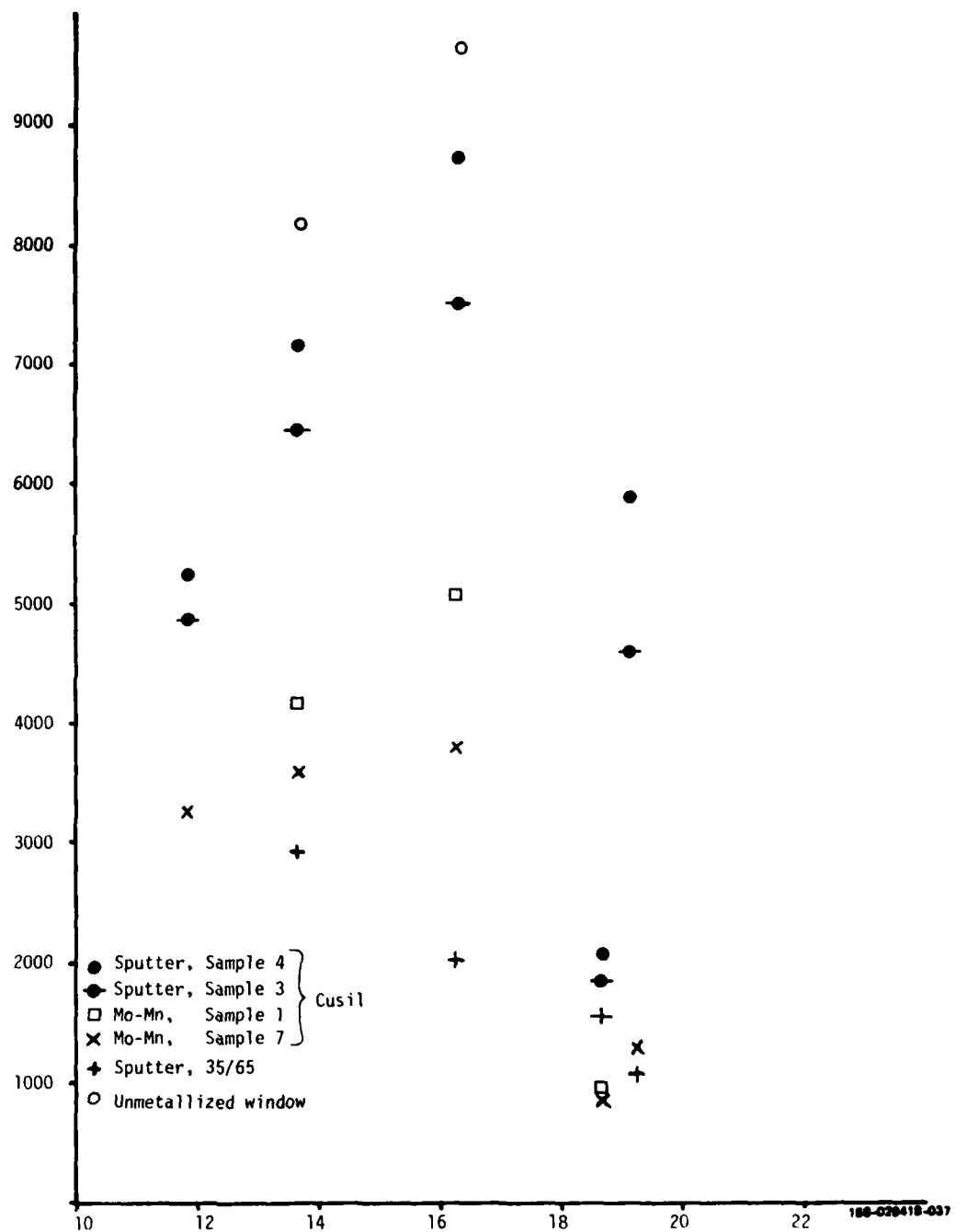


Figure 38. Average measured Q as a function of resonant frequency

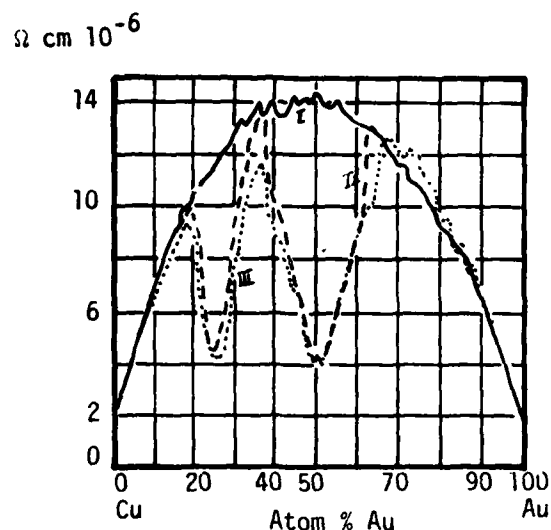


Figure 39a. Specific Resistivity of Au-Cu:*

- I: Misch crystal, at 0°C ———
 II: Tempered, at 0°C - - - - -
 III: Tempered, at 20°C

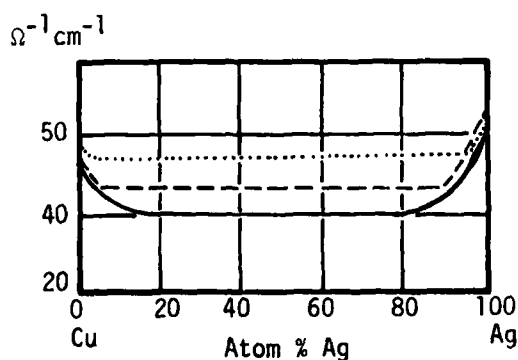


Figure 39b. Electrical Conductivity of Ag-Cu:

- I: Fast-cooled from 1100°C, rolled ———
 II: After 90 hr. at 750°C - - - - -
 III: After 100 hr. at 350°C

* Landolt-Bornstein: Zahlenwerte und Funktionen aus Physik, Chemie, Astronomie, Geophysik und Technik, Sixth Edition. Vol. II, Part 6.

unmetallized window, and if Q is the measured Q of the same cavity containing a brazed window, then:

$$\frac{1}{Q} = \frac{1}{Q_0} \left[1 + \frac{\delta - \delta_0}{\delta_0} \alpha \right] \quad (12)$$

$$\alpha = \frac{\int_{s'} H^2 ds}{\int_s H^2 ds}$$

where s' is the area of contact between the window and the cavity walls, and s the total wall surface of the cavity. The coefficient α , therefore, depends on the geometry of the brazed section and on the mode under consideration. Furthermore, δ and δ_0 are the skin depths of the brazing layer and of the silver plated cavity walls respectively. The knowledge of α is not necessarily required for a comparison between two brazing layers. For example, for a given resonating mode, the relation:

$$\frac{Q_0 - Q_1}{Q_0 - Q_2} = \frac{\delta_1 - \delta_0}{\delta_2 - \delta_0} \quad (13)$$

does not depend on α , but compares the values δ_1 and δ_2 . At the resonant frequencies of 13.7 and 16.3 GHz, the measured Q_0 's are respectively 8150 and 9650. The averaged Q for the two sputtered metallized samples in Figure 38 are respectively 6800 and 8100 (cusil braze), and the average Q for the Mo-Mn metallized windows at those frequencies are respectively 3875 and 4450. Thus, one obtains:

$$\frac{\delta_{sp} - \delta_0}{\delta_{Mo-Mn} - \delta_0} = \begin{cases} .32 \text{ at } 13.7 \text{ GHz} \\ .30 \text{ at } 16.3 \text{ GHz} \end{cases}$$

It is easily determined that:

$$\delta_{sp} \approx \frac{2}{3} \delta_0 + \frac{1}{3} \delta_{Mo-Mn} \quad (14)$$

Similarly, one finds the relation:

$$\delta_{sp} \approx \frac{4}{5} \delta_0 + \frac{1}{5} \delta_{Au-Cu} \quad (15)$$

In order to obtain the exact values of the skin depths, the coefficient α in equation 13 must be known. A calculation of α can be easily done by assuming the model discussed previously. Thus, if the window in the cavity can be simulated by a homogeneous dielectric filling the entire cavity, (dielectric constant $\bar{\epsilon} \approx 1.4$), then the magnetic field components are known (equation 6), and α can be calculated by integration. One obtains:

$$\begin{aligned} \alpha &= .034 \quad (1,0,2) \text{ mode} \\ \alpha &= .054 \quad (1,0,3) \text{ mode} \\ \alpha &= .062 \quad (1,0,4) \text{ mode} \\ \alpha &= .030 \quad (1,0,5) \text{ mode} \end{aligned} \quad (16)$$

Consider now relation 12 and the Q measured in Figure 38. At 13.7 GHz, $Q_0=8150$ and the maximum Q for the sputtered windows is 7150. From relation 12, one obtains:

$$\delta_{sp}/\delta_0 = 1 + (.14/\alpha_{1,0,3}) = 3.59 \quad (17a)$$

Similarly, at 16.3 GHz, one obtains:

$$\delta_{sp}/\delta_0 = 1 + (.11/\alpha_{1,0,4}) = 2.77$$

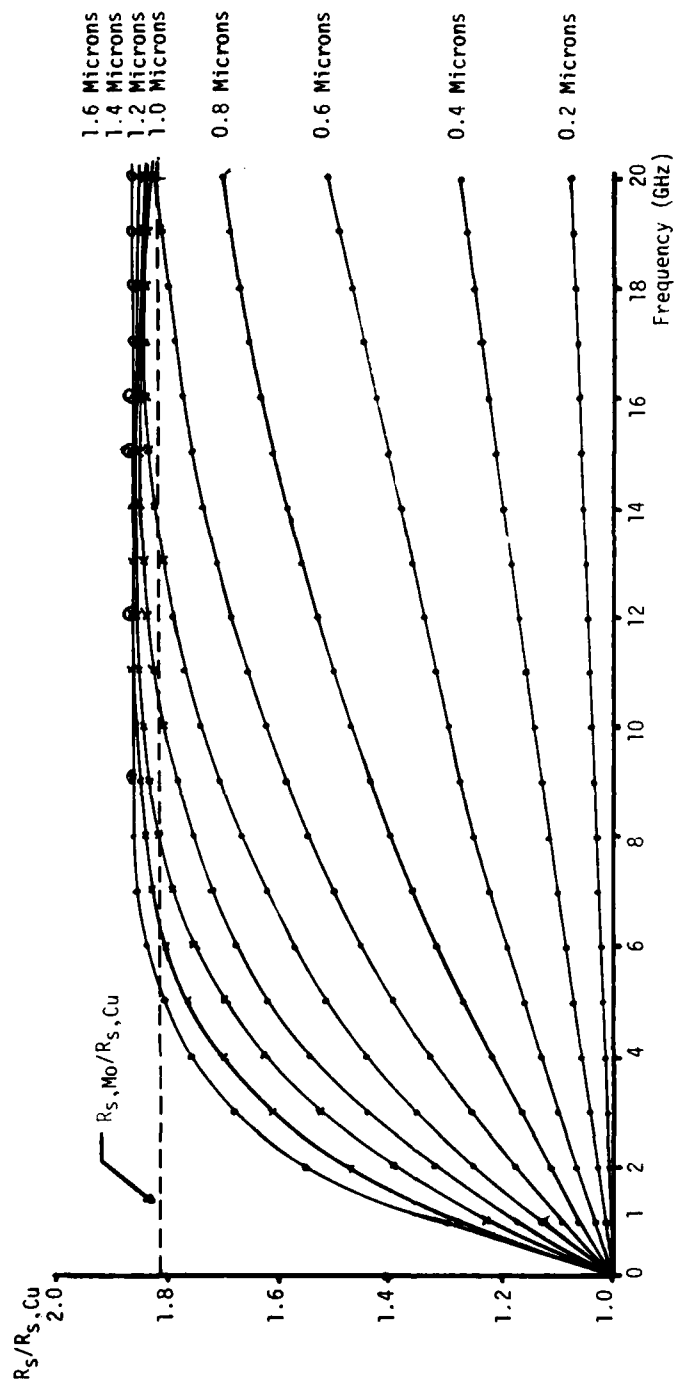
Experience in fabricating and testing CFA delay lines shows that these values are too high. This is particularly due to the small values of α . As mentioned above, a more detailed computer simulation of the electromagnetic field in the cavity containing the window has shown the amplitude of the magnetic field to be 2.38 times larger in the dielectric section (center) than at the cavity ends in the (1,0,4) resonating mode. Thus, an upper limit on the values of α can be assumed by multiplying the values of α in relation (16) by the square of 2.38. Under those conditions, the values of δ_{sp} in relation 17 become respectively 1.46 and 1.32. Thus, using the relations (14) and (15), it follows:

$$\begin{aligned}\delta_{sp} &\approx 1.40 \delta_{Cu} \text{ (Sputtered, Cusil braze)} \\ \delta_{MoMn} &\approx 2.20 \delta_{Cu} \text{ (Mo-Mn metal, Cusil braze)} \\ \delta_{AuCu} &\approx 3.00 \delta_{Cu} \text{ (Sputtered, 35/65 braze)}\end{aligned}\tag{18}$$

These results merit some discussion. Calculations have been made concerning the surface resistance of plane Cu plates coated with a thin layer of Moly. At approximately 15GHz, the surface resistance of such coated Cu plates is about 35% higher than the surface resistance of pure Cu plates (5000Å thick Mo layer), see figure 40. Furthermore, the influence of surface roughness becomes important at those frequencies. Thus, the value for δ_{sp} for cusil brazing seems reasonable.

It has been shown previously* that the attenuation in CFA meander lines was reduced by approximately a factor of two when the metallizing schemes were switched from Mo-Mn to sputtering. Since it was also found experimentally that the attenuation of meander lines increases proportional to the frequency instead of proportional to $f^{1/2}$, the ratio ($\delta_{Mo-Mn}/\delta_{sp}$) is found here to be 2.5, in reasonable agreement with the experimental observation.

* Contract No. F33615-76-C-1050.



156-028418-029

Figure 40. Surface resistance of Cu plated with Mo as a function of coating thickness and frequency

Thirdly, the use of Au/Cu alloy is found to increase the skin depth by approximately a factor of 3 when compared to pure Cu. Thus, the resistivity of the alloy increased by a factor of 9, neglecting the influence of the thin moly layer. This is in good agreement with the curve shown in Figure 39(a) where the intrinsic resistivity of Au/Cu alloy can be as much as 8 times higher than the resistivity of pure copper.

As such, the results presented in (18) have reasonable value, although some approximations were made, particularly due to the value of α .

Finally, it should be noted that those windows prepared by diffusion brazing exhibited extremely low Q's when tested in the cavities discussed here. This result implies again that the bonding layer was not homogeneous.

4.1.4 Circular Windows

A large number of circular windows corresponding to the shape discussed in Section 2.0 of the report were tested by similarly measuring the resonant frequencies and the Q's. It was consistently found that the Q's for Mo-Mn metallized windows were lower than those measured with sputter metallized windows, however, an accurate evaluation similar to the one made for rectangular waveguide was not made. The cavities tested were not silver plated, and as such, the variations from sample to sample, and from day to day, differed enough so that reliable interpretation of the data was not obtained.

5.0 CONCLUSIONS AND DISCUSSION

Using the Ti-Mo-Cu sputtering technique developed at Northrop in the past few years, three types of rf windows were successfully fabricated during this program. They include rectangular J-band waveguide windows, circular waveguide windows suitable for I or J band, and coaxial windows of dimensions suitable through J-band. Mechanical, thermal and RF properties were analyzed with respect to several variations of the sealing process, and were compared with similar windows fabricated by using the classical moly-manganese metalizing technique.

Table 21 shows a summary of some of the results obtained for waveguide windows. Grading from 1 (very good) to 5 (very poor) is somewhat arbitrary. This table, however, reveals the following.

- Tests of sputter-metallized waveguide windows showed that with Cusil (copper-silver eutectic) as brazing alloy, bond strength was high, the thermal barrier was nearly non-existent, and rf losses were low. The effective surface resistivity was found to be about 40% higher than copper, and can be almost fully accounted for by the 5000Å layer of molybdenum in the metallizing, and indicates no significant added contribution of the brazing alloy to the rf losses.

On the other hand, the combination of metallizing by sputtering and OFHC outside sleeves led to failure after only a few high temperature thermal cycles when OFHC was used; for Kovar sleeves, degradation with up to 50 thermal cycles was not observed.

- Tests of sputter-metallized waveguide windows with 35-65 gold-copper alloy as the braze material also indicated a low thermal barrier, probably

Table 21. Quality of Waveguide Window Seals

Braze Material	Base or Sleeve Material	Initial Bond Strength Flat Surface	Bond Strength After Thermal Cycling Disc in Flat Surface	Bond Strength Disc in Sleeves	Vacuum Integrity Initial	Thermal Integrity Thermal Cycling	Thermal Barrier	RF Losses
Sputter Metallized (Ti-Mo-Cu):								
Diffusion	None	2	--	2	--	5	1	5*
Liquid Braze	Cu-51 28Cu-72Ag	1	3	1	5	5	1	1
	Cu-51	--	2	--	3	1	2	--
	35Au-65Cu	2	2	2	4	3	2	5
	35-65	--	2	--	2	1	--	--
Mo-Manganese Metallized:								
Liquid Braze	Cu-51	--	3	--	3	2	2	3
	Cu-51	--	2	--	2	1	3	--
	35-65	--	3	--	3	2	2	--
	35-65	--	2	--	1	1	--	--
Sputtered Metallized (Zr-Mo-Cu):								
Diffusion	None	4	--	5	--	--	--	--
	Copper							

*Good diffusion bonds were not obtained in window form

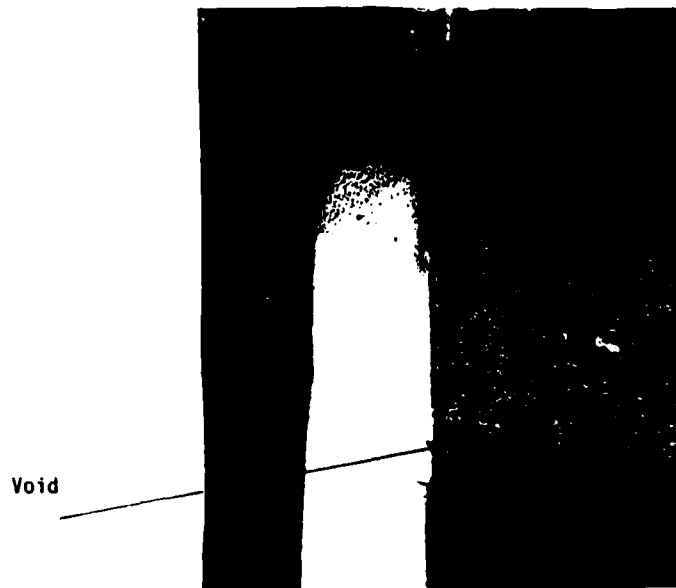
improved by the formation of fillets. RF losses were higher; the effective surface resistivity was three times as great as copper. The windows brazed by this process survived high temperature thermal cycling very well with Kovar sleeves; and moderately well with copper sleeves.

- Waveguide windows with moly-manganese metallization showed good bond strength and slightly greater thermal impedance. With Cusil as the braze material, the effective surface resistivity was 2.2 times the value in copper. The window assemblies made with moly-manganese metallizing in general withstood temperature cycling quite well.

The replacement of titanium by zirconium in the sputtering process is not recommended, since the bond strength is reduced from about 10,000 PSI to 6000 PSI.

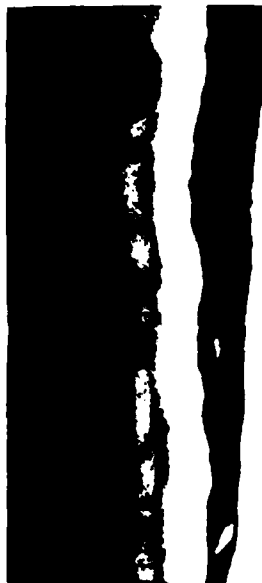
Experiments were also performed with pure silver and pure gold as brazing materials, and with copper-copper diffusion. Windows brazed with pure metals were characterized by poor vacuum integrity and low bond strength. In contrast with the success previously achieved with copper-to-copper diffusion bonds in meander circuits, efforts to make waveguide windows by this process were unsuccessful. Vacuum integrity was poor and rf losses were high, possibly because of significant voids at the interface (see figure 41).

Sputter metallization of the center hole of ceramic beads for coaxial windows has been demonstrated successfully. Coaxial window seals, where the seal is made between the center pin and the inside diameter of the ceramic, have been demonstrated to be repeatably vacuum tight and resistant to thermal cycling when the center conductor is molybdenum. Some seals with copper pins were initially tight, but as might be expected failed during the first few thermal cycles.



Cu-sleeve
Al₂O₃ disc
Moly-manganese
metallized

50X



Enlarged view of
voided area

945X

158-028418-040

Figure 41. Cross-sectional area of diffusion brazed Sample #35

The search for low rf loss, high thermally conductive metal to ceramic bonds has resulted in the development of the Ti-Mo-Cu ceramic metallization process by sputtering, and excellent results have been obtained. Therefore, this process is currently used in high power microwave tubes, and its applicability to rf windows has been demonstrated during this program. Simple calculations, however, have shown that the thickness of the molybdenum layer must be reduced as the frequency is increased. For example, a molybdenum thickness of less than 2000\AA is required in I/J band applications, and even smaller thicknesses will be required at millimeter wave frequencies. Therefore, one must consider the minimum limit thickness of molybdenum which must be applied so that the diffusion of copper to the ceramic is still inhibited. Indications are that diffusion of copper through a thin molybdenum layer (about 1500\AA) may have occurred during the fabrication of an I/J band CFA delay line.

It is therefore proper to consider whether another material could replace the molybdenum as diffusion barrier. In first approximation, and from an electrical standpoint, one would expect that the electrical resistivity of the new material must be smaller than molybdenum. Figure 42 shows, however, that such is not necessarily the case. Here the copper electrodes of a parallel plate waveguide model were coated with a layer (of thickness $d = 5000\text{\AA}$) of a material having the electrical resistivity ρ . The power loss due to the electrodes, normalized to the power loss one would expect if the layers were pure copper, is plotted as a function of material resistivity ρ , with the frequency (in GHz) as parameter. For $\rho = \rho_{\text{copper}}$, the ratio is equal to 1, and for infinite resistivity, the layer acts as a thin dielectric, so that

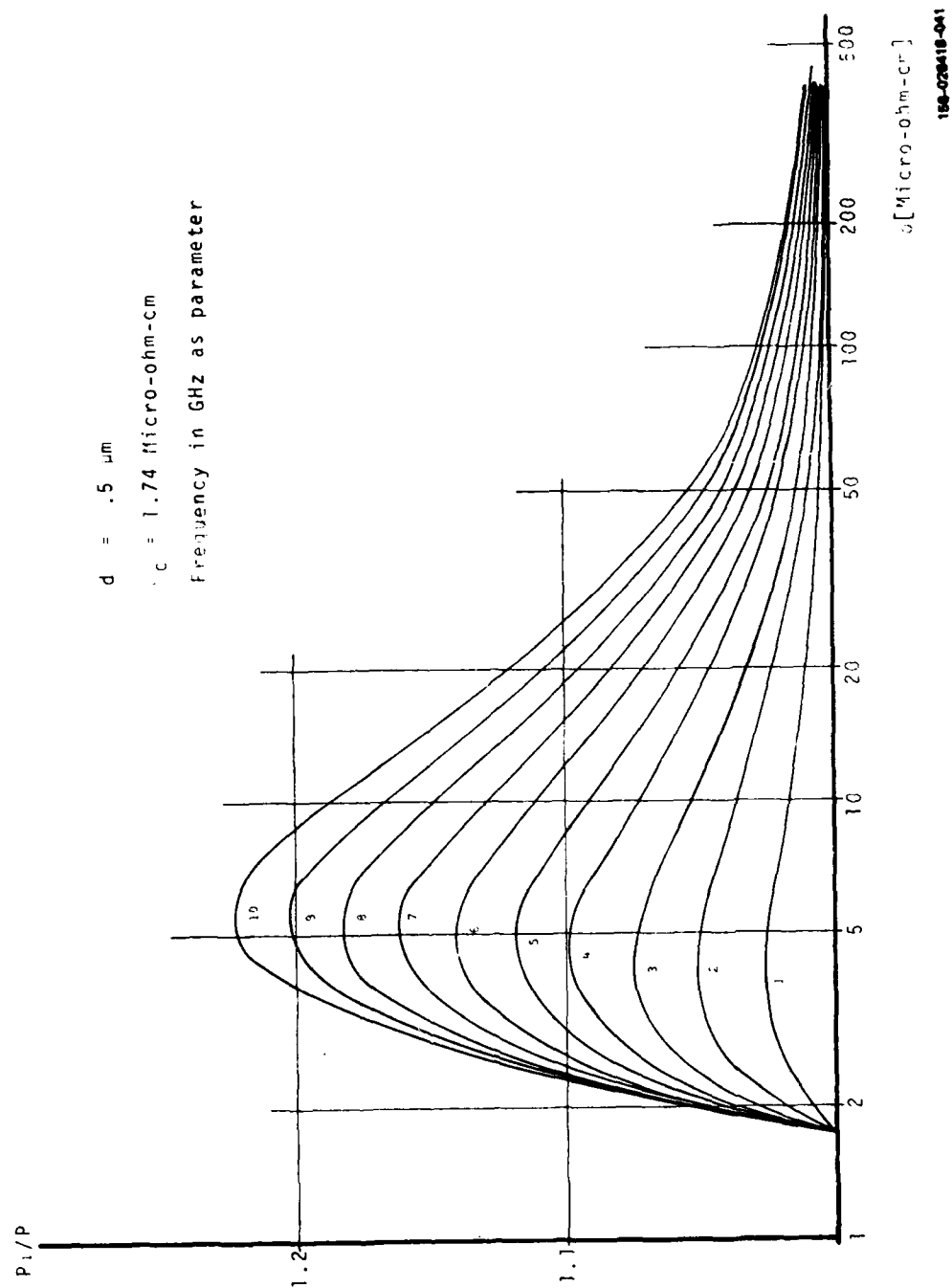


Figure 42. Relative surface resistivity of copper clad with molybdenum

the power ratio is again equal to one. It is seen in Figure 42 that the maximum power absorption of the coated electrodes occurs at around $\rho \approx 5$ micro-ohm-cm, a value corresponding to the resistivity of molybdenum. The position of the maximum increases to about 9×10^{-6} ohm-cm ($F = 10\text{GHz}$) as d is increased to $10,000\text{\AA}$, and reduces to about 4.8×10^{-6} ohm-cm at 2500\AA . Therefore, for high frequency applications, it is highly desirable to replace the molybdenum in the Ti-Mo-Cu metallizing process by a material of much larger (or much lower) resistivity than molybdenum. Table 22 shows a list of possible materials, their melting point, their electrical resistivity and their crystalline structure, which is believed to determine the diffusion rate of copper through the material.

The replacement of molybdenum as copper diffusion barrier is therefore proposed as future work. Furthermore, the possible application of diffusion bonding in small size windows should be further investigated.

Table 22. List of Different Elements with High Electrical Resistivity

Element	Symbol	Binary Alloys with Cu	Melting Point (°C)	Resistivity at 20°C ($\times 10^{-6}\Omega\text{cm}$)	Crystal Structure
Boron	B	No	2030	1.8×10^{12}	Orthorhombic
Columbium	Cb	--	2468	13.0	B.C.C. ⁺
Erbium	Er	No	1497	107.0	C.P.H. ⁺⁺
Gadolinium	Gd	No	1312	141.0	C.P.H.
Hafnium	Hf	No	2222	35.0	C.P.H.
Holmium	Ho	No	1461	87.0	C.P.H.
Lutetium	Lu	No	1652	79.0	C.P.H.
Molybdenum	Mo	No	2610	5.2	B.C.C.
Rhenium	Re		3180	193.0	C.P.H.
Samarium	Sm		1072	88.0	Rhombohedral
Scandium	Sc		1539	61.0	C.P.H.
Tantalum	Ta	No	2996	12.5	B.C.C.
Thulium	Tm	No	1545	79.0	C.P.H.
Tungsten	W	No	3410	5.5	B.C.C.
Vanadium	V	No	1900	25.0	B.C.C.
Yttrium	Y	No	1509	57.0	C.P.H.

⁺ B.C.C. - Designates body-centered cubic

⁺⁺C.P.H. - Designates close packed hexagonal